Investigating the Photochemistry of Provitamin D₃ as a Function of Liposome Properties

by

Danielle L. Sofferman

A dissertation submitted in partial fulfillment
of the requirements for the degree of
Doctor of Philosophy
(Applied Physics)
in The University of Michigan
2020

Doctoral Committee:

Professor Roseanne J. Sension, Chair
Professor Julie Biteen
Professor Cagliyan Kurdak
Professor Vanessa Sih
Professor Sarah Veatch

Danielle L. Sofferman

dnlesoff@umich.edu

ORCID iD: 0000-0001-7386-4019

DEDICATION

This dissertation is dedicated to all the people who have supported me throughout this journey.

ACKNOWLEDGEMENTS

Thank you, Mom, Dad, and David. Mom and Dad, you both have supported my every decision throughout my science career and were proud of my every accomplishment. Dad, thank you for working so hard to provide me with an undergraduate education at Adelphi University. Mom, thank you also for helping me pay for Adelphi as well. The opportunity that you both gave me ultimately led me to pursue and now complete a Ph.D. at the University of Michigan. Thank you, Mom, for always checking in to see if I made it home safe, and for visiting, even during the coldest times of the year. And thank you to my brother, David, for helping me move into my apartment when I first moved to Michigan. I love you guys!

Thank you, Rob. Thank you for all the love and support you have given me in the short time that we have been together. Your encouragement and support has helped me complete this dissertation. Thank you for standing by myside through one of the toughest years of my Ph.D. and for reassuring me that everything will work out in the long run.

Thank you, Professor Roseanne Sension. Thank you for this opportunity that allowed me to take my curiosity for science, problem solving and technical skills to a level I never imagined was possible. Thank you for challenging me to make the most compelling evidence-based arguments and pushing my creativity to come up with the next best experiment. Thank you, Professor Ken Spears for mentoring me and serving as a second advisor throughout the years. I have been very fortunate to have learned from you and have always appreciated your practical problem solving and technical skills.

Finally, thank you to my labmates, collaborators, and friends who have helped me make my years at Michigan so memorable and making this dissertation possible. Thank you, Dr. Ted Wiley for teaching me everything about our laser system, for having patience and allowing me to make mistakes and learn from them. Thank you, Dr. Nick Miller for pushing me to make the most compelling scientific arguments during a presentation. Thank you, Dr. Orko Konar and Dr. Joseph Mastron for working with me in the Laboratory for Ultrafast Multidimensional Optical Spectroscopy (LUMOS) to obtain the most important pieces of data for this dissertation. Thank you to the Veatch Group for your expertise on sample preparation and thank you to the Kopelman Group for allowing me to use your equipment to characterize my samples. Thank you to all my friends that I have made along the way, you all have helped shape Michigan into a home. Thank you, Kurdak, Cyndi and the rest of the Applied Physics family for supporting and believing in me throughout the years. I truly wouldn't have done this without any of you.

Table of Contents

LIST OF FIGURES

LIST OF TABLES

ABSTRACT

7-dehydrocholesterol (DHC, provitamin D_3) is the starting material that undergoes photochemical processes to turn into vitamin D_3 in mammalian skin membranes. The process starts when UV-B light penetrates through the outer layer of mammalian skin and converts DHC in the skin membrane into a previtamin D_3 species. The previtamin species can undergo further processes where it can relax to form vitamin D_3. Additionally, the Smith-Lemi-Opitz syndrome (SLOS), a condition fatal to developing embryos, is caused by the genetic inability to convert DHC into cholesterol, resulting in destabilization of the cell membrane. Thus, most lipid research has focused on the structural influences of DHC and cholesterol on synthetic lipids that closely mimic the cell membrane. The photochemical dynamics of DHC can also provide additional insight into the cell membrane environment, but has not been explored. By using membrane models to study the initial dynamics of vitamin D_3 formation, information about the photochemical process in the lipid environment can possibly be used to address issues that arise from the SLOS.

The ultrafast photochemical transformation of DHC, ergosterol (ergo, provitamin D_2) and DHC-acetate to previtamin D_3, D_2 and D_3-acetate occurs upon a ring-opening reaction in the excited state where a cyclohexadiene (CHD) chromophore embedded within the molecules opens to form a hexatriene previtamin D species. In order to capture the dynamics and conformational changes of the three provitamins, broadband transient absorption spectroscopy is used. This dissertation investigates the excited state ring-opening and ground state relaxation of DHC, ergo

and DHC-acetate in isotropic solution and anisotropic liposome environments. The solution measurements provide a baseline to explore the excited state and ground dynamics of the three molecules in a complex liposome environment. The primary lipid that is used in this work, 1,2-dipalmitoyl-sn-glycero-3-phosphocholine (DPPC), is reported to closely mimic the human skin and therefore allows us to study the initial steps involved in vitamin D production in a simple skin membrane model.

The excited state of DHC is well studied in isotropic solvents where the molecule ring opens to form a previtamin D_3 species with dynamics that are completed within 1-2 ps. On the ground state, the conformer relaxation process forms a stable previtamin D_3 species within 6-7 ps. In solution, ergo and DHC-acetate have similar spectra, photoproduct distributions, and excited state and ground state lifetimes as DHC.

However, unlike in solution, the cell membrane environment is hypothesized to stabilize the previtamin D conformation responsible for thermal formation of vitamin D. In this work we find that when DHC is incorporated into the DPPC lipid bilayer, the longest time constant is significantly slower than in solution, ca. 11 ps and 25 ps in the excited and ground state, respectively. To understand the photochemistry that takes place in biological skin membranes, DHC, ergo and DHC-acetate are investigated as a function of membrane parameters, such as hydrogen bonding, van der Waals interactions and lipid tail length. Dynamics in the excited state and ground state appear to be more significantly dependent on the lipid tail length than on the other parameters. The ring-opening reaction of DHC in the shortest lipid studied, 1,2-dilauroyl-sn-glycero-3-phosphocholine (DLPC) is completed within 6 ps. The photochemistry of DHC in DLPC suggests that the shorter tail length environment reduces the conversion efficiency of vitamin D_3 formation.

Chapter 1

Introduction

Introduction to The Photochemistry of 7-Dehydrocholesterol In The Skin Membrane

When skin is exposed to UV-B radiation, provitamin D_3 (7-dehydrocholesterol, DHC) in the epidermis converts to vitamin D_3, an essential compound for human survival. Wollweber *et al.*[1] have used computational models to study the formation of previtamin D_3 and found that the stratum basale to account for most of the production. An illustration of the skin and photochemical reaction is illustrated in Figure 1.1. The conversion takes place in a series of steps. First, the cyclohexadiene chromophore undergoes a ring-opening reaction to form a hexatriene previtamin D species (preD$_3$ Figure 1.1). From the gZg conformation, the molecule can undergo a thermal hydride shift followed by a relaxation to form vitamin D_3. Thus, the relative stabilities of the gZg and tZg conformation influence the rate of vitamin D_3 formation. Given excess exposure time to UV radiation, the photoisomerization of previtamin D_3 to tachysterol (the trans isomer of previtamin D) and to other side products, such as lumisterol can occur[2,3,4,5]. Although these side products are not relevant to human utilization of DHC, the accumulation of these side products needs to be monitored throughout transient and steady state measurements.
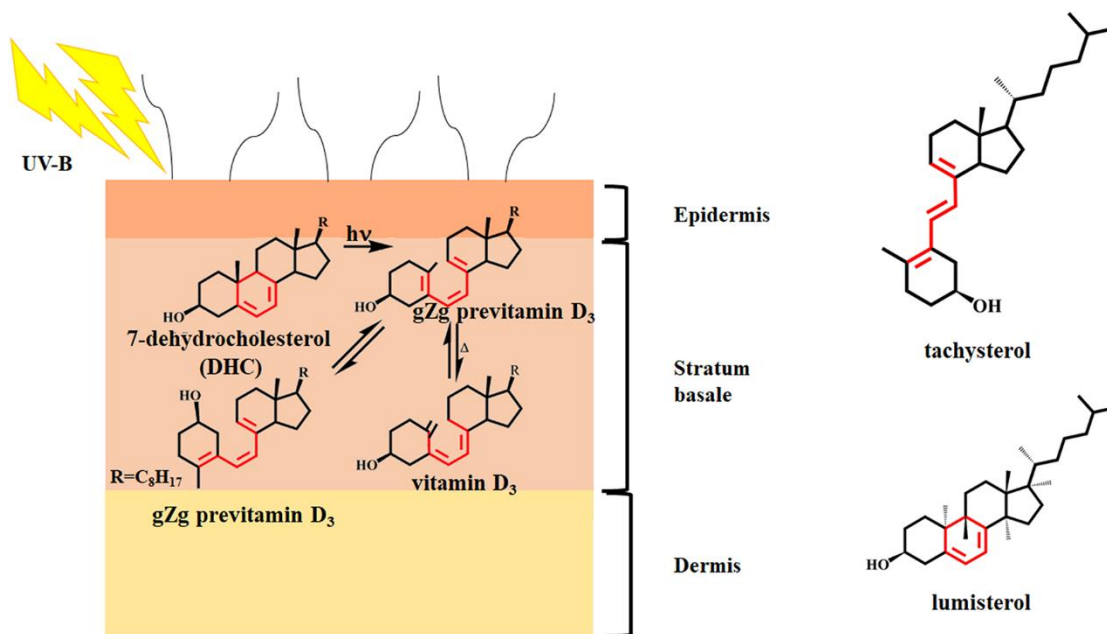
Figure 1.1: Photochemical process of DHC in skin. Following absorption of UV radiation, the cyclohexadiene chromophore (red) undergoes photochemical changes to convert DHC to vitamin D_3. Excess exposure of UV radiation can lead to the formation of tachysterol and lumiseterol.

The cyclohexadiene (CHD) chromophore is the photoactive component responsible for previtamin and vitamin D_3 formation[6,7,8,9,10,11,12] . CHD also serves as a photo switch in a number of other molecules such as α-terpinene[6], ergosterol (ergo, provitamin D_2) and DHC-acetate. A cartoon that illustrates the ring-opening of CHD along a potential energy surface is shown in Figure 1.2. The reaction is initiated by optically pumping the CHD chromophore from the S_0 ground state to the excited S_1 state. This reaction is followed by an ultrafast trajectory to the dark state and back to the ground state through a conical intersection that can result in conformational

relaxation back to CHD or formation of hexatriene photoproducts. The entire process is described as a "more or less" ballistic motion and happens within 50-100 fs[13,14,15,16].
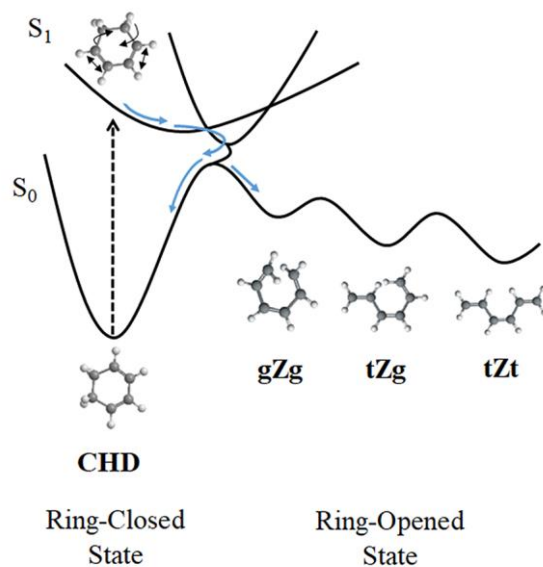
Figure 1.2: Photochemistry of CHD along the reaction coordinate. After the ring opens in the excited state, the molecule undergoes conformational relaxation in the ground state to form a stable tZt species.

DHC photochemistry compared to CHD photochemistry: The photochemistry of DHC is based on the photochemical reactions of cyclohexadiene as illustrated in Figure 1.3. However, the DHC molecule differs significantly from CHD in that it is larger and the conformational change in the ground state is constrained by the rings surrounding the cyclohexadiene chromophore.
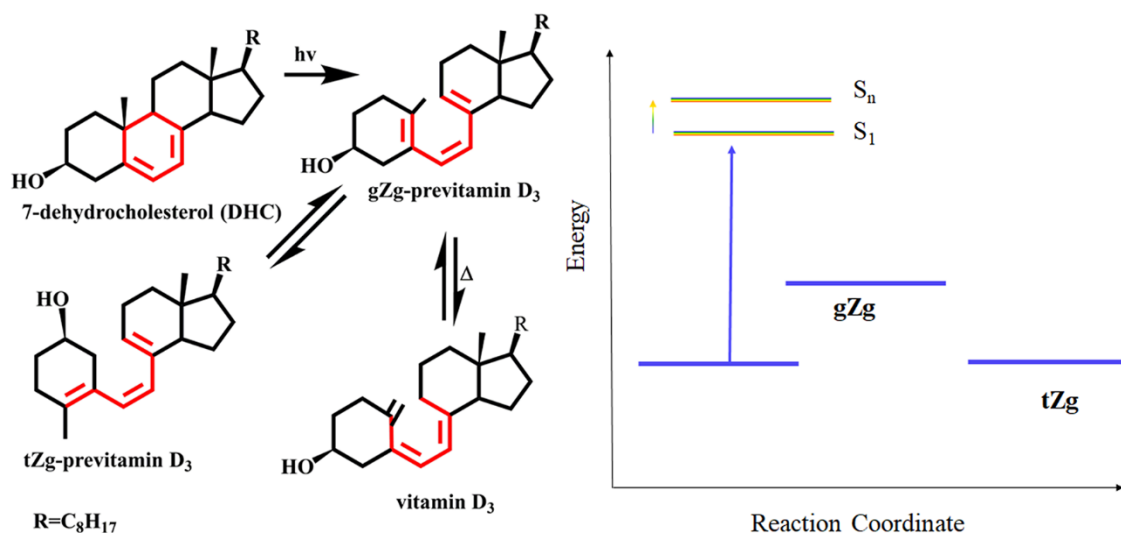
Figure 1.3: Photochemistry of DHC. As the molecule first ring opens, it moves from the excited state (S_1) to the ground state, where a previtamin D_3 species is formed. The gZg-previtamin D_3 is able to undergo a thermal hydride shift and relax to form vitamin D_3. Access to this channel is controlled by the relative stability of the gZg and tZg species.

The stereochemistry for DHC is different compared to CHD. Isolated CHD has two identical isomers, while DHC has only one preferred orientation. Isolated CHD only has C-H groups around the ring, whereas the ring embedded in DHC has additional C-C bonds that connect to the sterol rings (Figure 1.2 and Figure 1.3). The rings constrain the way the molecule can isomerize preventing full relaxation to the tZt conformation. In addition, DHC has substantially more vibrational modes compared to CHD (3N-6, with N = 72 and N = 14 respectively). The modes along the reaction coordinate are most relevant in the photochemical reaction. The other modes provide a bath that can take energy away from the chromophore.

One of the major experimentally observed differences between CHD and DHC is the excited state lifetime of these two molecules. DHC has a strong visible absorption that can be used to monitor the excited state lifetime[7,10,12]. Unlike DHC, the isolated cyclohexadiene chromophore does not have an excited state absorption in the visible range[15], therefore experimental measurements to measure mechanisms and pathways of the molecule on the potential surface includes mass spectroscopy[16,13], photoelectron spectroscopy[17], transient electron

diffraction[18,19,20]and femto-second x-ray spectroscopy[21]. The motion of isolated CHD along the

reaction coordinate (Figure 1.2) occurs within 50 to 100 fs, whereas the pathway for DHC from

the excited state to ground state is much slower (~1.8 ps). Tang *et al.*[12] demonstrated that the

DHC molecule has an effective barrier in the excited state, expressed as

$$DHC_{barrier} = \text{Intrinsic intramolecular barrier} + \text{Solvent barrier.}$$

 In contrast, the barriers for internal conversion in CHD are negligible[22].

On the ground state, the thermal relaxation of the CHD hexatriene photoproduct (Figure

1.2) is solvent dependent[23] while conformer relaxation for DHC in solution is solvent

independent, with the initial relaxation occurring on a time scale of 6 to 10 ps[6]. However, all the

experiments were performed in isotropic solution, a far cry away from the biologically relevant

environment of a cell membrane in human skin. To test the relative packing around the molecule,

in the upcoming chapters we will examine the photochemistry of DHC in an anisotropic lipid

bilayer environment, where the DHC molecule and photoproduct are constrained by the

environment. Liposomes described below and in Chapter 2 suit this purpose well and will allow

us to study the photochemical processes of DHC in a simple model of human skin.

α-Terpinene compared to DHC: While the CHD chromophore is the photoactive unit, a

small molecule more closely related to DHC is α-terpinene. This molecule, illustrated in Figure

1.4 also contains the cyclohexadiene chromophore, but the conformational relaxation of the

photoproduct is constrained by a methyl and propyl group attached to the ring.
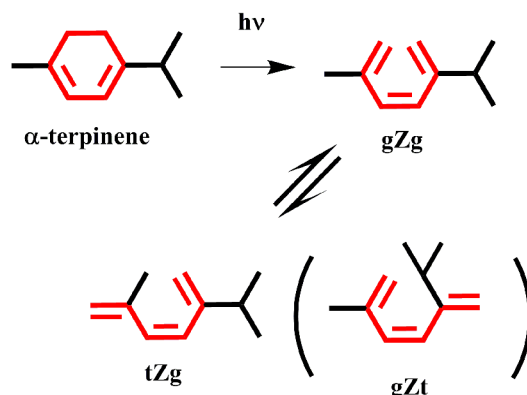
Figure 1.4: Chemical structure of α-terpinene and its photoproducts in the gZg, tZg and gZt conformation.

Arruda *et al.*[6] studied the ring-opening reaction of α-terpinene, through a combination of TD-DFT calculations, steady state absorption and transient absorption measurements[6]. Like DHC, this molecule exhibits an excited state absorption, although the lifetime of the excited state is much shorter, ca. 150 fs. Following excitation of α-terpinene and formation of the hexatriene product, both spectroscopic measurements and TD-DFT calculations suggest that most of the distribution relaxes to form a stable tZg conformer. The conformer relaxation process of the photoproduct occurs on a time scale of 6-7 ps, similar to that observed by DHC, and is not dependent on solvent viscosity or polarity. Thus, α-terpinene makes a good small model comparison to DHC.

The photochemical changes of α-terpinene, DHC and CHD are well studied in isotropic solvents, however the solution environment does not provide insight into how mammalian skin increases vitamin D production. In this work we focus on the photochemical ring-opening reaction and ground state conformer relaxation in synthetic lipid bilayers that are reported to mimic the human skin environment[24]. The most dominant lipid in human skin is reported to be phosphocholine. This lipid is reported to occupy ~20-50 (wt %) of the lipid distribution in human skin. The composition of pig skin is reported to closely mimic the lipid distribution in human skin. Thus, may serve as a close model in future work[25,26]. In human skin applications, sterols

have been used in concentrations of ~30-40mol-%[27,28]. Tian and Holick reported that both human skin and dipalmitoyl-sn-glycero-3-phosphocholine (DPPC) lipid bilayers increase the isomerization rate from previtamin D_3 to vitamin D_3 by a 10 fold compared to solution[24]. To compare our results to the accelerated isomerization rate reported by Tian and Holick, DPPC is the primary lipid used in this work. To mimic the skin environment and have defined membrane structure, the primary loading of sterol used is 30mol-%[29].

The lipid environment and DHC-analogs: DPPC contains two palmitoyl acyl chains, each with 16 carbons and no double bonds, (denoted by 16:0) and has a bilayer melting point (T_m) of 41 °C. The melting point (T_m) of a lipid bilayer from the gel to fluid phase is a function of tail length and saturation which allows us to examine how membrane fluidity impacts the photochemistry of the provitamins. The influence of membrane fluidity on the initial steps in vitamin D photosynthesis was tested in our measurements by using 1,2-disteroyl-sn-glycero-3-phosphocholine (DSPC, 18:0),1,2-dimyristoyl-sn-glycero-3-phosphocholine (DMPC, 14:0) and 1,2-dilauroyl-sn-glycero-3-phosphocholine (DLPC, 12:0). The DSPC, DMPC and DLPC bilayer melting points are at 55 °C, 24 °C, and -2 °C respectively. These lipids are illustrated in Figure 1.5. All of our measurements were done between 22 °C and 25 °C, near T_m for DMPC, below T_m for DPPC and DSPC and well above T_m for DLPC.

DSPC (18:0) **DPPC** (16:0) **DMPC** (14:0) **DLPC** (12:0)
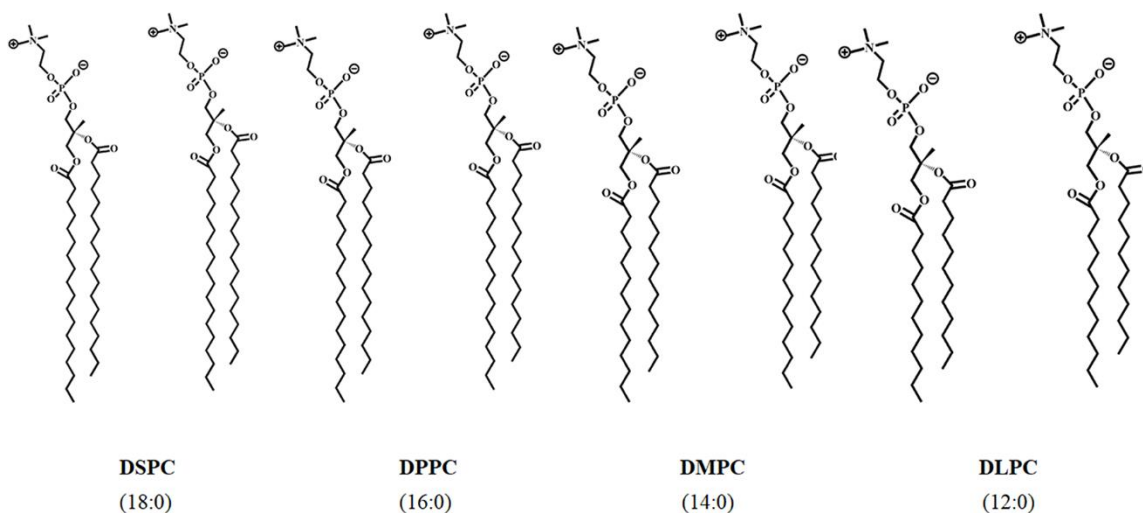
Figure 1.5: Illustration of DSPC, DPPC, DMPC and DLPC lipids without sterol.

To explore the excited state dynamics and the conformational relaxation of previtamin D on the ground state, we have studied naturally occurring sterols, DHC and ergo, as well as a synthetic variant, DHC-acetate. These molecules have a similar sterol structure to cholesterol (CHL), an essential structural component of mammalian cell membranes. A comparison of these molecules is shown in Figure 1.6. Ergo and DHC-acetate allow us to probe interactions with the lipid bilayer by changing the structure of the tail or preventing hydrogen bonding by the hydroxyl group.
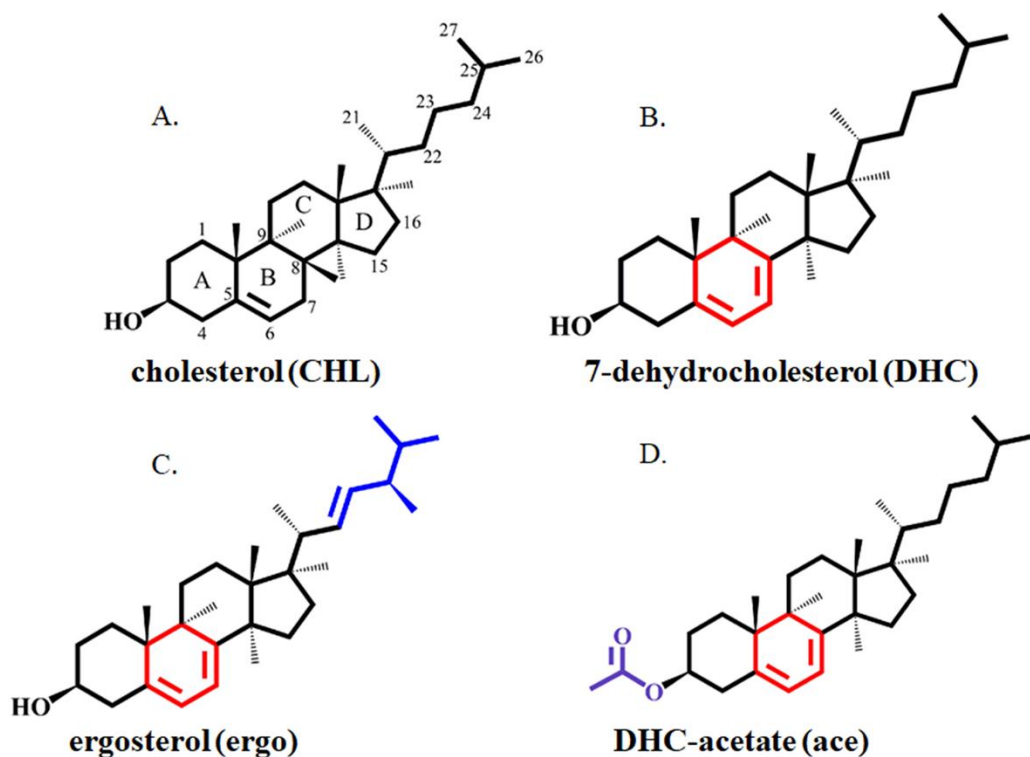
Figure 1.6: Chemical structure for (A) cholesterol, (B) DHC, (C) ergosterol and (D) DHC-acetate. DHC, ergo and DHC-acetate contain the cyclohexadiene chromophore (red) that allows the molecules to undergo photochemical changes, whereas cholesterol is not photoactive.

Cholesterol (Figure 1.6A) is made from DHC through DHCR7, an enzyme that removes the double bond in DHC. Cholesterol is not photoactive but is used to stabilize the cell membrane. It acts as a regulator that keeps the membrane from becoming too rigid or too fluid under phase changes. Cholesterol is used in our studies to test heterogeneity of the lipid phases and is used as a control to remove scattering contributions in steady state measurements.

The primary molecule of interest in this dissertation is DHC. As described above, DHC undergoes a photochemical transformation in a series of steps to form vitamin D_3. The isomerization of the molecule takes place from the ring-opening reaction of the cyclohexadiene chromophore embedded in the steroid skeleton as illustrated in Figure 1.6. This reaction has been studied extensively in solution and in theoretical simulations of the isolated molecule[6,7,8,10,11,12,30,31]. Ergo is a supplement of cholesterol in plants. It contains the

9

cyclohexadiene chromophore and undergoes a photochemical ring-opening reaction to form

vitamin D_2. Ergo differs from DHC and cholesterol in the tail structure, where there is a double

bond present on C22-C23 and a methyl group on C24 (see Figure 1.6C). This molecule is used in

our studies to test if van der Waals or packing interactions between the lipid tail and sterol tail

have an influence on conformer relaxation and excited state reaction rates. Another analog of

DHC is DHC-acetate. DHC-acetate as shown in Figure 1.6D has the same skeleton as DHC,

except there is an acetate group in place of the hydroxyl group. In our studies, we use this

molecule to test if the ring-opening reaction in liposomes is influenced by hydrogen bonding to

the lipid head group.

Tian and Holick's studies of the isomerization rate from previtamin D_3 to vitamin D_3

used kinetic and thermodynamic analysis to test the conversion rate as a function of liposome tail

length, fluidity and hydrogen bonding. Their model, illustrated in Figure 1.7 suggests that the

gZg conformer is stabilized in the lipid bilayer through hydrogen bonding between the phosphate

group of the lipid and –OH group of the molecule and van der Waals interactions with the lipid

tails[24]. The model for the way the sterol resides in the lipid bilayer has also been investigated

computationally. Molecular dynamics (MD) simulations have focused on the location of sterols

within the bilayer and on the interactions between the sterol and the bilayer. Y. Liu *et al.*[32]

performed MD simulations to compare DHC and cholesterol in DMPC for loadings of 11% and

33% DHC and cholesterol. Mass density profiles show that the sterol ring A (Figure 1.6) is near

the polar head group of the lipid and the alkane tail of the molecule is in the center of the

membrane and for a given loading, mass density profiles for DHC and cholesterol are similar.

Other MD studies done by Z. Cournia show that mass density profiles of cholesterol and ergo in

DPPC lipid bilayers are also similar[28]. The locations of these sterols are consistent with Tian and

Holick's membrane model[24].
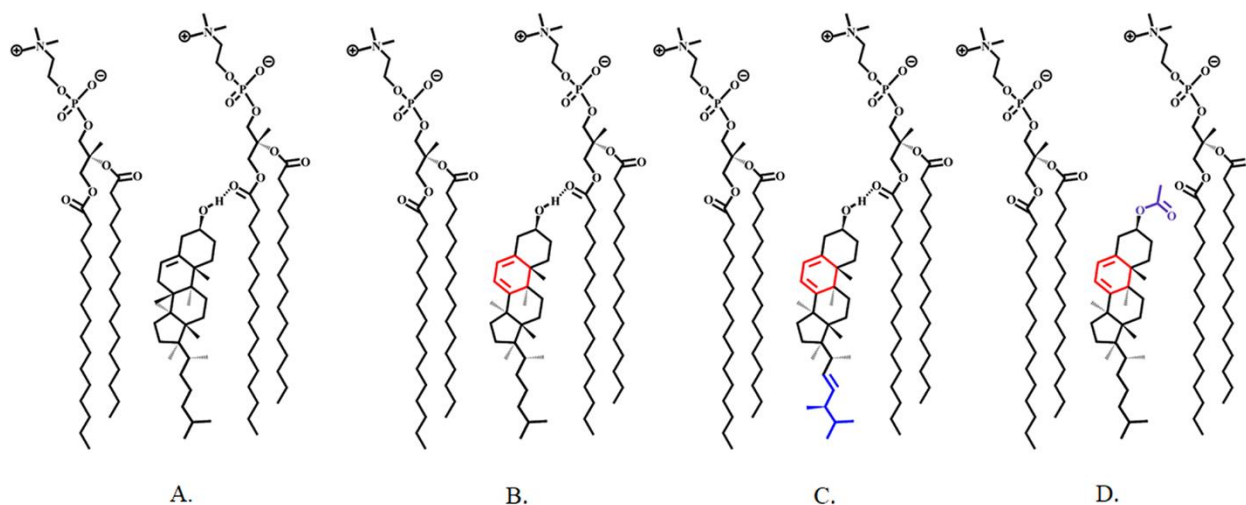
Figure 1.7: Illustration of lipid membrane model proposed by Tian and Holick for (A) CHL, (B) DHC, (C) ergosterol and (D) DHC-acetate in DPPC lipid bilayers.

Lipid bilayer effects with the incorporation of sterols: For the photochemistry explored in this work, there is a complex connection between understanding the environment and the photochemistry of the probed molecule, Table 1.1 summarizes, the effects of each individual sterol molecule on the DPPC lipid bilayer[33,34]. The check marks (✓) indicate the intermolecular forces between the sterol and the lipid. In addition to the location of the sterols, it may be also important to consider the orientation of the head group of the lipid. The zeta potential describes the orientation of the charge distribution at the lipid head group as illustrated in Figure 1.8. Depending on the orientation of the head group, the cyclohexadiene chromophore may interact differently with the lipid tails, thus altering the transient absorption data.

11

Table 1.1: Summary of sterol effects on the lipid bilayer.

Sterol	Hydrogen bonding with lipid	Different van der Waals interaction from sterol tail	Promotes domain formation effectively*	Zeta Potential Measurements (mV) **
cholesterol	✓	X	✓	-5
DHC	✓	X	X	-12.5
ergo	✓	✓	✓	-12.5
DHC-acetate	X	X	N/A	N/A

*Domain formation for 20mol-% and 40mol-% sterol loading in DPPC [33]
**Measurements for zeta potential for 30mol-% sterol loading in DPPC [33]
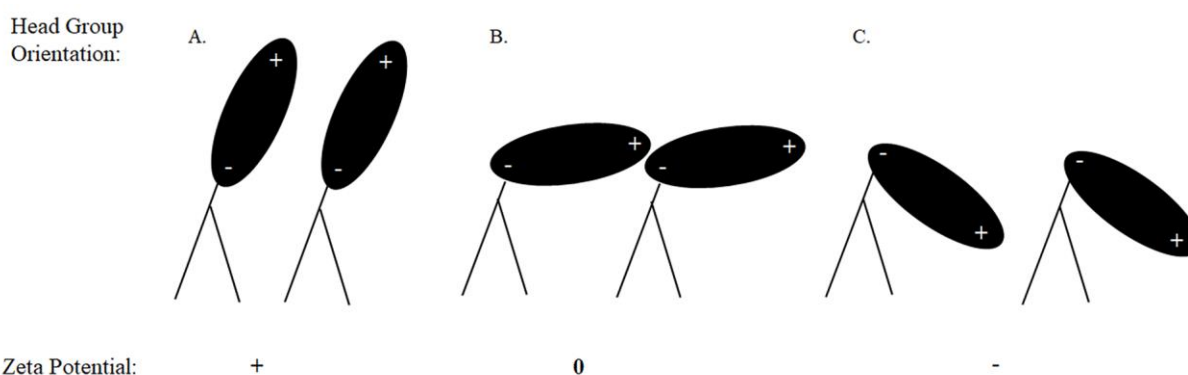
Figure 1.8: Illustration of the lipid head group orientation for (A) positive, (B) neutral and (C) negative zeta potentials.

A comparison between DHC and CHL on lipid properties: A major topic of interest in lipid research are the effects of DHC and cholesterol on the lipid bilayer. This topic addresses issues raised by the Smith-Lemi-Opitz syndrome (SLOS). The SLOS syndrome is a genetic deficiency in the ability to remove the double bond located between C7 and C8 in DHC to form cholesterol (Figure 1.6). The syndrome is fatal in developing embryos since the overproduction of DHC destabilizes the cell membrane.

Incorporation of sterols such as cholesterol and DHC influence the shape, melting point and phases of the lipid bilayer. It is therefore necessary to discuss the similarities and differences

for both DHC and cholesterol as this may 'weed out' any unnecessary assumptions about environmental effects that DHC (and other provitamins) may experience in the excited state and in the ground state. Figure 1.9 illustrates these lipid properties. The primary points are:

1. <u>Sterol tilt of the lipid bilayer</u>: Sterol tilt is defined by the angle between the lipid tails and the normal of the lipid membrane. The angle between the lipid tails, *sn*-1 and *sn*-2 relative to the sterol may increase or decrease the amount of space that the cyclohexadiene chromophore has when it ring opens or undergoes conformational relaxation.

2. <u>Lipid domains formation</u>: When sterol is incorporated into the lipid bilayer, two phases can coexists. The solid-ordered ('non-fluid') and liquid-ordered ('fluid') phase. These phases lead to regions where detergent resistant domains form. The sterol-rich and sterol-poor regions have been shown to be highly dependent on the type of incorporated sterol. This may be important to the observed photochemistry in this dissertation because it can change the heterogeneity of the environment, which may change vibrational modes of the molecule. It also may lead to signals coming from 'tightly packed molecules' in the solid-ordered phase and 'loosely packed molecules' in the liquid-ordered phase. Thus, it is hypothesized that each region can contribute to the lifetimes measured in transient data.

3. <u>Membrane fluidity (phase)</u>: Membrane fluidity and compressibility is a function of lipid tail length[35]. To account for the fluidity of the environment, it is hypothesized that a more fluid (less constrained) environment will cause the photochemical process of the provitamins to be faster than in a rigid one.
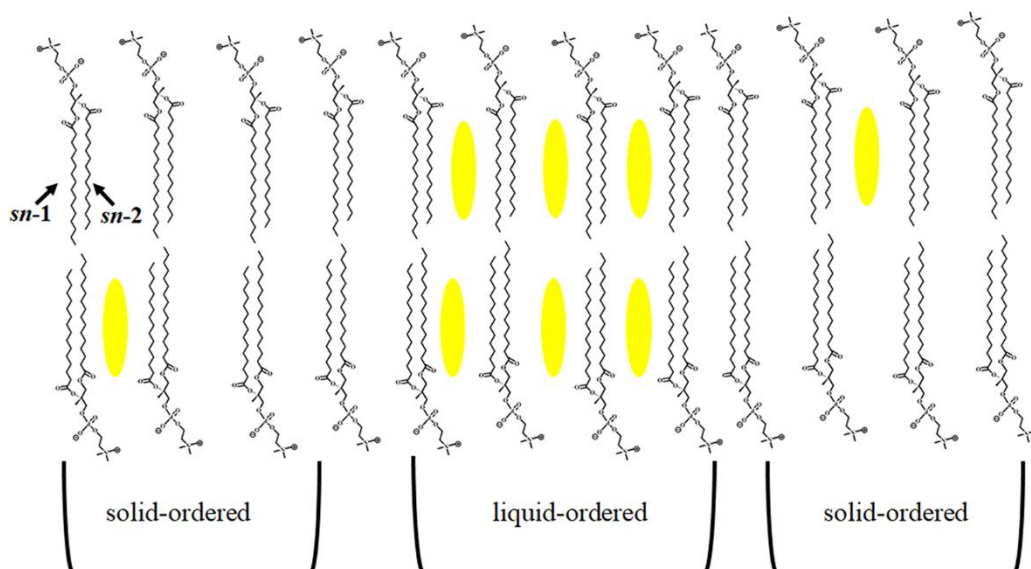
Figure 1.9: Illustration of the solid-ordered (sterol poor regions) and liquid-ordered (sterol rich) regions formed by the incorporation of sterol (represented by yellow ovals) in DPPC lipid bilayers. *sn*-1 and *sn*-2 are the names of the two acyl chains of the lipid.

Previous studies have focused on the sterol effects on lipid membranes for a variety of lipids and lipid mixtures, but have not explored photochemical motion of the sterols in these complicated environments. These studies have focused on Egg (chicken) PC, DMPC, and DPPC[32,33,36,37,38,39]. Figure 1.10 illustrates a comparison between DPPC and Egg PC. For our studies we consider only DPPC and DMPC. It is uncertain how Egg PC would influence the photochemistry of the provitamins in comparison to the experiments done in this dissertation.

DPPC   **Egg PC**
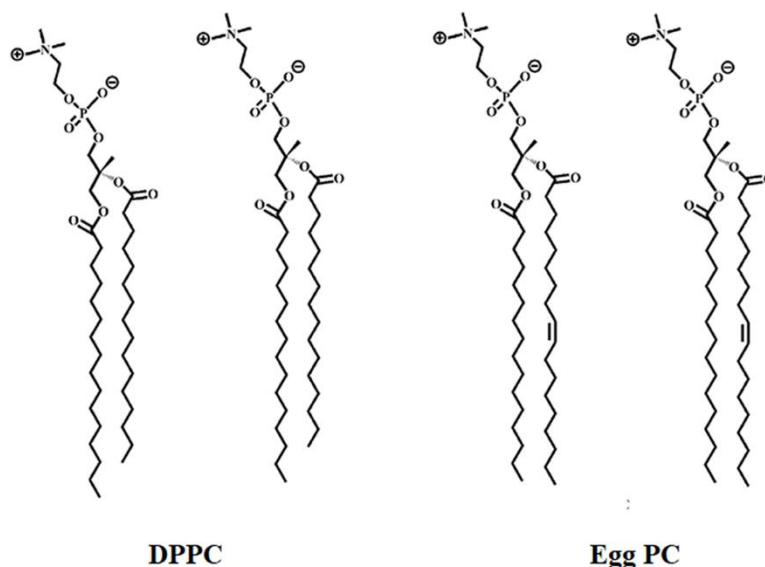
Figure 1.10: Comparison between DPPC (left) and Egg PC (right). The two lipids have the same head group however Egg PC has a double bond in the *sn*-2 chain.

   To understand the initial environment before any reaction dynamics occur, we must

consider the structural properties of the lipid environment. MD simulations have shown that the

DMPC sterol tilt between the *sn*-1 chain and *sn*-2 chain are primarily a function of sterol loading

rather than the type of sterol used (cholesterol or DHC)[32]. This is consistent with fluorescent

probe anisotropy measurements done by Bendoff and Winter[34]. At 30 °C, cholesterol and DHC

in DPPC lipid bilayers have a similar effect on the tilt angle of the fluorescent probe. For

temperatures below the melting point of DPPC, loadings of 10-30mol-% all exhibited a similar

order parameter of the fluorophore incorporated in the bilayer. Although the probe anisotropy is

probe selective, if sterol tilt has a significant influence on then the ring-opening process, transient

data for loadings between 10-30mol-% would most likely be indistinguishable. However, at

higher temperatures above the melting point for these loadings, there is a significant effect on the

anisotropy of the fluorescent probe and the ordering of the lipid bilayer, therefore we may expect

the heterogeneity of the lipid environment to influence the transient measurements.

Lipid domain formation has been shown to be different for the major sterols studied in our work. At a 20mol-% sterol loading in DPPC, domain formation is reported to be more favorable for ergo than DHC or cholesterol. However, at a 40mol-% loading, cholesterol forms domains more readily than DHC or ergo. The domain formation for DHC in EggPC is completely different. The solubility of a detergent, Titon X-100, is larger in EggPC than DPPC, suggesting that the EggPC membrane is more fluid than the DPPC membrane[33]. Computational MD simulations show results that contrast with the experimental work. MD simulations reported by Y. Liu *et al.*[32] predict that DHC and cholesterol do not individually effect domain formation differently for a particular loading. The results for 33mol-% DHC compared to 33mol-% cholesterol in DMPC lipids show a similar increase in membrane order compared to loadings of 11mol-% DHC and 11mol-% cholesterol. However, in experimental measurements DHC and cholesterol do not behave the same for a particular loading[39]. The inconsistency points to an incomplete understanding of the heterogeneity of lipid bilayers.

Differential scanning calorimetry has been used to determine phase transition temperatures as a function of sterol content. Benes *et al.*[40] studied the thermotropic phase transition of DHC and cholesterol in perdeuterated DPPC for loadings within the range of 0-50mol-%. The results above a sterol loading of 25mol-% show that cholesterol causes the phase transition to be broader and occur at a slightly lower temperature than the phase transition observed for liposomes that contain DHC. These reports are consistent with calorimetry studies on cholesterol and ergo in DPPC reported by Mannock *et al.*[41]. The broadness and melting temperature of the main transition peak with increasing sterol content is proposed to be a function of the sterol-rich and sterol-poor regions in the lipid membrane. Measurements in DPPC suggest that below the melting point, 30-50mol-% cholesterol favors sterol-rich regions since the

broadness of the transition peak increases with increasing sterol content. In contrast to this, loadings of DHC and ergo above 15mol-% are proposed to destabilize the sterol-rich regions more readily than cholesterol [40,41]. In DMPC, 30mol-% cholesterol puts the lipid membrane into the liquid-ordered phase, where sterol-rich regions exist[42]. For our time resolved measurements, we tested loadings between 15-30mol-% DHC and DHC mixed with cholesterol to test if the properties of the bilayer changed enough to show an influence the photochemistry of DHC.

An even bigger effect may be observed when DHC is incorporated into different lipids. Figure 1.1 shows DHC and ergo in each tail length that was studied in this work. The melting point of each of the lipids is indicative of the degree of fluidity. At room temperature the ridgidity of each lipid (in increasing order) is DLPC < DMPC < DPPC < DSPC[35,43], therefore it is hypothesized that the ring-opening and conformational relaxation will be the fastest in DLPC and the slowest in the DSPC membrane. With some caveats, this trend is observed in our measurements (See Chapters 4 and 6).
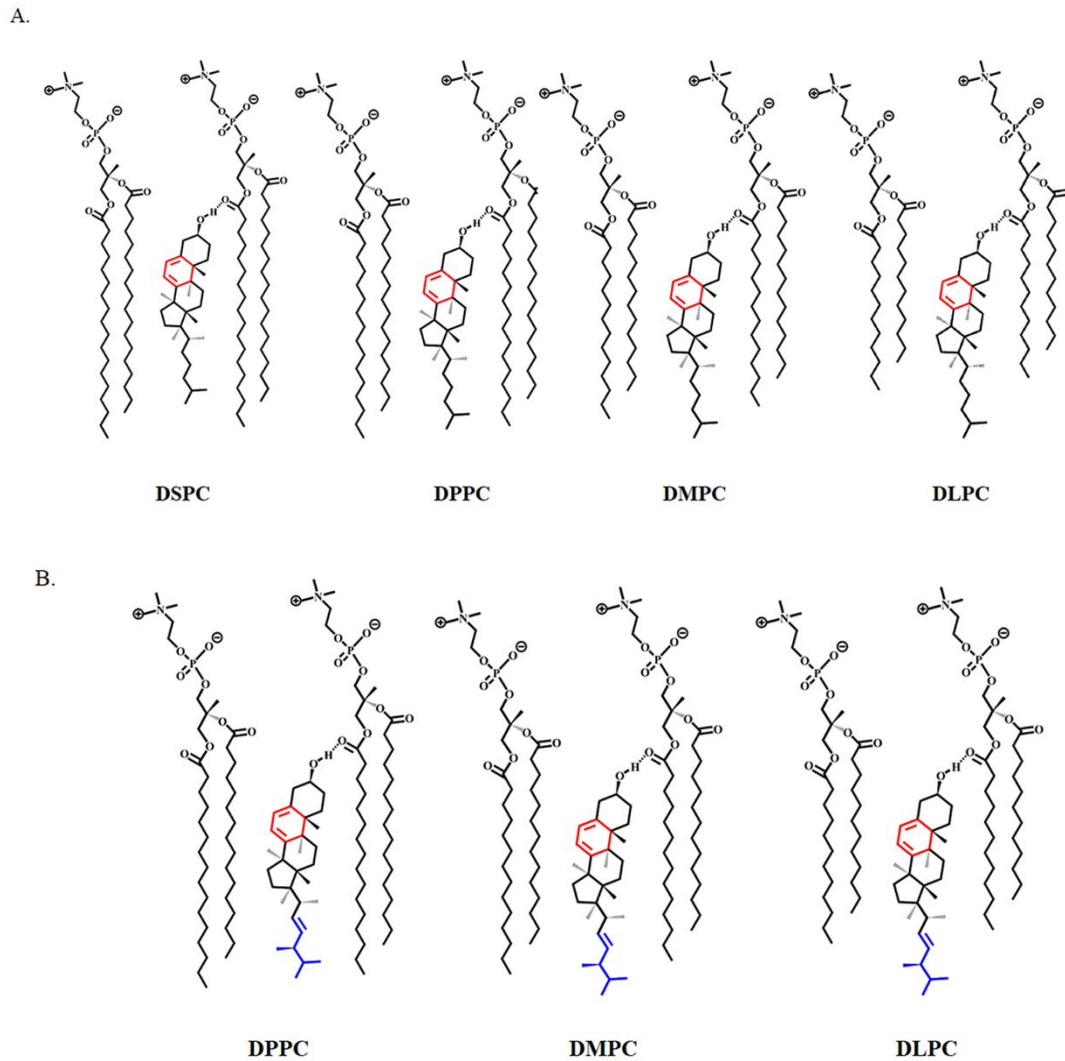
Figure 1.11: (A) DHC in DSPC, DPPC, DMPC and DLPC. (B) ergo in DPPC, DMPC and DLPC lipid bilayers.

Lipid mixtures have been used to model the SOL syndrome[39]. While this may provide structural information for a particular sterol or promote domain formation, this method introduces even more complexity into dynamical processes of the sterol. To simplify our experiments, lipid mixtures were not studied.

Time Resolved Photochemistry of DHC in Lipid Bilayers

While there are many reports on the effect of sterols on the lipid bilayer, there is not any work to date that investigates the transient dynamics of photochemically active sterols in the lipid bilayer. In our work here we use UV-Visible transient absorption measurements to probe the dynamics of the ring-opening and conformational relaxation dynamics in liposomes. The model proposed by Tian and Holick[24] provides the framework for analyzing the physical influences of the bilayer on the time constants we obtain for the ring-opening reactions of the three provitamins in the excited state as well as conformer dynamics on the ground state. DPPC is the primary lipid used in all experiments, which allows us to compare with Tian and Holick's proposed model and results in DPPC liposomes.

Outline of Dissertation

To probe provitamin D photochemistry, broadband UV-Visible transient absorption is utilized to capture excited state dynamics (Chapter 3, 4) and conformer relaxation (Chapter 5, 6).

Chapter 2 presents the experimental methods used for these studies. This includes details of the laser system used to generate femtosecond laser pulses to capture the photochemical reactions of provitamins in solution and liposomes, sample preparation of incorporating loading sterol into lipid bilayers, and characterization instruments used to determine liposome size and accumulation of photoproducts.

Chapters 3 describes the current and prior work using the visible excited state absorption (ESA) of DHC in solution to probe the excited state ring-opening reaction and presents new studies on ergo and DHC-acetate. The ESA is characterized as a S_1 (first excited state) to S_n (higher excited state) transition (Figure 1.2). The ring-opening is studied in 2-butanol and

hexadecane to provide a baseline for hydrogen bonding, carbon structure and packing effects that the molecules may experience in the lipid environment.

Chapter 4 presents the excited state ring-opening of DHC and analogs as a function of lipid parameters. These parameters include, heterogeneity between the solid-ordered and liquid-ordered regions, lipid tail length, hydrogen bonding, van der Waals interactions and membrane curvature. The analogs, ergo and DHC-acetate are used to interpret results of DHC in lipid bilayers to determine if van der Waals interactions or hydrogen bonding influence the excited state dynamics.

Chapter 5 examines the conformer relaxation of the three previtamin D species in 2-butanol and hexadecane. These dynamics are probed in the UV spectral region.

Chapter 6 uses the baseline measurements in solution (Chapter 5) to explore conformer relaxation in the liposome environment.

Chapter 7 summarizes the work described in this dissertation and presents future work that can help further understand the complex photochemistry of provitamin D in skin membrane models. These ideas may also be able to address issues related to SLOS.

References

(1)   Meinhardt-Wollweber, M.; Krebs, R. A Computational Model for Previtamin D(3) Production in Skin. *Photochem. Photobiol. Sci.* **2012**, *11* (4), 731–737.

(2)   Dmitrenko, O.; Orlova, T.; Terenetskaya, I. Medium Controlled Photochemistry of Provitamin D: From Solutions to Liquid Crystals. *J. Mol. Liq.* **2018**, *267*, 428–435.

(3)   Kostas, A. Generation of Previtamin D3 from Tachysterol3 : A Novel Approach for Producing Vitamin D3 in the Winter. *Bost. Univ. thesis* **2015**.

(4)   Cisneros, C.; Thompson, T.; Baluyot, N.; Smith, A. C.; Tapavicza, E. The Role of Tachysterol in Vitamin D Photosynthesis-a Non-Adiabatic Molecular Dynamics Study. *Physical Chemistry Chemical Physics*. 2017, pp 5763–5777.

(5)   Bayda, M.; Redwood, C. E.; Gupta, S.; Dmitrenko, O.; Saltiel, J. Lumisterol to Tachysterol Photoisomerization in EPA Glass at 77 K. A Comparative Study. *J. Phys. Chem. A* **2017**, *121* (12), 2331–2342.

(6)   Arruda, B. C., Peng, J., Smith, B. Spears, K. G., Sension, R. J. Photochemical Ring-Opening and Ground State Relaxation in α-Terpinene with Comparison to Provitamin D 3 Photochemical Ring-Opening and Ground State Relaxation in α-Terpinene with Comparison to Provitamin D 3 Brenden C . Arruda , Jian Peng , Broc Smith , K. *J. Phys. Chem.* **2012**.

(7)   Anderson, N. A.; Shiang, J. J.; Sension, R. J. Subpicosecond Ring Opening of 7-Dehydrocholesterol Studied by Ultrafast Spectroscopy. *J. Phys. Chem. A* **1999**, *103* (50), 10730–10736.

(8)   Anderson, N. A.; Sension, R. J. Solvent Dependence of Excited State Lifetimes in 7-Dehydrocholesterol and Simple Polyenes. *ACS Symp. Ser.* **2002**, *820*, 148–158.

(9)   Fuss, W.; Ho, T.; Hering, P.; Kompa, K. L.; Lochbrunner, S. Ring Opening in the Dehydrocholesterol - Previtamin D System Studied by Ultrafast Spectroscopy. **1996**, 921–927.

(10)   Smith, B. D.; Spears, K. G.; Sension, R. J. Probing the Biexponential Dynamics of Ring-Opening in 7-Dehydrocholesterol. *J. Phys. Chem. A* **2016**, *120* (33), 6575–6581.

(11)   Tang, K.-C.; Sension, R. J. The Influence of the Optical Pulse Shape on Excited State Dynamics in Provitamin D3. *Faraday Discuss.* **2011**, *153*, 117.

(12)   Tang, K. C.; Rury, A.; Orozco, M. B.; Egendorf, J.; Spears, K. G.; Sension, R. J. Ultrafast Electrocyclic Ring Opening of 7-Dehydrocholesterol in Solution: The Influence of Solvent on Excited State Dynamics. *J. Chem. Phys.* **2011**, *134* (10).

(13)   Garavelli, M.; Page, C. S.; Celani, P.; Olivucci, M.; Schmid, W. E.; Trushin, S. A.; Fuss, W. Reaction Path of a Sub-200 Fs Photochemical Electrocyclic Reaction. *J. Phys. Chem. A* **2001**, *105* (18), 4458–4469.

(14) Pemberton, C. C.; Zhang, Y.; Saita, K.; Kirrander, A.; Weber, P. M. From the (1B)

      Spectroscopic State to the Photochemical Product of the Ultrafast Ring-Opening of 1,3-

      Cyclohexadiene: A Spectral Observation of the Complete Reaction Path. *J. Phys. Chem. A*

      2015, *119* (33), 8832–8845.

(15) Lochbrunner, S.; Fuss, W.; Schmid, W. E.; Kompa, K. L. Electronic Relaxation and

      Ground-State Dynamics of 1,3-Cyclohexadiene and Cis-Hexatriene in Ethanol. *J. Phys.*

      Chem. A **1998**, *102* (47), 9334–9344.

(16) Kosma, K.; Trushin, S. a; Fuss, W.; Schmid, W. E. Cyclohexadiene Ring Opening

      Observed with 13 Fs Resolution: Coherent Oscillations Confirm the Reaction Path. *Phys.*

      Chem. Chem. Phys. **2009**, *11* (1), 172–181.

(17) Kuthirummal, N.; Rudakov, F. M.; Evans, C. L.; Weber, P. M. Spectroscopy and

      Femtosecond Dynamics of the Ring Opening Reaction of 1,3-Cyclohexadiene. *J. Chem.*

      Phys. **2006**, *125* (13). h

(18) Wolf, T. J. A.; Sanchez, D. M.; Yang, J.; Parrish, R. M.; Nunes, J. P. F.; Centurion, M.;

      Coffee, R.; Cryan, J. P.; Gühr, M.; Hegazy, K.; et al. Electron Diffraction. **2019**, *11*

      (June).

(19) Cardoza, J. D.; Dudek, R. C.; Mawhorter, R. J.; Weber, P. M. Centering of Ultrafast

      Time-Resolved Pump-Probe Electron Diffraction Patterns. *Chem. Phys.* **2004**, *299* (2–3),

      307–312.

(20) Ruan, C. Y.; Lobastov, V. A.; Srinivasan, R.; Goodson, B. M.; Ihee, H.; Zewail, A. H.

      Ultrafast Diffraction and Structural Dynamics: The Nature of Complex Molecules Far

      from Equilibrium. *Proc. Natl. Acad. Sci. U. S. A.* **2001**, *98* (13), 7117–7122.

(21)   Attar, A. R.; Bhattacherjee, A.; Pemmaraju, C. D.; Schnorr, K.; Closser, K. D.; Prendergast, D.; Leone, S. R. Femtosecond X-Ray Spectroscopy of an Electrocyclic Ring-Opening Reaction. *Science (80-.).* **2017**, *356* (6333), 54–59.

(22)   Arruda, B. C.; Sension, R. J. Ultrafast Polyene Dynamics: The Ring Opening of 1,3-Cyclohexadiene Derivatives. *Phys. Chem. Chem. Phys.* **2014**, *16*, 4439–4455.

(23)   Harris, D. A.; Sension, R. J. Solvent Dependent Conformational Relaxation of Cis-1,3,5-Hexatriene. *Femtochemistry VII* **2006**, 189–192.

(24)   Tian, X. Q.; Holick, M. F. A Liposomal Model That Mimics the Cutaneous Production of Vitamin D3: Studies of the Mechanism of the Membrane-Enhanced Thermal Isomerization of Previtamin D3 to Vitamin D3. *J. Biol. Chem.* **1999**, *274* (7), 4174–4179.

(25)   Wertz, P. W. Epidermal Lipids. *Semin.Dermatol.* **1992**, *11* (0278-145X (Print)), 106–113.

(26)   Gray, G. M.; Yardley, H. J. Lipid Compositions of Cells Isolated from Pig, Human, and Rat Epidermis. *J. Lipid Res.* **1975**, *16* (6), 434–440.

(27)   Keller, R. K.; Arnold, T. P.; Fliesler, S. J. Formation of 7-Dehydrocholesterol-Containing Membrane Rafts in Vitro and in Vivo, with Relevance to the Smith-Lemli-Opitz Syndrome. *J. Lipid Res.* **2004**, *45* (2), 347–355.

(28)   Favus, J. Vitamin D. *Society* **1999**, *60637*, 250–287.

(29)   Briuglia, M. L.; Rotella, C.; McFarlane, A.; Lamprou, D. A. Influence of Cholesterol on Liposome Stability and on in Vitro Drug Release. *Drug Deliv. Transl. Res.* **2015**, *5* (3), 231–242.

(30)   Tapavicza, E.; Meyer, A. M.; Furche, F. Unravelling the Details of Vitamin D
        Photosynthesis by Non-Adiabatic Molecular Dynamics Simulations. *Phys. Chem. Chem.*
        Phys. Phys. Chem. Chem. Phys **2011**, *13* (13), 20986–20998.

(31)   Kim, J.; Tao, H.; White, J. L.; Petrovic, V. S.; Martinez, T. J.; Bucksbaum, P. H. Control
        of 1,3-Cyclohexadiene Photoisomerization Using Light-Induced Conical Intersections. *J.*
        Phys. Chem. A **2012**, *116* (11), 2758–2763.

(32)   Liu, Y.; Chipot, C.; Shao, X.; Cai, W. The Effects of 7-Dehydrocholesterol on the
        Structural Properties of Membranes. *Phys. Biol.* **2011**, *8* (5), 056005.

(33)   Chen, C.; Tripp, C. P. A Comparison of the Behavior of Cholesterol, 7-
        Dehydrocholesterol and Ergosterol in Phospholipid Membranes. *Biochim. Biophys. Acta -*
        Biomembr. **2012**, *1818* (7), 1673–1681.

(34)   Bernsdorff, C.; Winter, R. Differential Properties of the Sterols Cholesterol, Ergosterol,
        Beta-Sitosterol, Trans-7-Dehydrocholesterol, Stigmasterol and Lanosterol on DPPC
        Bilayer Order. *J. Phys. Chem. B* **2003**, *107* (38), 10658–10664.

(35)   Guo, Y.; Pogodin, S.; Baulin, V. A. General Model of Phospholipid Bilayers in Fluid
        Phase within the Single Chain Mean Field Theory. *J. Chem. Phys.* **2014**, *140* (17).

(36)   Róg, T.; Pasenkiewicz-Gierula, M.; Vattulainen, I.; Karttunen, M. Ordering Effects of
        Cholesterol and Its Analogues. *Biochimica et Biophysica Acta - Biomembranes*. 2009.

(37)   Kasian, N. A.; Vashchenko, O. V.; Gluhova, Y. E.; Lisetski, L. N. Effect of the Vitamin D
        Photosynthesis Products on Thermodynamic Parameters of Model Lipid Membranes.
        Biopolym. Cell **2012**, *28* (2), 114–120.

(38)   Yamamoto, J.; Borch, R. Photoconversion of 7-Dehydrocholesterol to Vitamin D3 in Synthetic Phospholipid Bilayers. *Biochemistry* **1985**, *24* (13), 3338–3344.

(39)   Staneva, G.; Chachaty, C.; Wolf, C.; Quinn, P. J. Comparison of the Liquid-Ordered Bilayer Phases Containing Cholesterol or 7-Dehydrocholesterol in Modeling Smith-Lemli-Opitz Syndrome. *J. Lipid Res.* **2010**, *51* (7), 1810–1822.

(40)   Benesch, M. G. K.; Lewis, R. N. A. H.; McElhaney, R. N. A Calorimetric and Spectroscopic Comparison of the Effects of Cholesterol and Its Immediate Biosynthetic Precursors 7-Dehydrocholesterol and Desmosterol on the Thermotropic Phase Behavior and Organization of Dipalmitoylphosphatidylcholine Bilayer Membrane. *Chem. Phys. Lipids* **2015**, *191*, 123–135.

(41)   Benesch, M. G. K.; Mannock, D. A.; Lewis, R. N. A. H.; McElhaney, R. N. A Calorimetric and Spectroscopic Comparison of the Effects of Ergosterol and Cholesterol on the Thermotropic Phase Behavior and Organization of Dipalmitoylphosphatidylcholine Bilayer Membranes. *Biochemistry* **2009**, *50* (46), 9982–9997.

(42)   De Meyer, F. J. M.; Benjamini, A.; Rodgers, J. M.; Misteli, Y.; Smit, B. Molecular Simulation of the DMPC-Cholesterol Phase Diagram. *J. Phys. Chem. B* **2010**, *114* (32), 10451–10461.

(43)   Bui, T. T.; Suga, K.; Kuhl, T. L.; Umakoshi, H. Melting-Temperature-Dependent Interactions of Ergosterol with Unsaturated and Saturated Lipids in Model Membranes. *Langmuir* **2019**, *35*, 10640–10647.

Chapter 2

Experimental Methods for Transient Absorption and Steady State Measurements

Introduction to Experimental Background

All of the experiments presented in this dissertation require the use of ultrashort pulses for time resolved studies of the excited electronic state dynamics and ground state conformer dynamics. The primary technique used is ultrafast broadband transient absorption (TA) spectroscopy in the UV-Visible region. This technique utilizes a two pulse sequence where one pulse (the pump) optically excites a percentage of molecules in the sample and a second pulse (the probe) is time delayed and spatially overlapped with the pump in the excited sample volume, capturing changes in the chromophore.

Laser Instrumentation

Femtosecond pump-probe transient absorption measurements were performed by using two kHz Ti-Sapphire laser systems.

Sension lab laser system and experimental parameters: The first system is a lab-built system. A KM labs Ti-Sapphire oscillator produces an 88 MHz pulse train with a bandwidth of ~30 nm centered at ~800-815 nm. The pulse train is sent to a grating stretcher that adds a wavelength dependent path length to stretch the pulses temporally.

A Quantum Technologies pulse picker is used to reduce the pulse train to 1 kHz. The selected pulse is sent into a multipass amplifier and overlapped spatially and temporally with a Quantronix DARWIN YAG: YLF pulse centered at 527 nm to generate ~800 mW- 1 W of power. The pulses are then compressed by using a grating compressor to have a duration of ~60 fs. A beam splitter is used to generate the pump and probe pulses. The pump pulses at 272 nm are generated by frequency tripling the 800-810 nm fundamental by using two β-barium borate (BBO) crystals. The visible probe range from 350-800 nm is created by using a 100 mm focusing lens to focus the fundamental wavelength (800-810 nm) onto a translating Calcium Fluoride (CaF_2) crystal. A KG3 filter is placed after the generation of the continuum to remove residual 800 nm light. In the case of the UV continuum (250-600 nm) the continuum is created by focusing the second harmonic (400-405 nm) into the CaF_2 crystal, a 1 cm path length of nickel sulfate is placed after the generation of the continuum to absorb residual 405 nm. The probe is then focused with a concave, f = 500 mm mirror onto the sample and overlapped spatially and temporally with the pump pulse in a 0.5mm quartz flow cell that is connected to a sample reservoir via Viton tubing. The sample is continuously pumped with a Cole-Parmer peristaltic pump throughout the experiment to prevent the build-up of photoproduct in the sampled volume. The pump and probe spot size are typically kept at ~160 μm and ~80 μm, respectively. Experiments required 6-8 TA scans; each time point averaged 297 difference spectra that were collected and analyzed in custom written LABVIEW software.

For excited state measurements in solution and lipid bilayer environments, molecules were pumped at 272 nm and probed with a visible continuum ranging from 350-800 nm. This allows us to capture the initial excited state of the provitamin D species characterized by a visible absorption band peaking at 480 nm. These results are presented in Chapters 3 and 4.

The conformer relaxation of the previtamin D photoproducts were probed using a broadband continuum spanning the range from 250-600 nm. A short pass filter was used to remove visible contributions to scale visible to UV intensities appropriately. These results are presented in Chapters 5 and 6. All measurements for visible and UV studies were carried out with a pump energy of ~250-350 nJ, and probe energy of ~1 μJ, with relative polarizations of the pump and probe at magic angle (54.7°) at the sample to eliminate orientational effects.

LUMOS facility laser system and experimental parameters: The second laser system used was in the LUMOS facility at the University of Michigan. Time resolved conformer relaxation along with some ring-opening measurements of the provitamins in lipid bilayers were acquired by exciting a thin sheet (~300 μm) of sample formed by a wire guided flow apparatus at 265 nm. For liposome experiments, a wire guided flow reduced the amount of pump scatter into the spectrometer and allowed us to remove coherent artifacts in the visible region of the spectrum. The sample was continuously circulated with a Cole-Parmer peristaltic pump throughout the experiment. The pump and probe spot size were typically kept at ~100 μm and ~90 μm, respectively. Experiments required 4-6 TA scans; each averaged 1500 difference spectra at each time point that were collected and analyzed in custom written LABVIEW software.

Transient absorption: The observable quantity is the difference in absorption, ΔA. This quantity allows us to quantify excited state and conformational behavior of the provitamins in solution and in the lipid bilayer.

$$\Delta A(\lambda, t) = -\log\left(\frac{<I_{pump-on}>}{<I_{pump-off}>}\right) \tag{2.1}$$

Where I is the Intensity for the pump on/ off. The absorbance, A, is dependent on the concentration (c) of the sample, the extinction coefficient (ε) and path length (l) of the sample. This relationship is described by the beer lambert law,

$$A(\lambda, t) = \varepsilon c l \qquad (2.2)$$

For these experiments the absorption is ~0.3-0.5 OD in a 1 mm path length. The difference signal was obtained by using a synchronized Thorlabs M1000 optical chopper operating at 500 Hz to block and allow every other pump pulse. In TA measurements, the signal strength, ΔA, depends on the absorbance of the sample, the fraction of sample excited, and the time delay. Spectra at various time delays between the pump and probe were achieved by using a NEWPORT ESP 300 mechanical delay stage that was controlled through LABVIEW.

The probes in both laser systems are "chirped" such that the blue wavelengths arrive at an earlier time than the redder ones. In order to set all wavelengths at the same time delay, where the pump and probe initially overlap (time zero), the chirp is removed from each individual scan by fitting and subtracting out a third order polynomial using LABVIEW[1]. To obtain lifetimes, τ_i, in the respected probe regions, the average "chirp corrected" file is fit by a custom python code that uses a Levenberg-Marquardt least squares algorithm to globally fit the data[2]. In the model, the data is fit to a sum of decaying exponentials, with rate constants, k_i, and amplitudes, δ_i (λ,t), and a non-decaying exponential (i.e k = 0) to account for solvent effects.

$$\sum_1^\infty \delta_i(\lambda, t)e^{-k_i t} = \delta_1(\lambda, t)e^{-k_1 t} + \delta_2(\lambda, t)e^{-k_2 t} + \delta_3(\lambda, t)e^{-k_3 t} + \cdots$$

$$\tau_i = \frac{1}{k_i} \qquad (2.3)$$

The associated amplitudes, $\delta_i(\lambda, t)$ across a range of wavelengths are known as the decay associated difference spectra (DADS). The DADS are used in Chapters 3, 4, 5 and 6 to identify the species and/or processes behind the lifetimes obtained.

Sample Preparation / Characterization

For all experiments the sterols used, 7- dehydrocholersterol (98%), 7-dehydrocholesterol-acetate (98%), and ergosterol (98%) (See Figure 1.6) were obtained from Santa Cruz biotechnology, Steraloids, Inc. and Sigma Aldrich, respectively. The lipids, 1,2- distearoyl-sn-glycero-3-phosphocholine (DSPC), 1,2-dipalmitoyl-sn-glycero-3-phosphatidylcholine (DPPC), 1,2-dimyristoyl-sn-glycero-3-phophocholine (DMPC) and 1,2 dilauroyl-sn-glycero-3-phosphocholine (DLPC), were purchased dissolved in chloroform from Avanti Polar Lipids Inc. All sterols and lipids were used without further purification.

Sample preparation of liposomes: Samples of the provitamins in lipids were prepared to have a final concentration of ~2 mM. All experiments were calibrated for an optical density ~0.3-0.7 OD at the excitation wavelength. For liposome experiments, samples were prepared by mixing desired amounts of dried sterol/ chloroform (purchased from Sigma Aldrich) with the appropriate amount of lipid. A thin-film of sterol-lipid was formed by evaporating the solvent by using a rotary evaporator for ~2 hours. Following the formation of the thin-film, 20 mL of deionized water obtained from using a Millipore Synergy Purification System was added for hydration and was continuously stirred for ~30 minutes above the transition temperature of the respective lipid: DSPC (55 °C), DPPC (41 °C), DMPC (24 °C), and DLPC (-2 °C) [3,4]. The vesicles were then homogenized using an Avestin Liposofast LF-50 Extruder that was held above the transition temperature of the lipid. The vesicles were passed twice through a 400 nm pore membrane and twice through a 100 nm pore membrane (obtained from Sigma Aldrich). For

curvature studies, larger and smaller vesicles were obtained by passing the sample twice through a 200 nm membranes or an extra four times through a 50 nm membrane, respectively (both pore sizes were purchased from Avestin).

Alternative methods: Extrusion is not the only way to reduce the size of liposomes, other methods include freeze thaw[4,5] and sonication[6,7]. In the freeze thaw method, the round bottom flask that contains the aqueous solution is passed multiple times between a liquid nitrogen bath and a warm water bath, held above the phase transition of the lipid-sterol mixture. The sample is hand stirred in a circular motion in both the liquid nitrogen and warm water bath to evenly distribute heat around the solvent. The process is repeated until the desired particle size is reached. Sonication uses a sound probe to generate high frequencies to break up the multilamellar vesicles into smaller ones. Table 2.1 outlines the general advantages and disadvantages of each method.

Table 2.1: Advantages and disadvantages of the different methods that can be used to downsize lipid particle size.

Method	Advantage	Disadvantage
Extrusion	• Wide range of membrane pore sizes available to get desired liposome size, multiple passes leads to more homogeneous sample	• Size characterizations done here are in agreement with literature showing that the resulting liposomes may have some variation from the membrane pore size
Sonication	• Widely more available than extruders and does not require cryogenic gases	• Heat generated from high energy can rupture, oxidize lipids, can degrade entrapped solute molecules • Inhomogeneous distribution of particle size • Do not easily control size
Freeze Thaw	• Improves encapsulation efficiency for water soluble drugs	• Do not have control of size and distribution of particles

Sample Characterization

Liposome size characterization: Liposome size was characterized with the use of a (Beckman Coulter) Delsa Nano C Particle Analyzer. The technique used for particle characterization is Dynamic Light Scattering (DLS) in which a laser beam interacts with a sample of particles to determine the average size and spread of the distribution. Here the translational diffusion coefficient, D_t is determined by approximating the particles as a sphere undergoing Brownian motion. Intensity fluctuations are collected by time delaying the incident

electric field and information about the diffusion rate of the particles is obtained by fitting to the second order autocorrelation function,

$$g^2(q;\tau) = \frac{<I(t)I(t+\tau)>}{<I(t)>^2} \qquad (2.4)$$

where I is the intensity, τ is the time delay and q is the wavevector. The first order correlation function is given by,

$$(q;\tau) = 1 + \beta[g^1(q;\tau)]^2 \qquad (2.5)$$

where β is a correction factor for laser alignment. The simplest approach is to consider a monodisperse sample such that only the first order correlation function is a decaying exponential in time delay with decay parameter, Γ. The decay parameter is given by[8]

$$\Gamma = \frac{4\pi\eta_0}{\lambda}\sin(\frac{\theta}{2})\,D_t = q^2 D_t \qquad (2.6)$$

where η_0 is the refractive index of the sample and θ is the angle at which the detector is located with respect to the sample cell and λ is the incident laser wavelength. From equation 2.6 the translational diffusion coefficient can be extracted and related to the Stokes Einstein equation to give the hydrodynamic diameter of the particles:

$$D(H) = \frac{kT}{3\pi\eta D_t} \qquad (2.7)$$

where k is Boltzmann's constant, T is absolute temperature and η is viscosity. In the sample preparation, pore membrane filters of 50 and 100 nm resulted in liposome sizes that were slightly larger than the pore size. In contrast, the larger pore size of 200 nm resulted in liposome sizes that were slightly smaller than the pore size[4,9]. The measured average liposome size and

distribution of liposomes are summarized in Table 2.2-2.6. For DLPC, liposome size was only measured for DHC and ergosterol. DHC-acetate was not able to be incorporated into the bilayer since the acetate group makes the molecule less lipophlic. All error bars in this dissertation are reported as the standard deviation.

Table 2.2 Size and polydispersity of a 30mol-% loading of DHC in DSPC liposomes before and after TA experiments.

Provitamin in DSPC	Average Size (Before TA) (nm)	Polydispersity (Before TA) (nm)	Average Size (After TA) (nm)	Polydispersity (After TA) (nm)
DHC	170.17 ± 2.18	0.11 ± 0.02	Not Measured	Not Measured

Table 2.3: Size and polydispersity of various loadings of sterol in DPPC liposomes before and after TA experiments.

Sterol in DPPC lipid bilayers	Average Size (Before TA) (nm)	Polydispersity (Before TA) (nm)	Average Size (After TA) (nm)	Polydispersity (After TA) (nm)
30mol-% DHC	149.29 ± 6.04	0.08 ± 0.02	145.28 ± 7.12	0.08 ± 0.03
15mol-% DHC	171.8 ± 7.38	0.11 ± 0.03	Not Measured	Not Measured
15/15mol-% DHC/cholesterol	171.92 ± 3.54	0.11 ± 0.02	Not Measured	Not Measured
30mol-% DHC-acetate	151.87 ± 4.67	0.06 ± 0.02	151.10 ± 4.52	0.14 ± 0.02
30mol-% ergosterol	160.64 ± 9.80	0.07 ± 0.26	162.21 ± 11.70	0.08 ± 0.02
30mol-% cholesterol	158.69 ± 5.41	0.08 ± 0.03	172.27 ± 3.41	0.18 ± 0.02
15mol-% cholesterol	121.5 ± 0.90	0.02 ± 0.20	Not Measured	Not Measured

Table 2.4: Size and polydispersity of a 30mol-% sterol loading in DMPC liposomes before and after TA experiments.

Provitamin in DMPC	Average Size (Before TA) (nm)	Polydispersity (Before TA) (nm)	Average Size (After TA) (nm)	Polydispersity (After TA) (nm)
DHC	172.37 ± 2.47	0.06 ± 0.03	169.55 ± 5.78	0.09 ± 0.04
ergosterol	200.33 ± 2.16	0.12 ± 0.09	Not Measured	Not Measured

Table 2.5: Size and polydispersity of a 30mol-% sterol loading in DLPC liposomes before and after TA experiments.

Provitamin in DLPC	Average Size (Before TA) (nm)	Polydispersity (Before TA) (nm)	Average Size (After TA) (nm)	Polydispersity (After TA) (nm)
DHC	159.44 ± 10.48	0.10 ± 0.05	162.28 ± 1.20	0.12 ± 0.06
ergosterol	200.33 ± 2.16	0.19 ± 0.14	210.57 ± 1.21	0.24 ± 0.01

Table 2.6: Size and polydispersity of a 30mol-% loading of DHC in DPPC liposomes as function of membrane pore filter size before and after TA measurements.

Membrane Pore Size (nm)	Average Size (Before TA) (nm)	Polydispersity (Before TA) (nm)	Average Size (After TA) (nm)	Polydispersity (After TA) (nm)
50	78.77 ± 3.86	0.12 ± 0.05	77.93 ± 3.36	0.11 ± 0.06
100	149.29 ± 6.04	0.08 ± 0.02	145.28 ± 7.12	0.08 ± 0.03
200	193.80 ± 1.08	0.12 ± 0.02	189.83 ± 4.70	0.12 ± 0.05

Percentage of Molecules Excited

The percentage of molecules excited is an important factor to consider during absorption measurements as small sample volumes and high pump powers can cause the sample to photolyze faster and increase the magnitude of nonlinear contributions from solvents. The presence of nonlinear effects can distort the actual signal. Low sample volume and high pump power increases the risk of taking measurements on multiple product species during the course of the experiment. For measurements taken in this dissertation, the sample concentration, pump energy and volume were all calibrated to excite ~10% or less of the total volume estimated by,

$$Percentage\ excited = \left. photons_{absorbed} \middle/ molecules_{pump-focus} \right. \tag{2.8}$$

where photons $_{absorbed}$ are the number of molecules absorbed per pump pulse and molecules $_{pump-focus}$ are the number of molecules in the pump volume. For liposome characterization, the dynamic light scattering instrument provides insight about the size distribution of the particles, but does not provide any information on how many liposomes are in a given volume of the pump during a TA experiment. The distribution of liposomes in the volume of the beam should be considered as different size particle distributions from shot to shot can distort the overall photochemical properties of the molecule of interest, also to characterize the signal:noise, it is important to understand how many scatters are in present in the beam path. The number of liposomes can be approximated as,

$$N_{total} = \frac{4\pi}{a}\left[\frac{d^2}{2} + \left(\frac{d}{2} - h\right)^2\right] \tag{2.9}$$

where d is the diameter of the liposome, 'a' is the head group area and h is the bilayer thickness. To get the number of liposomes per mL,

$$N_{liposome\ per\ mL} = \frac{M\ x\ 6.02x10^3}{N_{total} * 1000} \tag{2.10}$$

where M is the molar concentration of the lipid. Now in the given volume of the beam, since the exposed volume can be approximated as a cylinder, equation 2.10 yields $\sim 1.3 \times 10^{32}$ liposomes / laser shot. Since the number of particles in the exposed volume is very large, the law of large numbers applies, suggesting that each laser shot contains the same distribution and average size of particles.

TA Scans and Steady State Measurements

Photoproduct accumulation was monitored by measuring the UV-VIS spectrum after each TA scan with use of a Shimadzu UV-2600 spectrometer. Steady state photolysis experiments were done by measuring the UV-VIS spectrum after irradiating the sample with a mercury arc lamp (7 A, 125 V power supply) from Oriel Corporation . The lamp was placed directly in the sample holder of the spectrometer to avoid repositioning the cuvette between scans. Measurements for the three provitamins in liposomes were taken using an optical diffuser to cut down on the intensity of the lamp, solution measurements were taken unfiltered. The spectra for monitoring photoproduct accumulation and obtaining steady state spectra were acquired from 200-800 nm with a step size of 0.1 or 0.2 nm in a 1 mm cuvette.

Scattering Analysis

The ground state spectra of the three provitamins in the lipid bilayer sit on top of a scattering curve that is invisible to signal strength in TA measurements. A Rayleigh scattering approximation can be used to derive an analytic fit to remove the scattering background. The intensity of the scattered light is given by[10],

$$I_0 \left(\frac{1 + \cos^2\Theta}{2R^2} \right) \left(\frac{2\pi}{\lambda} \right)^4 \left(\frac{n^2 - 1}{n^2 + 1} \right)^2 \left(\frac{d}{2} \right)^6 \tag{2.11}$$

where I_0 is the incident light intensity, R is the distance to the particle, Θ is the scattering angle, n is the index of refraction and d is particle size. Averaging overall scattering angles yields the scattering cross section, σ defined as:

$$\left(\frac{2\pi^5}{3} \right) \left(\frac{d^6}{\lambda^4} \right) \left(\frac{n^2 - 1}{n^2 + 1} \right)^2 \tag{2.12}$$

While the Rayleigh approximation is a simple model to analyze monodisperse particle size scattering behavior, it does not account for the size distribution that is present in our liposome samples. Besides the inhomogeneous distribution of particles, other complications that may arise are coupled scattering issues from the high concentration of scatters and different scattering degrees across the spectrum. A better method to remove the scattering contribution is to subtract out a spectrum of cholesterol loaded liposomes with the same loading and taken under the same conditions. For these measurements, the best fit was determined by comparing the baseline from 500-800 nm, where there are not absorption contributions from the provitamins and there is the least amount of scattering. The two different methods of background subtraction are shown in Figure 2.1.
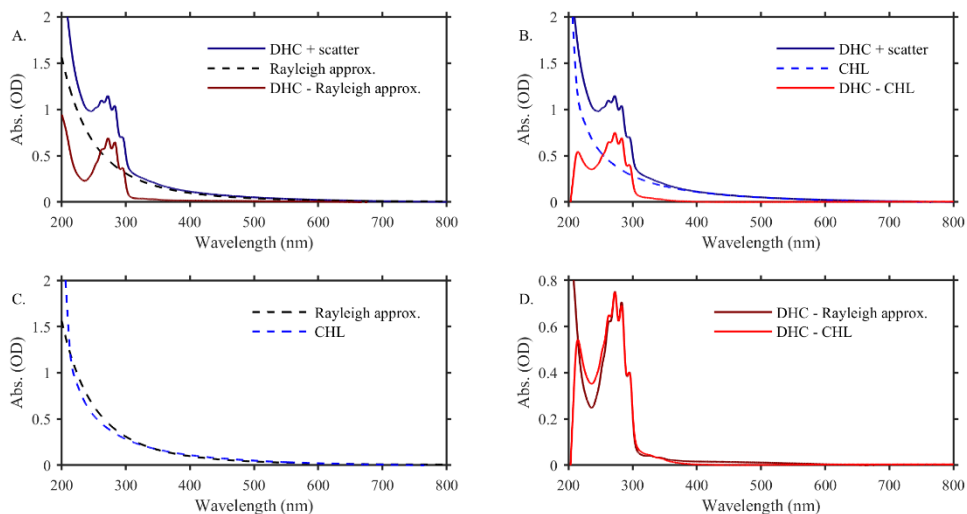
Figure 2.1: UV-VIS spectra of DHC in DPPC liposomes (dark blue) and subtracted scattering background (dark red and red) using (A) Rayleigh approximation (dashed black) and (B) a 30mol-% loading of cholesterol (CHL) in DPPC (dashed blue) for the background removal. (C) A comparison of the different scattering curves and (D) corresponding spectra of DHC with scatter contributions removed, scaled to relative intensities.

In comparison to the Rayleigh approximation, cholesterol backgrounds prepared in DPPC liposomes yield a curve that fits better to the scattering curve. Therefore, the background in steady state measurements, discussed in Chapter 6 is removed by subtracting out cholesterol loaded liposomes. It should also be noted that the absorption spectrum goes to zero at ~305 nm in solution, however a small absorption is still present in the lipid bilayer environment and has yet to be determined if the absorption is real or if an artifact from the scattering fit. The order parameter, x, may show why the Rayleigh approximation does not work as well as cholesterol in our experiments. Figure 2.2 shows the order parameter plotted for an average size of 150 nm particles, with the assumption that most of the scattering is coming from the larger species. The order parameter is defined as $2\pi r/\lambda$, where r is the radius of particle, and λ is the incident wavelength. This parameter sets the criteria for the type of scattering present (i.e Rayleigh for small particles, Mie for large particles).
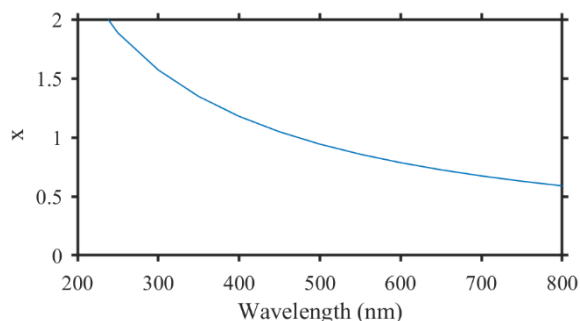
Figure 2.2: Order parameter, x, for 150 nm particles. Rayleigh scattering (450 nm< λ<700 nm) for x<<1, Mie scattering (390 nm<λ<450 nm) for x~1 and Geometric shape scattering (λ<390 nm) for x>>1.

Since the sample is composed of a size distribution of particles, an alternative form of the

Rayleigh approximation that may have to be used in our analysis is derived by replacing d^6 in

equation 2.11 and 2.12 with,[11]

$$\langle d^6 \rangle = 15\langle d \rangle^4 \sigma^2 + 45\langle d \rangle^2 \sigma^4 + 15\sigma^6 \qquad (2.13)$$

Despite the complicated nature of the scattering distribution, the scattering could possibly be

wavelength specific to the provitamin D spectra since all three molecules have vibronic

transitions within 260-290 nm. Therefore, even if a homogeneous distribution was present the

detector may still pick up different degrees of scattering contributions across the spectrum.

Background calibration for steady state measurements: In order to properly remove the

scattering background in steady state measurements, cholesterol loaded liposomes were used as a

calibration since the sterol does not undergo any photochemical changes. The following may

contribute to the scattering background observed in the liposome data:

1. <u>Diffusion</u>: The sample is not monodisperse, therefore it is possible that a different size distribution can be probed from scan to scan.

2. <u>Photochemical changes</u>: The photochemistry of the provitamins may change the morphology of the liposome slightly such that the background is not constant from scan to scan.

3. <u>Heat from the lamp</u>: The lamp heats up to ~50 °C which is ~34 °C greater than the room temperature of the lab. The longer measurements may have a different background due to the liposomes slightly heating.

Diffusion was tested by repeating multiple consecutive scans without exposing the sample to UV radiation. For example, if diffusion played a significant role then the background would be expected to change from scan to scan. Figure 2.3 shows the difference spectra of 3 consecutive scans of 30mol-% cholesterol in DPPC without UV irradiation. The data suggests that the probed volumes for each scan encompasses approximately the same distribution since the scattering contribution subtracts out.
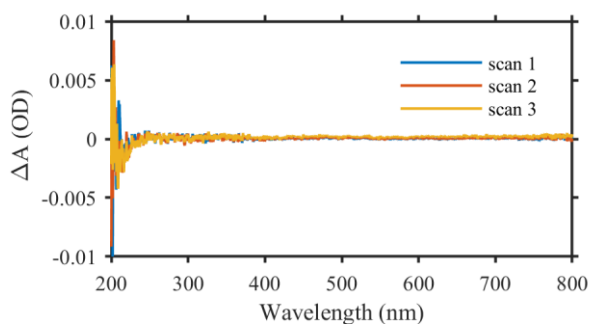
Figure 2.3: Difference spectra of a 30mol-% loading of cholesterol in DPPC taken without irradiation to test reproducibility of each scan.

It is difficult to separate effects on the lipid bilayer from the photochemical changes that occur by irradiating the provitamins or from heating effects on the lipids. To monitor any significant liposome change in the size distribution during the experiment, size analyses were done before

and after for comparison. If the background is significantly dependent on the photochemical

changes or heat from the lamp, then any notable difference would be apparent in size analysis.

Physical motion of the cuvette, in and out of the sample holder may introduce artifacts on

the surface of the cuvette, which may contribute to the scatter. To avoid surface artifacts on the

cuvette from scan to scan, the cuvette remained in the sample holder and the pen lamp was

inserted and removed. This not only minimized surface artifacts on the cuvette but allowed for a

reproducible positioning of the pen lamp from scan to scan. Additionally, an optical diffuser was

used to attenuate the intensity of the pen lamp which slowed down the chemical reaction of the

provitamins to capture the previtamin species before an accumulation of side products occurred

and possibly a change in liposome background. Figure 2.4A and 2.4C show a comparison of the

difference spectra of cholesterol loaded liposomes with attenuated and full intensity,

respectively. Figure 2.4B shows two methods of removing the background contribution to

reconstruct the steady state previtamin D_3 species in liposomes (Chapter 6). The substantial

change of the distribution shown in Figure 2.4C was also picked up by light scattering

measurements, whereas the subtle differences in Figure 2.4A have sizes within the noise

measurements of the original distribution. In both cases, changes in background are evident

around 250 nm that may be a consequence of the mercury lamp's intense line at 253 nm.
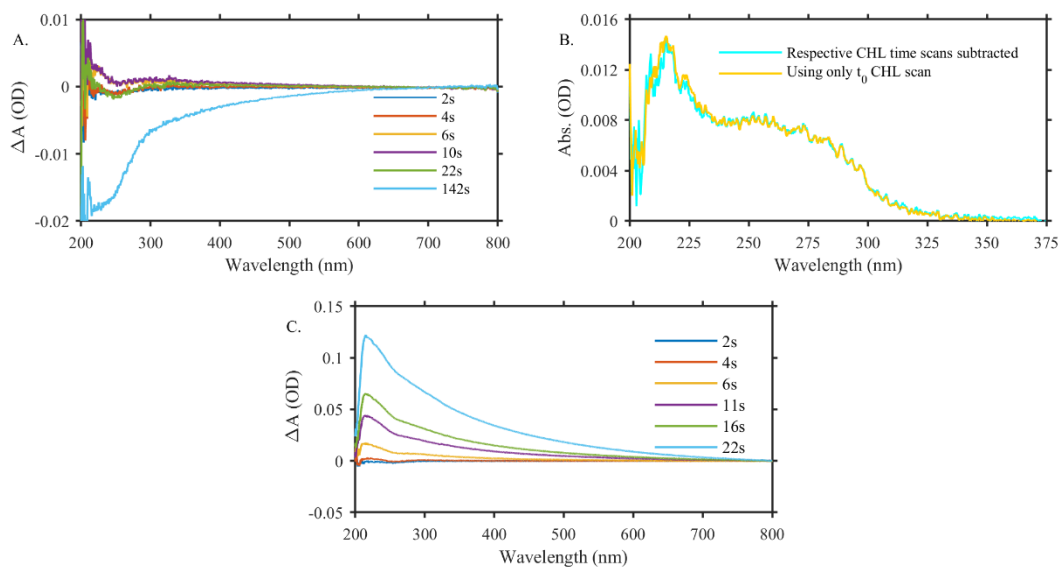
Figure 2.4: Difference spectra of a 30mol-% loading of cholesterol in DPPC taken with (A) attenuated irradiation and used in (B) to reconstruct the previtamin D_3 spectrum by subtracting out respective cholesterol time scans to remove liposome background contributions compared to only using only the t_0 cholesterol scan for removing the background. (C) Full intensity on cholesterol loaded liposomes produces a substantial change in the scattering background.

For steady state measurements of the three provitamins, the molecules are resonant within the wavelengths where the cholesterol scans (Figure 2.4A) change. Figure 2.4B shows a comparison between the shape of the reconstructed previtamin D_3 species by either removing the background at the respective time step or only using the t_0 background. The differences in background are nearly negligible at early times. Therefore, Chapter 6 only uses the t_0 cholesterol scan to reconstruct the previtamin D species. To further minimize background changes of the liposomes and photoproduct accumulation, steady state measurements scans within the first 8s are used to reconstruct the steady state photoproduct.

Solvent Signals

Visible continuum: For all TA measurements, a solvent background was collected immediately after the measurements on provitamin-lipid samples to identify contributions from solvated electron and 2-photon signals from the solvent. The background could arise from either the lipids or the surrounding water solvents. A power study was conducted for a comparison of cholesterol in DPPC vs. water for 620 nJ, 420 nJ and 240 nJ. These measurements confirmed that the background signal was mostly due to the presence of solvated electrons in water[12] and therefore, a water background was used as the solvent background for liposome experiments. Figure 2.5 shows spectra and kinetics for measurements at 240 nJ, all measurements in this dissertation were taken between 240-320 nJ.
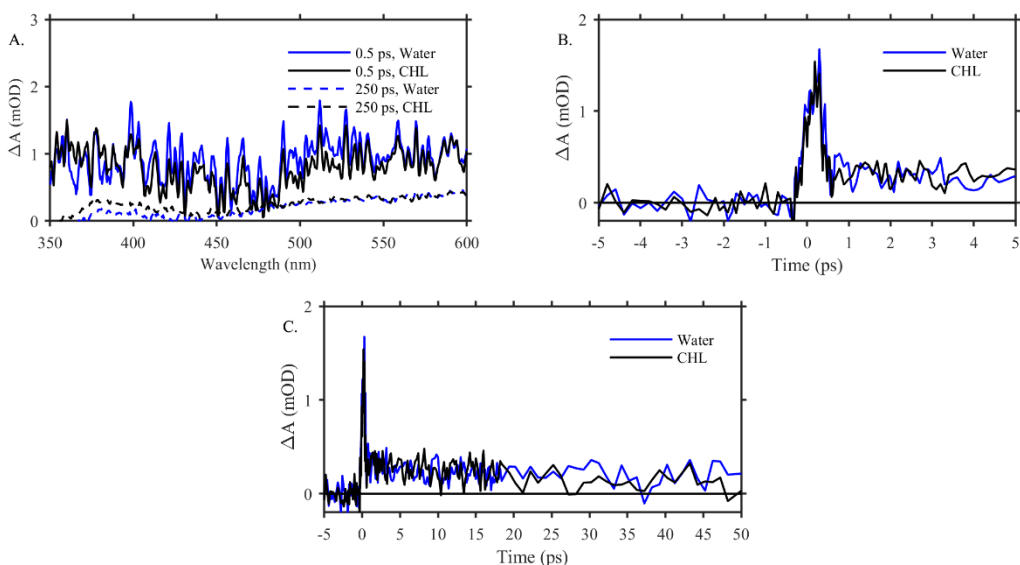
Figure 2.5: Comparison of selected time delays for a 30mol-% loading of cholesterol in DPPC and water (only) solvent. Both solvents excited at 240 nJ. Time delays at (A) 500 fs and (B) 250 ps. Corresponding kinetics at 480 nm in (C) early times and (D) late times.

Solvent background tests were also conducted in LUMOS to identify and minimize contribution from solvent effects due to the shorter pulse duration of the pump. The strength of the solvated electron signal impacts the resolution of early time scale kinetics, which are important in looking

45

at the ESA of the three provitamins (Chapter 4). Figure 2.6 shows solvated electron spectra for

with and without pulse broadening. In order to minimize the solvated electron effects[12] (between

550-700 nm) shown in Figure 2.6B, the pump was sent through 5-11 mm of CaF_2.
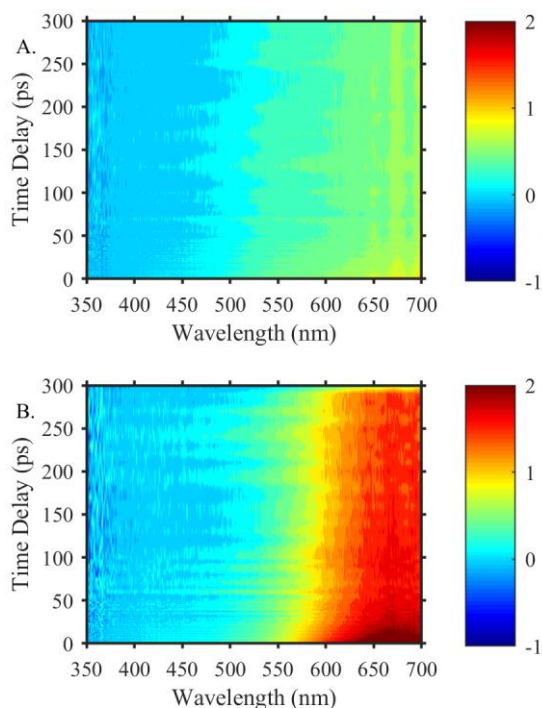
Figure 2.6: Contour plots of solvated electron signal in water (A) with broadened pulse using 5-11 mm of CaF_2 and (B) without pulse broadening. Data taken in LUMOS.

UV continuum: TA data of provitamins in liposomes show that there is a persistent offset

at all positive time delays. To understand where the offset orientates from, pump power studies,

pulse duration studies, and solvent studies were conducted.

Pump power studies were conducted for powers of 150 nJ, 300 nJ and 460 nJ as illustrated in

Figure 2.7.
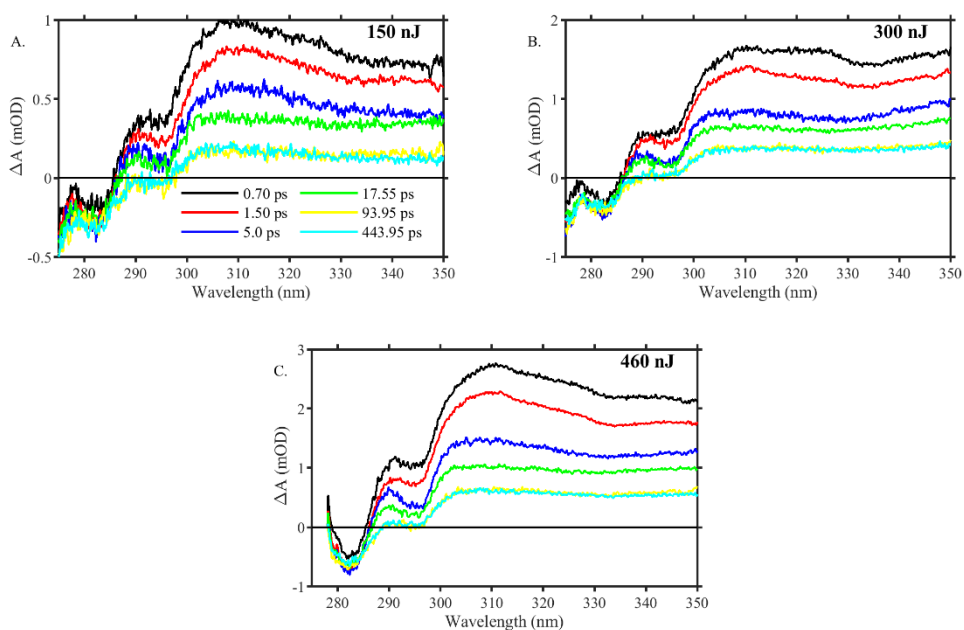
Figure 2.7: Selected time delays following excitation of a 30mol-% loading of DHC in DPPC in the UV region as a function of pump power. Pump powers tested at (A) 150 nJ, (B) 300 nJ and (C) 460 nJ. The legend in plot A is the same for all plots.

The offset appears to be linear with the increasing power, suggesting that there is not a nonlinear signal coming from the molecules or from the background.

Pulse length variations was also used to determine if the observed background signal is from nonlinear signals of the molecules or water. For this experiment the pump duration was elongated from ~50 fs to ~150 fs using 11 mm of CaF_2 and the time delay was taken out an additional 300 ps. Figure 2.8 shows that the residual background becomes nearly a constant offset at around 50 ps and is similar to that observed with shorter pulses.
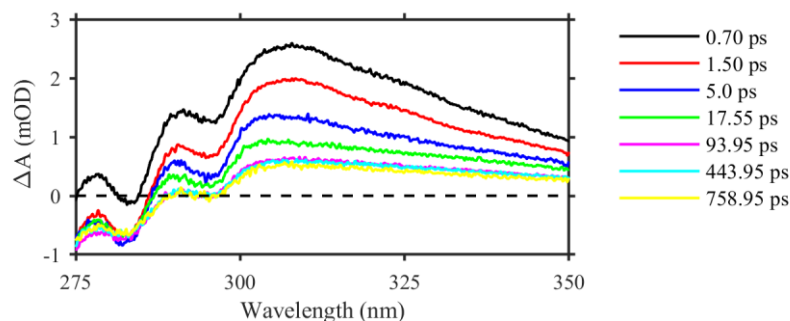
Figure 2.8: Selected time delays following excitation of a 30mol-% loading of DHC in DPPC in the UV region with increased pulse duration.

The solvent background for both cholesterol loaded liposomes and water indicate that the offset does not come from the solvent. The solvent scans shown in Figure 2.9 suggest that cholesterol loaded liposomes and water are comparable and fall short of the actual background in the provitamin spectra at long times. The nonlinearities in the UV make it difficult to reproduce the exact spectra and all spectra exhibit the same baseline < 0.2 mOD in water.
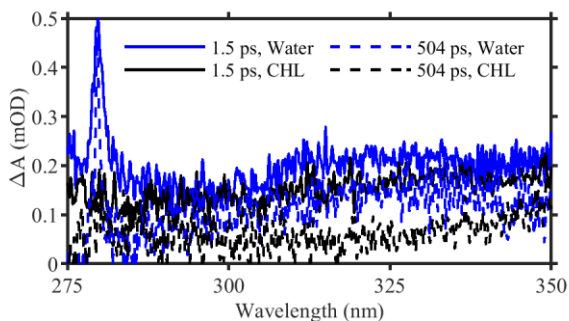
Figure 2.9: Comparison of UV spectra at selected time delays between water (blue) and a 30mol-% loading of cholesterol (CHL) in DPPC (black) pumped at 265 nm, 300 nJ.

Thermal lensing and coherent artifacts: Although the long-lived signal is not from the solvent, it could arise from thermal effects in the sample. The idea of thermal lensing comes from the geometric setup of femtosecond laser systems[13]. The conditions for thermal lensing are as follows:

1. <u>Absorbing species</u>: The absorbing species is resonant with the pump wavelength, where the energy is first absorbed then dumped into the surrounding medium which locally heats the solvent. Equation (2.1) becomes: log(PUMP OFF) –log(PUMP ON) = log(reference + background+ heat dissipated effect)– log(pumped molecules signal+ background + heat absorbed), where the background accounts for a baseline and the heat dissipated effect comes from a sub population of molecules in the pump-probe overlap volume dumping energy into the solvent. The localized increase/decrease of solvent temperature causes a refractive index change of the probe, and produces an observable offset in the signal.

2. <u>Power</u>: The pump power used for a given spot size is one of the factors that determines the percentage of molecules excited. An increase in power increases the number of excited absorbing species, thus increases the thermal gradient induced on the solvent that contributes to thermal lensing. For the experiments done in this dissertation, increasing the pump power would not only cause more spatial distortion of the probe, but it would also lead to solvated electron effects that may distort early time kinetics in the visible region. Therefore, experiments in LUMOS where done under conditions where the solvated electron effect was minimized while still maintaining a good signal:noise ratio. In the UV, conditions were optimized to the peak signal around 305 nm.

Summary of Solvent Background Analysis

All data analyzed in this dissertation required the use of a component that is very much longer than the time scale of the data set. This signal is referred to as a solvent or permanent signal in the fits to the data obtained in the visible and UV region, respectively. Some of the data required the use of a Gaussian placed at time-zero to account for coherent artifacts. Nonlinear tests were done to determine if the offset observed in the UV time resolved spectra was a function of provitamin or solvent properties. To test nonlinear liposome properties, cholesterol scans, solvated electron and power tests were conducted. The results show that these do not contribute to the observed background, therefore we assign the contribution to thermal lensing. It should also be noted that the decay curve in the excited state never fully goes to baseline and has been attributed in recent studies to a solvated electron effect[14]. Although there is a solvated electron effect in water, the strongest absorption is from ~550 nm- to the end of our continuum (~800 nm), whereas time lineouts of the provitamins greater than ~7.5 ps show a nearly flat spectra across the visible continuum. The solvent only water scans show an increasing amplitude from high to low frequency. In provitamin data sets, the solvated electron signal from the aqueous medium is greatly diminished since the provitamins are resonant with the pump. If one was to use shorter pulses or increase the power of the pump to the point that saturates the absorption of the molecules, then solvated effects would distort the data on the red edge. The observed background in the provitamin scans decreases with an offset with increasing time delays, which may be indicative of a localized heating to a cooling process.

References

(1)   Megerle, U.; Pugliesi, I.; Schriever, C.; Sailer, C. F.; Riedle, E. Sub-50 Fs Broadband Absorption Spectroscopy with Tunable Excitation: Putting the Analysis of Ultrafast Molecular Dynamics on Solid Ground. *Appl. Phys. B Lasers Opt.* **2009**, *96* (2–3), 215–231.

(2)   Wiley, T. E.; Konar, A.; Miller, N. A.; Spears, K. G.; Sension, R. J. Primed for Efficient Motion: Ultrafast Excited State Dynamics and Optical Manipulation of a Four Stage Rotary Molecular Motor. *J. Phys. Chem. A* **2018**, *122* (38), 7548–7558.

(3)   Benesch, M. G. K.; Lewis, R. N. A. H.; McElhaney, R. N. A Calorimetric and Spectroscopic Comparison of the Effects of Cholesterol and Its Sulfur-Containing Analogs Thiocholesterol and Cholesterol Sulfate on the Thermotropic Phase Behavior and Organization of Dipalmitoylphosphatidylcholine Bilayer Membranes. *Biochim. Biophys. Acta - Biomembr.* **2016**, *1858* (2), 168–180.

(4)   Sou, K.; Naito, Y.; Endo, T.; Takeoka, S.; Tsuchida, E. Effective Encapsulation of Proteins into Size-Controlled Phospholipid Vesicles Using Freeze-Thawing and Extrusion. *Biotechnol. Prog.* **2003**, *19* (5), 1547–1552.

(5)   Traikia, M.; Warschawski, D. E.; Recouvreur, M.; Cartaud, J.; Devaux, P. F. Formation of Unilamellar Vesicles by Repetitive Freeze-Thaw Cycles: Characterization by Electron Microscopy and 31 P-Nuclear Magnetic Resonance. *Eur. Biophys. J.* **2000**, *29* (3), 184–195.

(6)   Klein, R. . The Detection of Oxidation in Liposome Preparations. Biochim. Biophys. 1970, pp 486–489.

(7)   Dahlgren, Karl, Emilsoon, Pia, Hansson, Gunnar and Samuelson, B. PREPARATION AND CHARACTERISTICS OF LIPOSOMES Lipids Cholesterol Was Purchased from Calbiochem . Sphingomyelin Was Prepared. *J. Immunol. Methods* **1981**, *44*, 223–234.

(8)   Goldburg, W. I. Analysis of Macromolecular Polydispersity in Intensity Correlation Spectroscopy: The Method Of. *A Study Brownian Motion Using Light Scatt. Am. J. Phys.* **1999**, *67* (1999), 1093.

(9)   Ong, S. G. M.; Chitneni, M.; Lee, K. S.; Ming, L. C.; Yuen, K. H. Evaluation of Extrusion Technique for Nanosizing Liposomes. *Pharmaceutics* **2016**, *8* (4), 1–12.

(10)   Seinfeld, J. H.; Pandis, S. N. *ATMOSPHERIC From Air Pollution to Climate Change SECOND EDITION*; 2006.

(11)   Cox, A. J.; DeWeerd, A. J.; Linden, J. An Experiment to Measure Mie and Rayleigh Total Scattering Cross Sections. *Am. J. Phys.* **2002**, *70* (6), 620–625.

(12)   Shi, X.; Long, F. H.; Lu, H.; Eisenthal, K. B. Femtosecond Electron Solvation Kinetics in Water. *J. Phys. Chem.* **1996**, *100* (29), 11903–11906.

(13)   HARATA, A.; YAMAGUCHI, N. Photothermal Lensing Signal Enhancement by the

Transient Absorption of Photoexcited States in Liquid Solutions. *Anal. Sci.* **2005**, *16* (7),

743–749.

(14)   Tang, K. C.; Rury, A.; Orozco, M. B.; Egendorf, J.; Spears, K. G.; Sension, R. J. Ultrafast

Electrocyclic Ring Opening of 7-Dehydrocholesterol in Solution: The Influence of

Solvent on Excited State Dynamics. *J. Chem. Phys.* **2011**, *134* (10).

Chapter 3

Excited State Dynamics of Provitamins in Solution

Introduction

The ring-opening of 7-dehydrocholesterol (DHC) plays an essential role in vitamin D formation in mammalian cells. Upon excitation with UV-B radiation, the cyclohexadiene chromophore embedded within the molecule allows DHC to undergo a ring-opening reaction to form a previtamin D species, which is later on converted to the useful vitamin D_3. The initial ring-opening process of DHC that is explored in this chapter is illustrated in Figure 3.1.
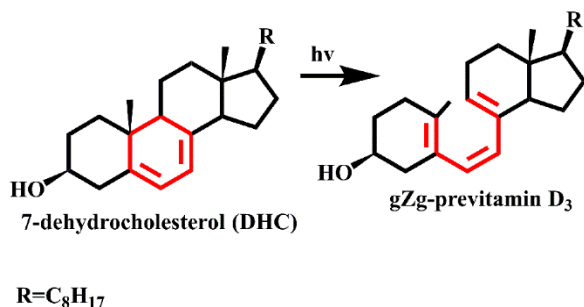
Figure 3.1: Initial ring-opening of DHC. In the ring-opening reaction, the cyclohexadiene chromophore (red) embedded within the molecule ring opens to form a previtamin D_3 species.

Another biologically relevant photochemical process is the conversion of provitamin D_2 (ergo) to vitamin D_2. The photochemistry involved in forming vitamin D_2 from ergo is analogous to the formation of vitamin D_3, but happens in a plant membrane environment. DHC-acetate also contains the cyclohexadiene chromophore that turns into a vitamin D –acetate compound.

This compound is not biologically relevant, but allows us to test the lipid environment as discussed in more detail in Chapter 4 and 6. Here we present a study of the excited state dynamics of ergo and DHC-acetate in 'simple' isotropic solution environments and compare the results with DHC.

The time scale for the ring-opening of the cyclohexadiene chromophore in DHC using ultrafast pump-probe techniques has been studied extensively in solution[1,2,3,4,5,6,7,8]. Anderson *et al.*[1] showed that DHC exhibits a strong excited state absorption (ESA) peaking around 480 nm. This is assigned to an S_1 to S_n transition. In our experiments we utilize a white light continuum spanning between 350-800 nm to capture the S_1 to S_n transition of ergo and DHC-acetate. In previous work, this strong absorption of DHC was measured in a variety of solvents[4]. A global fitting analysis of the data showed that the decay dynamics in 2-butanol are best modeled using a biexponential with time constants of ~ 0.5 ps and 1.8 ps. The specific time constants depend weakly on the solvent. Martinez *et al.*[9] has performed ab initio nonadiabatic molecular dynamics to quantify the biexponential nature on the excited state of DHC. Through these simulations, the biexponential decay is attributed to nonequilibrium dynamics, where the two time constants arise from a bifurcation of the population of molecules decaying down to the ground state. The 0.5 ps component is attributed to the fast (i.e "ballistic" or coherent) motion of molecules from the S_1 excite state to ground state while the 1.8 ps component is assigned to the internal conversion of trapped molecules on the excited state moving through the conical intersection after relaxation. To extend our studies of the ring-opening process, we examine ergo and DHC-acetate in isotropic solution environments. These results provide a baseline control for the liposome studies presented in the next chapter.

Results

Ground state spectra of provitamins in solution: The excited state of ergo and DHC-acetate was studied in 2-butanol and in hexadecane. We chose these two solvents because DHC has been extensively studied in 2-butanol and hexadecane has the same tail structure as the DPPC lipid used in most of our liposome studies. The ground state spectra of ergo and DHC-acetate are presented in Figure 3.2 and compared to DHC. The DHC spectra are in agreement with those reported previously [4,10].
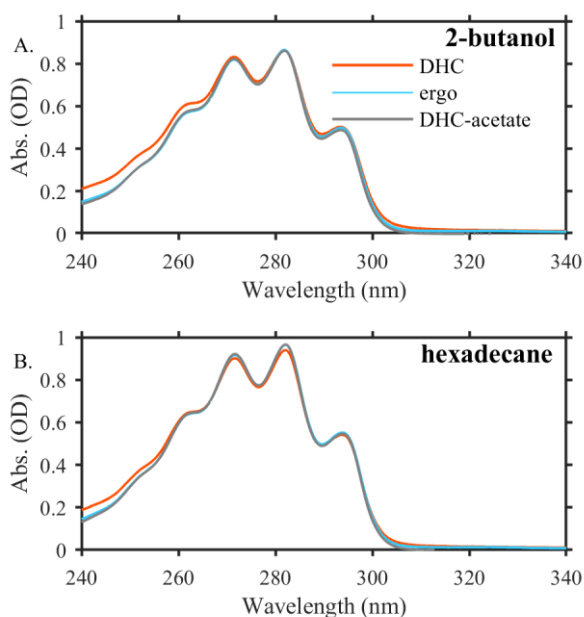
Figure 3.2: Ground state spectra of provitamins in (A) 2-butanol and (B) hexadecane, scaled to the same relative intensity. The legend in the first plot is the same for the second plot.

The peaks in the absorption spectrum in Figure 3.2 are nearly identical between the three provitamins. The spacing of about 1350 cm^{-1} corresponds to a $C = C$ stretch. In wavelength dependent studies from 266 nm to 297 nm, Smith *et al.*[2] demonstrated that the kinetics and biexponential nature of DHC is independent of pump wavelength. The pump wavelength used in these experiments is 272 nm and is resonant with the 0-2 vibronic transition.

Time resolved measurements of the excited state: The visible transient absorption spectra of DHC, DHC-acetate and ergo were measured in 2-butanol. Lineouts at selected time delays are plotted in Figure 3.3. In time resolved experiments, it is observed that the ESA shape and peak at 480 nm of ergo and DHC and DHC-acetate are nearly identical.
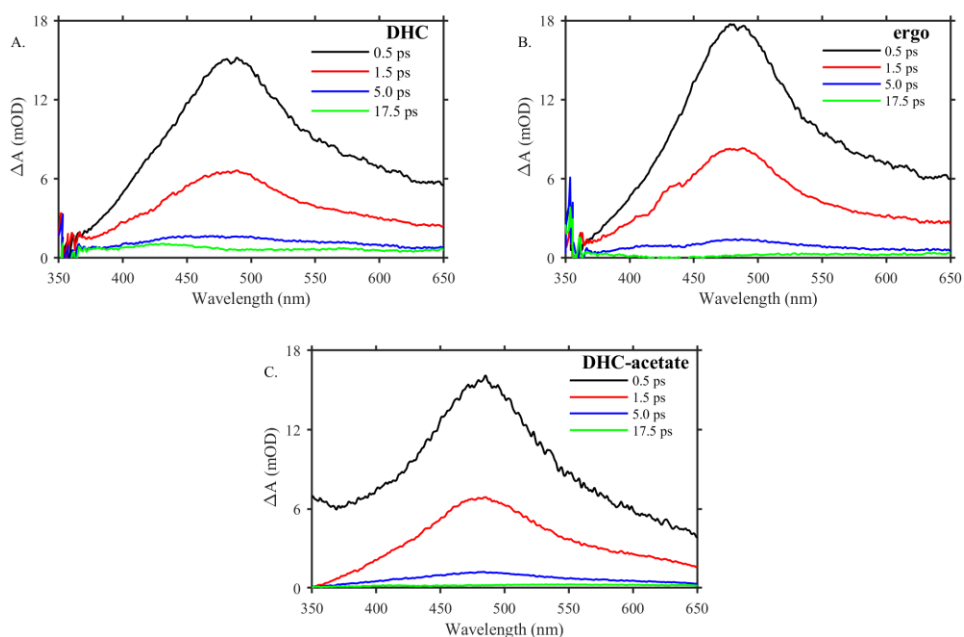
Figure 3.3: Selected time delays of (A) DHC, (B) ergo and (C) DHC-acetate in 2-butanol.

The data collected for ergo and DHC-acetate was fit to a sum of exponential decay components using a global analysis routine[11]. To minimize the residuals (difference between the data and the fit), the fit required at least two exponential decay components. The amplitudes or decay associated difference spectra (DADS) of these components give physical insight into the distribution of molecules that contribute to the biexponential decay. A cartoon description of the amplitudes (selected wavelength from the DADS) is shown in the Figure 3.4. The biexponential decay is attributed to a ballistic population (red molecules) and a trapped population (green molecules) that takes a longer time to relax to the ground state[9].

$\tau_1 = 0.53 \pm 0.04$ ps
$\tau_2 = 2.17 \pm 0.09$ ps

Ring-Closed State   Ring-Opened State
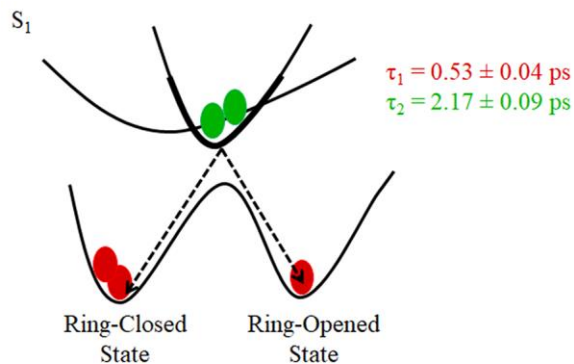
Ratio of Ballistic Population vs. Trapped Population
1.5 : 1

Figure 3.4: A cartoon representation of the amplitudes (at 480 nm in the DADS spectrum) for DHC in 2-butanol illustrating the trapped sub-population (green) of molecules in the S_1 excited state and the "ballistic" population (red) of molecules that immediately decays from the excited state to ground state.

Figure 3.5 shows the DADS for each component obtained after the global fitting analysis. The fast, ca. 0.55 ps component (red) corresponds to the population of molecules that immediately decays to the ground state. The slow component ca. 2.15-2.50 ps component (green) corresponds to the internal conversion of trapped molecules that do not immediately make it down to the ground state (as illustrated in Figure 3.4) and the long lived solvent component (blue) is assigned to solvent effects that include solvated electron signals and thermal lensing. The time constants obtained from the global fit for ergo are similar to DHC, but the decay of DHC-acetate is somewhat longer than DHC. The time constants are summarized in Table 3.1.

58
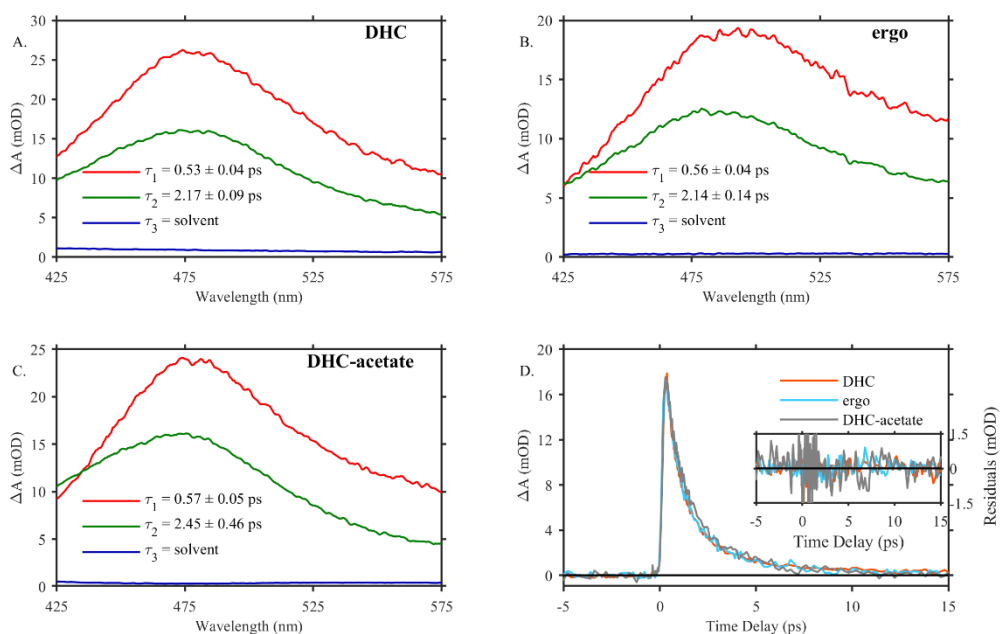
Figure 3.5 : (A-C) DADS obtained from global fits of (A) DHC, (B) ergo (C) DHC-acetate in 2-butanol. (D) Kinetics and residuals (box) of DHC (orange), ergo (light blue) and DHC-acetate (gray) plotted at 480 nm. Kinetics scaled to relative intensity.

Table 3.1: Time constants obtained from global fits across a wavelength range ~350-650 nm for DHC, ergo and DHC-acetate in 2-butanol.

Provitamin	τ_1 (ps)	τ_2 (ps)	τ_3 (ps)
DHC	0.53 ± 0.04	2.17 ± 0.09	>>50
ergo	0.56 ± 0.04	2.14 ± 0.14	>>50
DHC- acetate	0.57 ± 0.05	2.45 ± 0.46	>>50

The visible transient absorption spectra of DHC, DHC-acetate and ergo was also measured in hexadecane. Lineouts at selected time delays are plotted in Figure 3.6. In hexadecane, the ESA peak and shape of ergo and DHC-acetate are similar to DHC. The ESA spectrum of DHC-acetate appears to have a longer lived signal than ergo and DHC, consistent with the behavior observed

in 2-butanol.
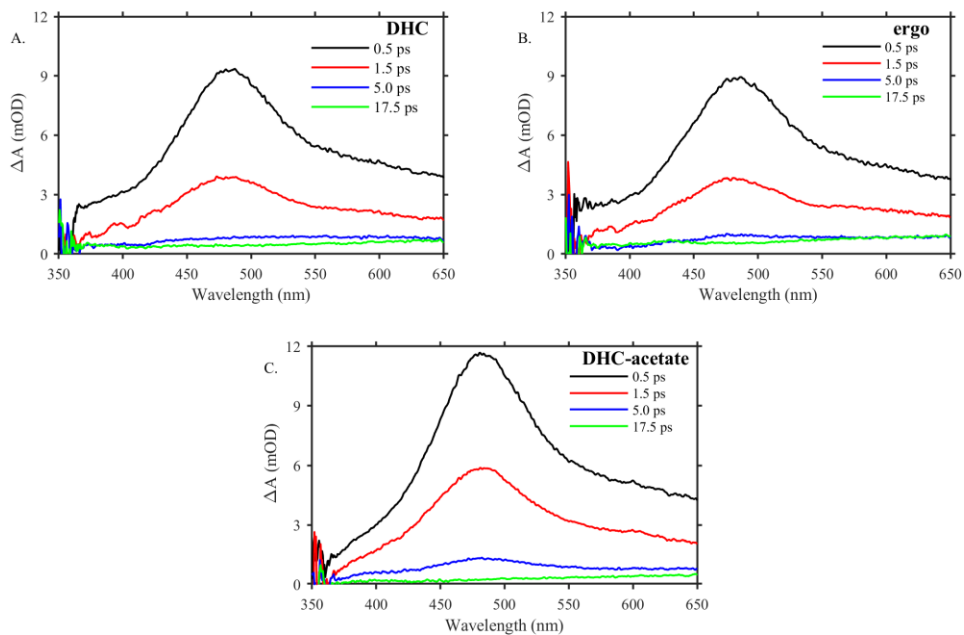
Figure 3.6: Selected time delays of (A) DHC, (B) ergo and (C) DHC-acetate in hexadecane.

The transient spectra were fit using the same global fitting technique routinely used in analyzing the data in 2-butanol. The kinetics between the three provitamins in hexadecane follow a similar trend as in 2-butanol. In the alkane solvent, ergo and DHC are similar. However, the long component of DHC-acetate is longer in hexadecane than in 2-butanol. Figure 3.7 shows the DADS and kinetics for the three provitamins in hexadecane. The time constants are summarized in Table 3.2. The DADS components represent the trapped and untrapped population distribution as described above for the three provitamins in 2-butanol.
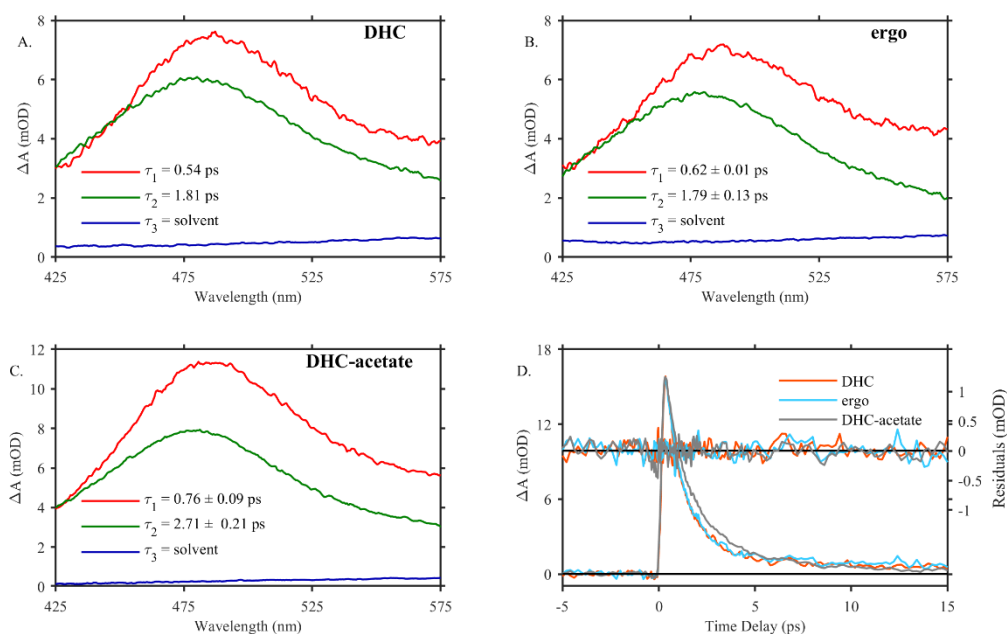
Figure 3.7: (A-C) DADS obtained from global fits of (A) DHC, (B) ergo and (C) DHC-acetate in hexadecane. (D) Kinetics and residuals of DHC (orange), ergo (light blue) and DHC-acetate (gray) plotted at 480 nm. Kinetics scaled to relative intensity.

Table 3.2: Time constants obtained from global fits across a wavelength range ~350-650 nm for DHC, ergo and DHC-acetate in hexadecane. DHC Measurement without error bars were only taken one time and produced results within error of previous experiments[4].

Provitamin	τ_1 (ps)	τ_2 (ps)	τ_3 (ps)
DHC	0.54	1.81	>>50
ergo	0.62 ± 0.01	1.79 ± 0.13	>>50
DHC- acetate	0.76 ± 0.09	2.71 ± 0.21	>>50

Comparison of time resolved data in 2-butanol and hexadecane: In order to gain physical insight into the biexponential behavior, we use the amplitudes of each time constant at the absorption peak (480 nm) to quantify the distribution of the trapped vs. untrapped populations. Figure 3.8 shows that the bifurcation of the population of excited state molecules that take a longer time to decay (slow component) compared to the population of molecules that make it to the ground state immediately (fast component) are the same between the three provitamins and do not change significantly from a polar to a non-polar environment.

61
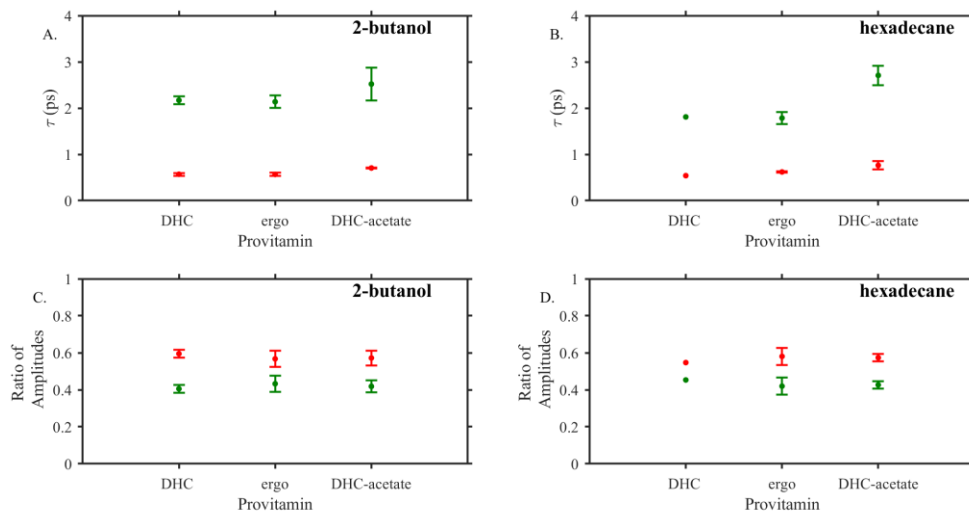
Figure 3.8: Summary of time constants for the three provitamins in (A) 2-butanol and (B) hexadecane. Fraction of the slow decay (green) and fast decay (red) component relative to the total amplitude of the decay components at 480 nm in (C) 2-butanol and (D) hexadecane. Here the slow and fast components represent the distribution of molecules that are trapped (slow time constant) and untapped (fast time constant) in the excited state.

The time constants for the fast and slow components following excitation of DHC in solution are temperature dependent[4]. At 29 °C the time constants are 0.56 ± 0.06 ps and 1.81 ± 0.02 ps in 2-butanol and 0.55 ± 0.22 ps and 1.4 ± 0.20 ps in hexadecane. In our experiments, we monitored the sample temperature to be ~24 °C in 2-butanol and ~25 °C in hexadecane which may increase the time constants slightly compared to the measurements reported at 29 °C. In our measurements, the temperature is the same within error for the two solvents.

The time constants observed for DHC and ergo are similar to each other in both solvents. This is unsurprising since the sterol structure around the chromophore is identical. The solvent viscosity for 2-butanol is slightly higher than hexadecane (3.10 cP and 3.03 cP, respectively)[12], although not sufficient to explain the differences between the time constants observed in the two solvents. In 2-butanol, DHC and ergo have the ability to hydrogen bond to the solvent, which may account for the longer lifetime observed compared to hexadecane.

For DHC-acetate, however, the lifetime appears to be longer than DHC and ergo in both solvents. The longer lifetimes observed for DHC-acetate in 2-butanol ($\tau_1 = 0.76 \pm 0.09$ and $\tau_2 = 2.45 \pm 0.46$ ps) and in hexadecane ($\tau_1 = 0.57 \pm 0.05$ and $\tau_2 = 2.71 \pm 0.21$ ps) may suggest two things about the ring-opening process. First, the sterol rings near the cyclohexadiene chromophore may influence the ring-opening process (Figure 1.6) and the larger acetate group could slow down this process. Second, hydrogen bonds between the alcohol and the acetate group could affect the lifetime in 2-butanol.

Based on the observations of the ring-opening reaction in 2-butanol and hexadecane, we hypothesize that hydrogen bonding may restrict motion and slow down the ring-opening reaction of DHC and ergo in the liposome environment. We also hypothesize that in the liposome environment, DHC-acetate may be slightly different from DHC and ergo because it cannot hydrogen bond with the lipid head group.

Conclusion

The purpose of these studies was to test the provitamin D_3 analogs, ergo and DHC-acetate in a simple environment where DHC is already well studied. The excited state dynamics are similar for all three molecules. Our results show that the depletion of molecules from the excited state to the ground state is best modeled as a biexponential decay, with a fast component that represents molecules moving straight from the excited to ground state and a slow component that represents a sub-population of trapped molecules on the excited state surface that takes a longer time to return to the ground state. The amplitudes of these components are similar for all three provitamins and do not vary significantly between the polar 2-butanol environment and the non-polar hexadecane environment. In comparison with DHC, it was observed that the double bond in ergo does not influence the ring-opening dynamics. The measured life times of ergo ($\tau_1 =$

0.56 ± 0.04 ps and $\tau_2 = 2.14 \pm 0.14$ ps) and DHC ($\tau_1 = 0.53 \pm 0.04$ ps and $\tau_2 = 2.17 \pm 0.09$ ps) in 2-butanol are slightly slower than in hexadecane ($\tau_1 = 0.62 \pm 0.01$ ps, $\tau_2 = 1.79 \pm 0.13$ ps and $\tau_1 = 0.54$ ps, $\tau_2 = 1.81$ ps, for ego and DHC respectively). The difference between the lifetimes observed in 2-butanol and hexadecane is small, but may come from hydrogen bonding in the alcohol environment. Measurements on DHC-acetate show a slightly longer decay compared to DHC and ergo in both solvents. This may arise from the larger size of the acetate group when compared with the hydroxyl group. The differences between the lifetimes observed for DHC-acetate in hexadecane ($\tau_1 = 0.57 \pm 0.05$ and $\tau_2 = 2.71 \pm 0.21$ ps) and 2-butanol ($\tau_1 = 0.76 \pm 0.09$ and $\tau_2 = 2.45 \pm 0.46$ ps) may arise from a very slight polarity dependence. Further testing is required to test solvent displacement or mass effects from the hydroxyl and acetate groups.

The studies in this chapter show that the initial ring-opening of DHC, ergo and DHC-acetate do not vary significantly from each other in polar and non-polar isotropic solutions. The next chapter will discuss the ring-opening process of the three provitamins in biologically relevant lipid bilayer membranes. The two significant results from this chapter that are relevant to the lipid membrane come from the hydrogen bonding (2-butanol) and long alkane tail (hexadecane) environments. The fits from the global analysis suggest that these parameters do not significantly change the decay dynamics between the three provitamins in a free solution environment. Therefore, any significant changes in the liposomes can be attributed to the environment and are not inherent properties of the specific molecules.

References

(1)   Anderson, N. A.; Shiang, J. J.; Sension, R. J. Subpicosecond Ring Opening of 7-Dehydrocholesterol Studied by Ultrafast Spectroscopy. *J. Phys. Chem. A* **1999**, *103* (50), 10730–10736.

(2)   Smith, B. D.; Spears, K. G.; Sension, R. J. Probing the Biexponential Dynamics of Ring-Opening in 7-Dehydrocholesterol. *J. Phys. Chem. A* **2016**, *120* (33), 6575–6581.

(3)   Fuss, W.; Höfer, T.; Hering, P.; Kompa, K. L.; Lochbrunner, S.; Schikarski, T.; Schmid, W. E. Ring Opening in the Dehydrocholesterol-Previtamin D System Studied by Ultrafast Spectroscopy. *J. Phys. Chem.* **1996**, *100* (2), 921–927.

(4)   Tang, K. C.; Rury, A.; Orozco, M. B.; Egendorf, J.; Spears, K. G.; Sension, R. J. Ultrafast Electrocyclic Ring Opening of 7-Dehydrocholesterol in Solution: The Influence of Solvent on Excited State Dynamics. *J. Chem. Phys.* **2011**, *134* (10).

(5)   Meyer-Ilse, J.; Akimov, D.; Dietzek, B. Ultrafast Circular Dichroism Study of the Ring Opening of 7-Dehydrocholesterol. *J. Phys. Chem. Lett.* **2012**, *3* (2), 182–185.

(6)   Tang, K.-C.; Sension, R. J. The Influence of the Optical Pulse Shape on Excited State Dynamics in Provitamin D3. *Faraday Discuss.* **2011**, *153*, 117.

(7)   Arruda, B. C., Peng, J., Smith, B. Spears, K. G., Sension, R. J. Photochemical Ring-Opening and Ground State Relaxation in α-Terpinene with Comparison to Provitamin.*J Phys. Chem.* **2012**.

(8)   Anderson, N. A.; Sension, R. J. Solvent Dependence of Excited State Lifetimes in 7-Dehydrocholesterol and Simple Polyenes. *ACS Symp. Ser.* **2002**, *820*, 148–158.

(9)   Snyder, J. W.; Curchod, B. F. E.; Martinez, T. J. GPU-Accelerated State-Averaged Complete Active Space Self-Consistent Field Interfaced with Ab Initio Multiple Spawning Unravels the Photodynamics of Provitamin D3. *J. Phys. Chem. Lett.* **2016**, *7* (13), 2444–2449.

(10)   Arruda, B. C., Peng, J., Smith, B. Spears, K. G., Sension, R. J. Photochemical Ring-Opening and Ground State Relaxation in α-Terpinene with Comparison to Provitamin.*J Phys. Chem.* **2012**.

(11)   Wiley, T. E.; Konar, A.; Miller, N. A.; Spears, K. G.; Sension, R. J. Primed for Efficient Motion: Ultrafast Excited State Dynamics and Optical Manipulation of a Four Stage Rotary Molecular Motor. *J. Phys. Chem. A* **2018**, *122* (38), 7548–7558.

(12)   Lide, D. R.; Baysinger, G. CRC Handbook of Chemistry and Physics: A Ready-Reference Book of Chemical and Physical Data. *Choice Rev. Online* **2004**, *41* (08), 41-4368-41–4368.

Chapter 4

The Provitamin Excited State Dynamics in Lipid Bilayers

Introduction

In ultrafast studies of the excited state absorption (ESA) of DHC, the ring-opening dynamics were primarily measured in organic solvents. However, the main photochemistry that happens in human skin takes place in a lipid matrix, organic solvents are not good models of this environment. In the lipid model proposed by Tian and Holick[1], hydrogen bonding, van der Waals interactions and lipid tail length are some of the factors that influence that rate of vitamin D_3 production from a previtamin species. In this chapter we investigate the ring-opening mechanism of DHC and analogs, ergosterol (ergo) and DHC-acetate solvated in lipid bilayers. Figure 4.1 illustrates the primarily lipid, 1,2-dipalmitoyl-sn-glycero-3-phosphatidylcholine (DPPC) used in our measurements. The studies presented here are used as a basis to understand the first steps in vitamin D production in mammalian skin. The formation of previtamin D will be analyzed in terms of the heterogeneity of the lipid matrix, hydrogen bonding (DHC-acetate), van der Waals interactions (ergo), membrane tail length (using 1,2- distearoyl-sn-glycero-3-phosphocholine (DSPC), 1,2-dimyristoyl-sn-glycero-3-phophocholine (DMPC), and 1,2 dilauroyl-sn-glycero-3-phosphocholine (DLPC)) and liposome curvature.
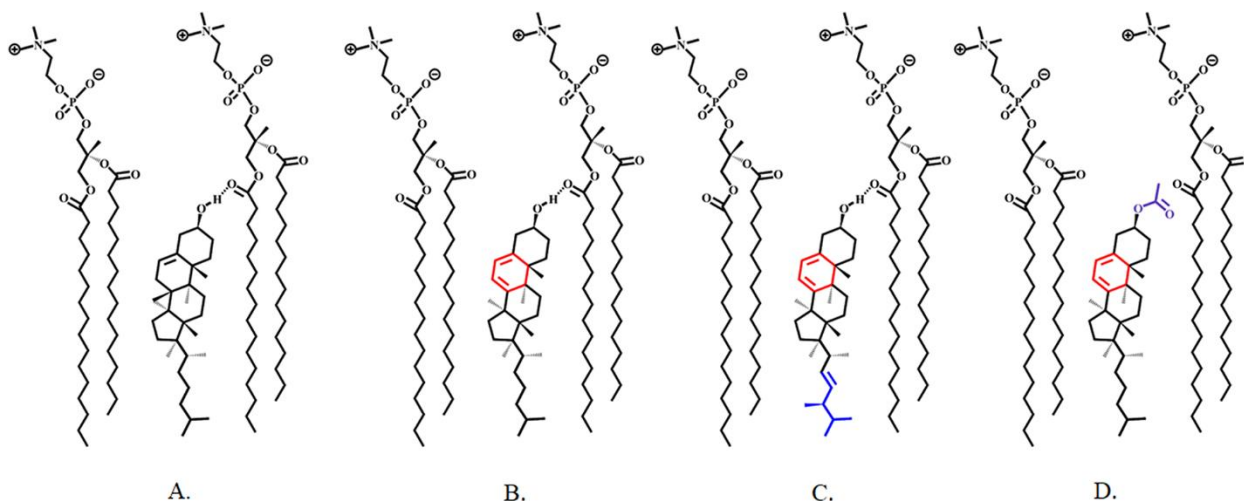
Figure 4.1: (A) cholesterol, (B) DHC, (C) ergo and (D) DHC-acetate in the DPPC lipid bilayer. Only cholesterol, DHC and ergo are capable of hydrogen bonding to the lipid head group.

Results and Discussion

Ground state absorption of provitamins in DPPC liposomes: The steady state absorption spectra of the three provitamins are shown in Figure 4.2. The steady state spectrum of DHC appears broader on the blue side compared to its analogs ergo or DHC-acetate, which look similar. This may be real, or may be an artifact of the background subtraction as discussed in chapter 2.
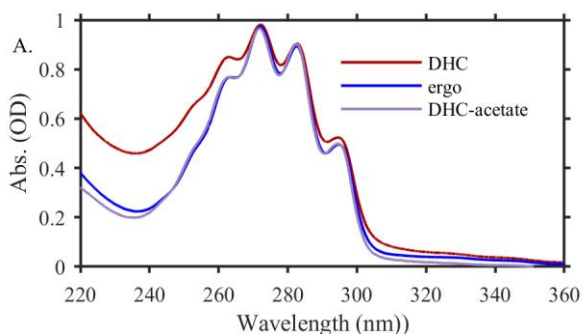
Figure 4.2: Steady state spectra of 30mol-% loadings of DHC, ergo and DHC-acetate in DPPC liposomes. All spectra scaled to be ~1 OD at ~ 272 nm.

It should also be noted that the transitions in the steady state absorption spectra for DHC and analogs are shifted about 1 nm to the red in liposomes compared to solution. This shift becomes important when looking at steady state photolysis measurements (see Chapter 6).

Transient absorption of provitamins in DPPC liposomes: In this study, we will focus, primarily on a 30mol-% loading of DHC in the liposomes. Cholesterol loaded liposomes are reported to be the most stable at this particular loading[2]. It is essential to form stable, spherical particles for size control and reproducibility. The biological loading of DHC is reported to be 30-50mol-% in human skin[3,4,5].

As shown in Chapter 3, the peak of the excited state visible absorption (ESA) of DHC and analogs occurs at 480 nm. Figure 4.3 shows the absorption spectra and excited state decay for DHC in DPPC lipid bilayers compared to 2-butanol.
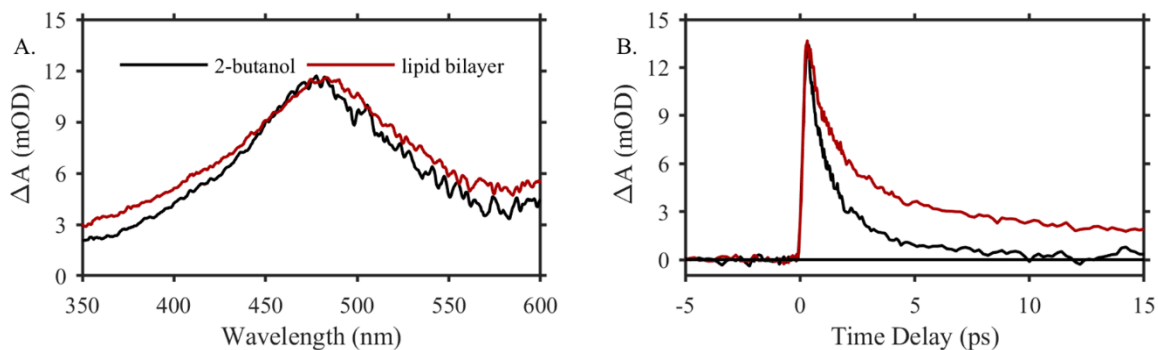
Figure 4.3: (A) Excited state absorption spectra averaged from 0.5 to 2 ps for a 30mol-% loading of DHC in DPPC lipid bilayers (red) and DHC in 2-butanol (black). The spectra are scaled to the same peak intensity. A solvent background averaged from 50 to 300 ps was subtracted from the data. (B) The excited state decay of a 30mol-% loading of DHC measured at 480 nm in DPPC lipid bilayers (red) compared to DHC in 2-butanol solution (black). The legend in plot A is the same for plot B.

Analysis of our TA data reveals that the excited state decay of DHC in the lipid membrane is best modeled as a biexponential decay (Figure 4.4A and 4.4C), but the lifetime of the ESA is distinctively longer ($\tau_1 = 1.30 \pm 0.13$ ps, $\tau_2 = 11.60 \pm 0.93$ ps) than in solution ($\tau_1 = 0.53 \pm 0.04$ ps, $\tau_2 = 2.17 \pm 0.09$ ps, see also Figure 4.3B). The overall shape of the absorption spectrum is comparable to what is observed in solution (see Chapter 3).
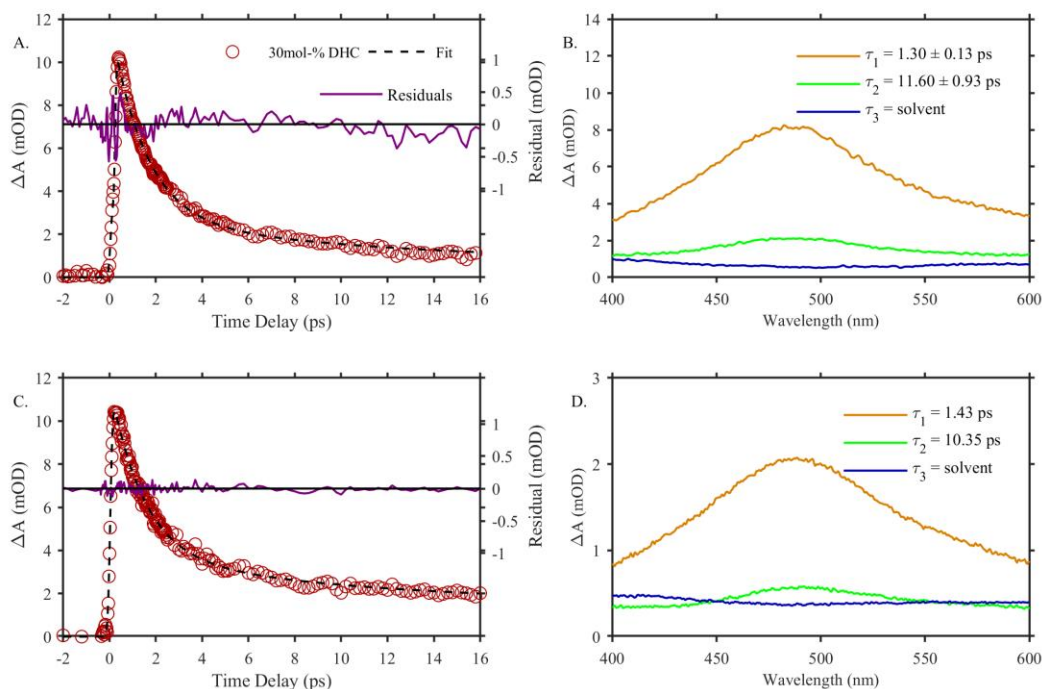
Figure 4.4: Transient kinetics of a 30mol-% loading of DHC in DPPC, fits (black dashed) and residuals (dark purple) at 480 nm taken from two independent measurements (A) with a flow cell and an instrument response function (IRF) ~300 fs or (C) with a wire guided flow apparatus in LUMOS and an IRF ~200 fs. DADS plotted in (B) and (C) for flow cell and wire guided flow measurements, respectively.

In order to determine what influences the long component, multiple experiments were carried out to test tested the influence of the (1) heterogeneity of the membrane, (2) sterol interaction between the molecule and membrane, (3) lipid tail length, and (4) membrane curvature.

Heterogeneity Tests

Liposomes with three different loadings were used to probe the effect of heterogeneity of the membrane on the excited state lifetime. Measurements were taken for 30mol-% DHC, 15mol-% DHC loadings and with a 15/15 mol-% DHC/CHL mixed loading. The results are summarized in Figure 4.5 and Table 4.1. The DADS (decay associated difference spectra) and decay dynamics within our signal to noise do not show significant differences.
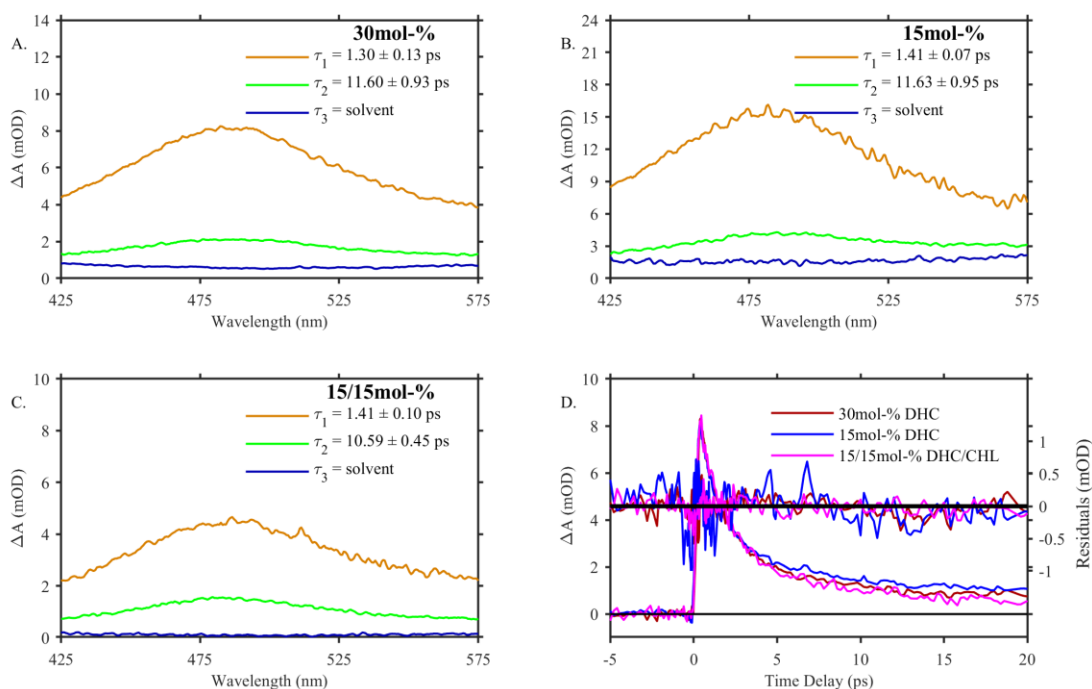
Figure 4.5: (A-C) DADS obtained after global fits to loadings of (A) 30mol-% DHC, (B) 15mol-% DHC, (C) 15/15mol-% DHC/CHL in DPPC lipid bilayers and (D) kinetics and residuals from the fit at 480 nm for DHC loadings of 30mol-% (red), 15mol-% (blue) and a mixed DHC/CHL loading of 15/15 mol-% (magenta) DHC. The kinetics traces are scaled to the same peak intensity.

Table 4.1: Time constants obtained from global fits across a wavelength range of ~350-650 nm for a 30/0mol-%, 15/0mol-% loading and 15/15mol-% DHC/CHL mixed loading in DPPC lipid bilayers.

Sterol Loading/ Sterol	τ_1 (ps)	τ_2 (ps)	τ_3 (ps)
30mol-% DHC	1.30 ± 0.13	11.60 ± 0.93	>>300
15mol-% DHC	1.41 ± 0.07	11.63 ± 0.95	>>300
15/15mol-% DHC/CHL	1.41 ± 0.10	10.59 ± 0.45	>>300

The time constants observed for different loadings of DHC appear to be nearly identical within error. The amplitudes (DADS at 480 nm) show that the fast and slow components (Figure 4.5A-C) also do not show distinctive differences, but are different compared to solution (Chapter 3).

Sterol Interaction between The Lipid Membrane and Molecule

Analogs of provitamin D_3 were used to determine if the tail structure of the molecule (ergo) or the absence of hydrogen bonding to the lipid head group (DHC-acetate) influences the excited state dynamics. In comparison to DHC in liposomes, the shape of the spectrum for ergo and DHC-acetate are similar where there is a strong excited state absorption at ~480 nm. This is shown in Figure 4.6.
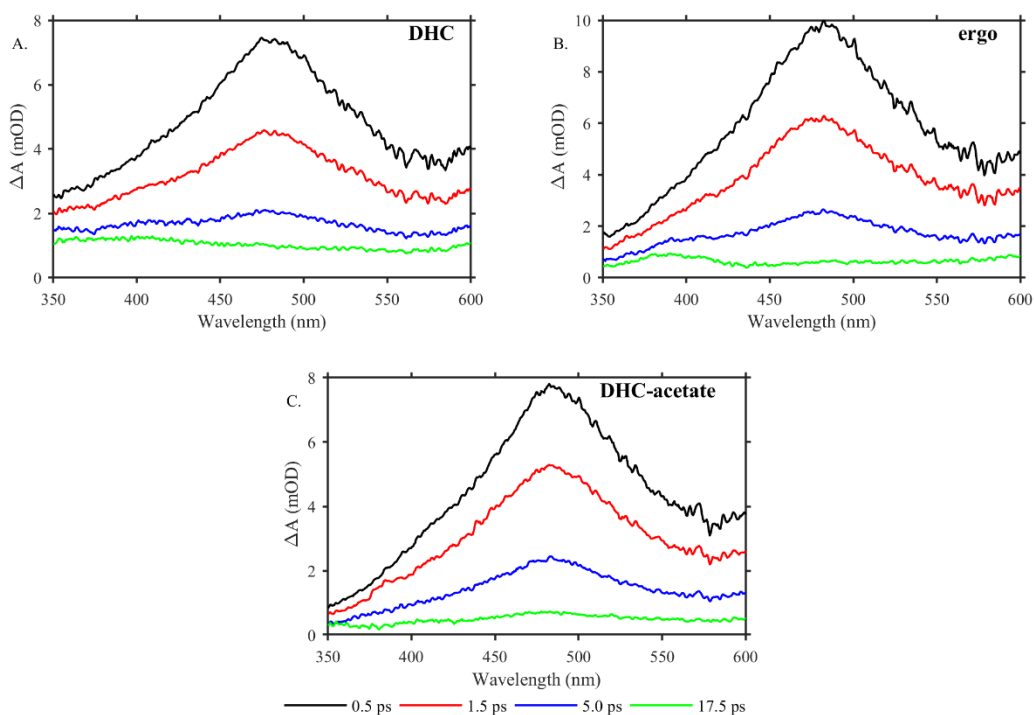
Figure 4.6: Selected time delay lineouts for 30mol-% loadings of (A) DHC, (B) ergo and (C) DHC- acetate in DPPC lipid bilayers. The legend on the bottom is the same for all three plots.

Fits to the data, illustrated in Figure 4.7 and summarized in Table 4.2 show that both ergo and

DHC-acetate exhibit a biexponential decay, with longer time constants than observed in solution

(Chapter 3). Measurements of the three provitamins were taken on the same day in order to

ensure that the same noise level and IRF were similar. This enabled an accurate comparison and

are in agreement with the data that was measured on different days.
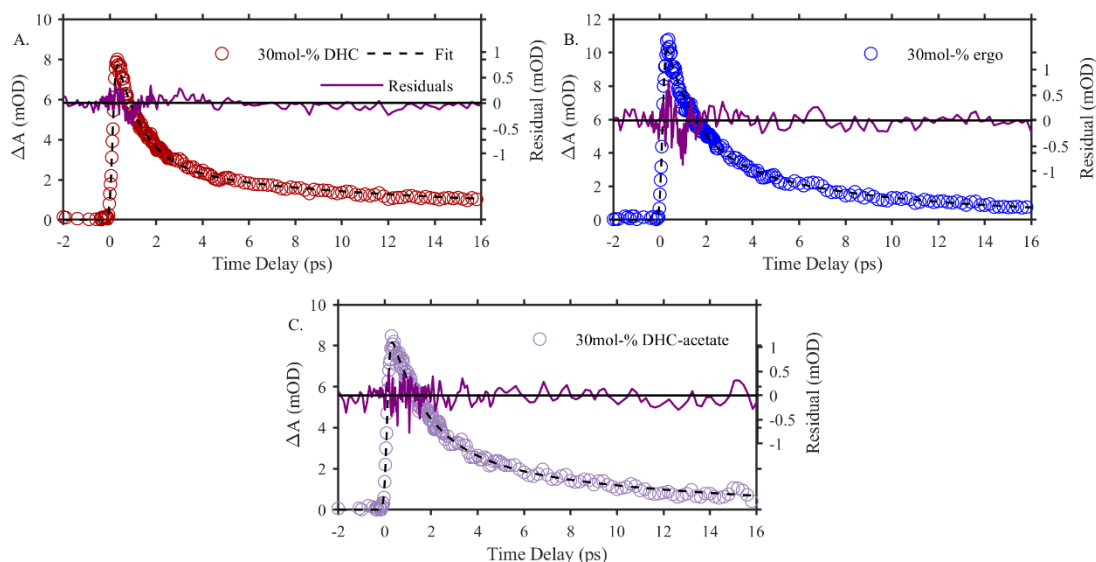
Figure 4.7: Fits (black dash) and residuals (dark purple) at 480 nm for 30mol-% loadings of (A) DHC (red circles), (B) ergo (blue circles) and (C) DHC-acetate (light purple) in DPPC lipid bilayers.

Table 4.2: Time constants obtained from global fits to 30mol-% loadings of DHC, ergo and DHC acetate in DPPC lipid bilayers across a wavelength range of ~350-650 nm.

Sterol Loading/ Sterol	τ_1 (ps)	τ_2 (ps)	τ_3 (ps)
30mol-% DHC	1.30 ± 0.13	11.60 ± 0.93	>>300
30mol-% ergo	1.37 ± 0.29	7.80 ± 1.27	>>300
30mol-% DHC-acetate	1.49 ± 0.10	9.07 ± 1.00	>>300

The data shows that in DPPC liposomes, the second component, τ_2 is longer for DHC than for ergo or DHC-acetate. The double bond located in the tail of ergo results in a more ordered lipid environment compared to DHC[6,7]. This may influence the excited state lifetime. The amplitudes of the fast and slow component also provide insight into potential differences. These are plotted in Figure 4.8. The amplitudes of the long component in DPPC is significantly larger for ergo and DHC-acetate than for DHC. Unlike the isotropic solution environment (Chapter 3), the DPPC

lipid bilayer can cause a different bifurcation between the fast and slow populations. Figure 4.8 illustrates the difference in the DADS for each of the provitamins.
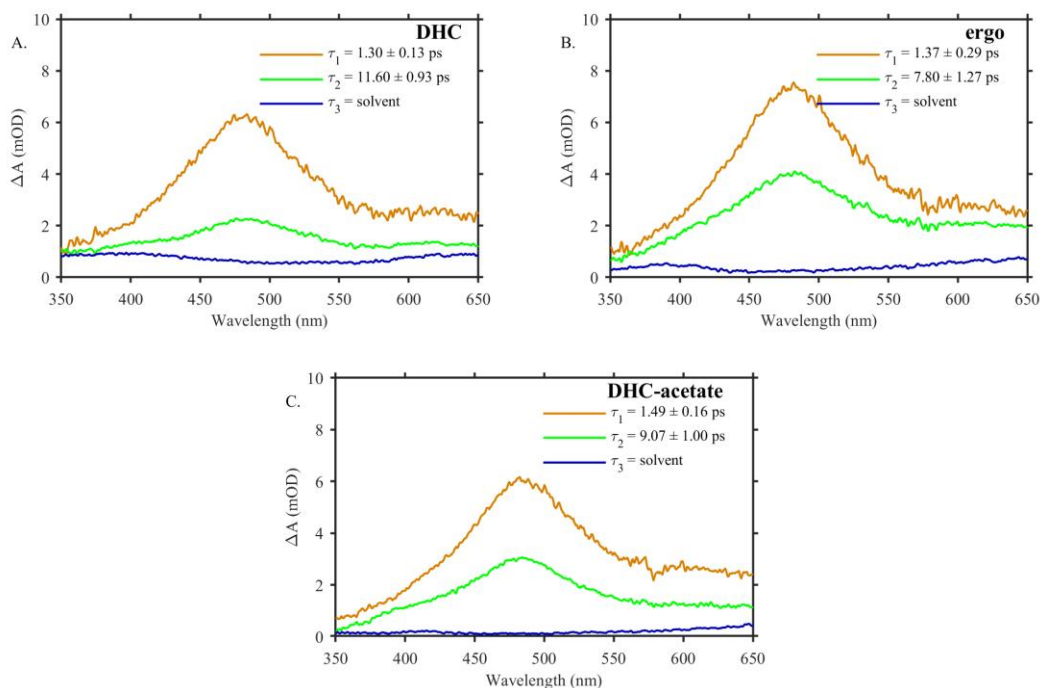
Figure 4.8: DADS obtained after a global fit to 30mol-% loadings of (A) DHC, (B) ergo and (C) DHC-acetate in DPPC lipid bilayers.

Lipid Tail Length

The fluidity of a membrane is dependent on the intermolecular interactions between the phospholipid tails, such as lipid packing. Theoretical mechanical properties of phospholipid bilayers reported by Guo *et al.*[8] shows that the compressibility of the lipid bilayer decreases with increasing phospholipid tail length. Experimental work done by Bui *et al.*[9] show that at 20°C, DPPC and DLPC lipids are in the gel phase and liquid phase, respectively. In order to test the influence of lipid tail length on DHC, ring-opening measurements were made in liposomes where the lipid tail length was varied from 18-12 carbons (DSPC (18) >DPPC (16) > DMPC (14) > DLPC (12)). Figure 4.9 illustrates the provitamins in the lipid bilayers that are explored in

this section.

A.

DSPC   DPPC   DMPC   DLPC

B.

DPPC   DMPC   DLPC
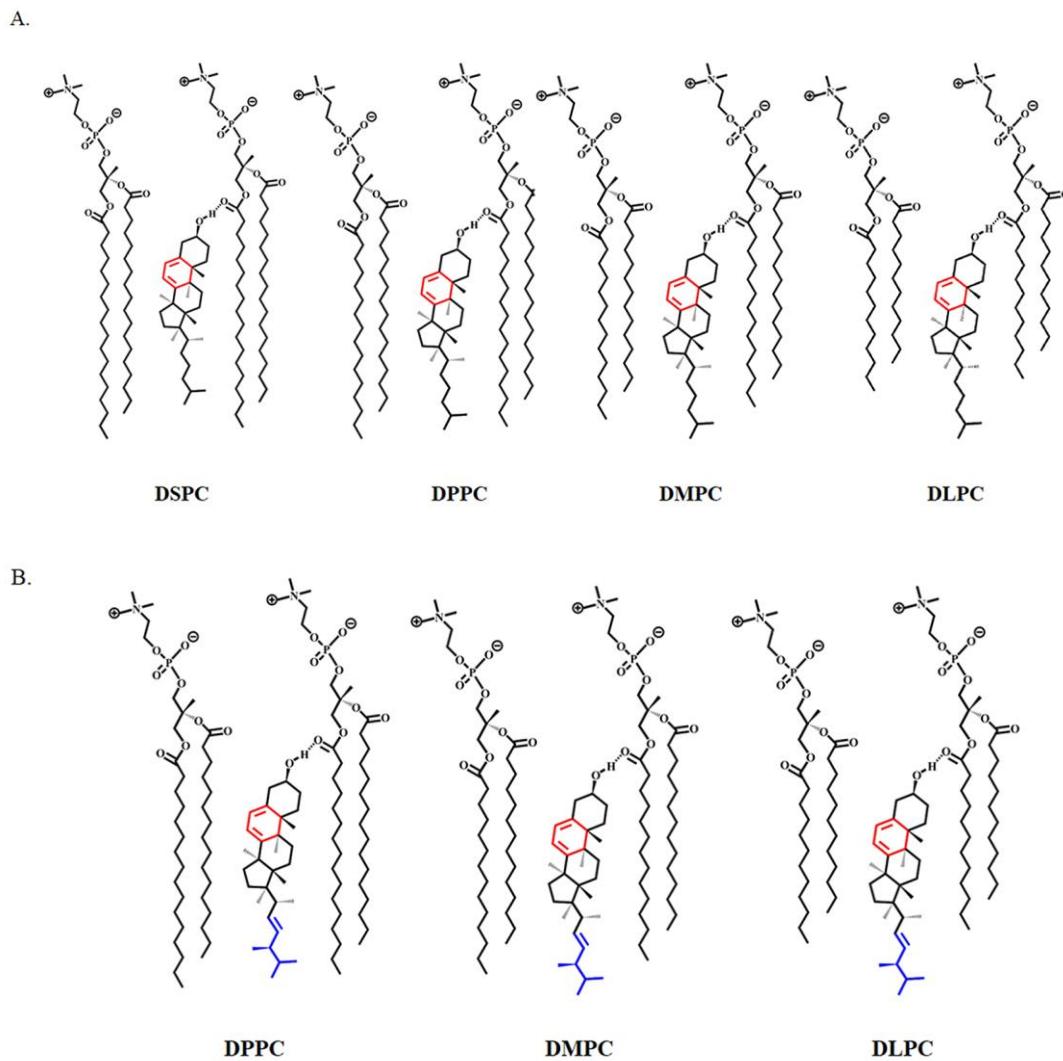
Figure 4.9: (A) DHC and (B) ergo in various chain length lipids.

The excited state spectra of DHC in the various tail lengths are plotted in Figure 4.10. The shape

of the ESA in DSPC, DMPC and DLPC liposomes are similar to the shape observed in DPPC.
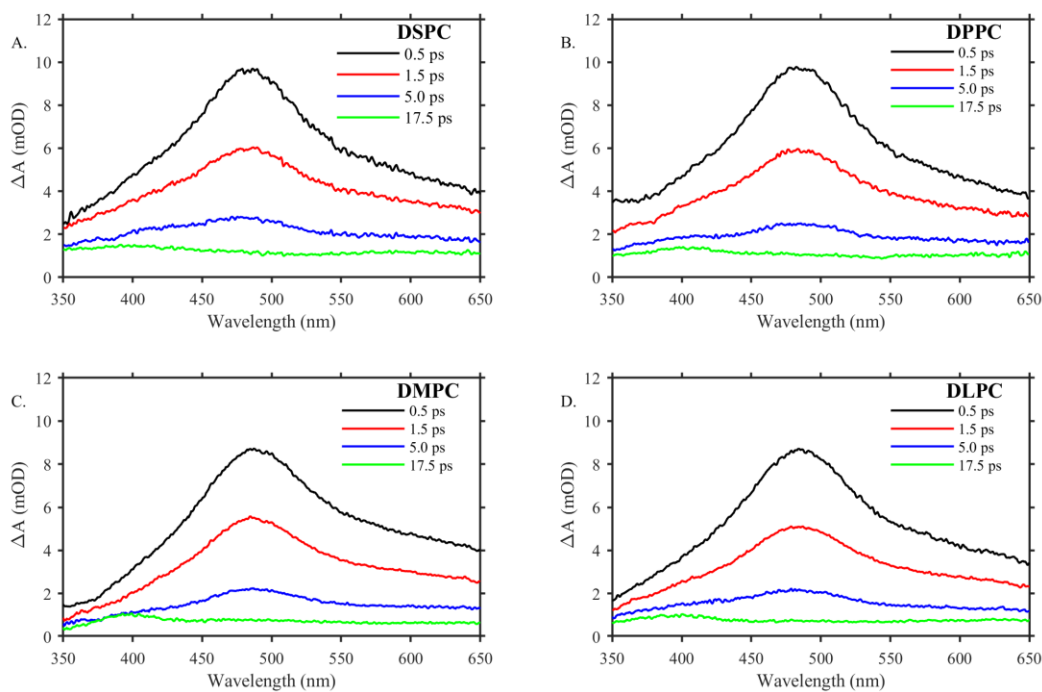
Figure 4.10: Comparison of the excited state absorption of a 30mol-% loading of DHC in (A) DPPC, (B) DSPC, (C) DMPC and (D) DLPC liposomes.

The excited state decays of DHC in DSPC and DPPC are essentially the same, therefore we did not use DSPC for any further experiments. However, in comparison to a 30mol-% loading of DHC in DPPC, the shorter tail lengths of DMPC and DLPC result in faster excited state dynamics. The amplitudes and kinetics of DHC both appear to approach a 'solution' like behavior with decreasing tail length, but are still much longer than solution. Figure 4.11 show the fits and residuals to the decay of DHC in the various lipid tail lengths. The time constants, fits and amplitudes are summarized in Table 4.3.
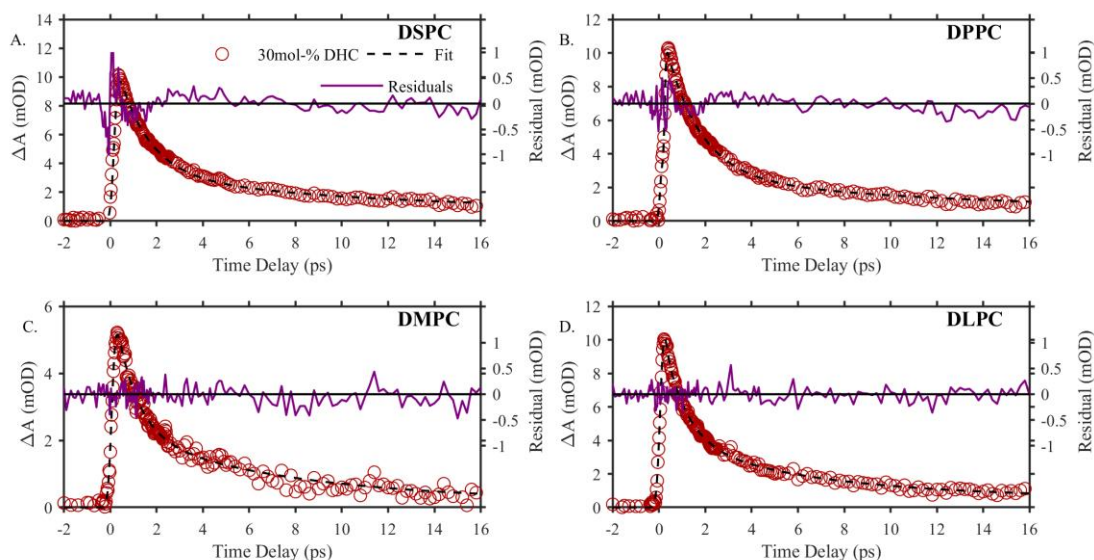
Figure 4.11: Fits (black dash) and residuals (purple) to a 30mol-% loading of DHC (red circles) in (A) DSPC, (B) DPPC, (C) DMPC and (D) DLPC at 480 nm.

Table 4.3: Table of time constants and amplitudes. Fast (A1) and slow (A2) decay components relative to the total amplitudes obtained for a 30mol-% loading of DHC in DPPC, DSPC, DMPC and DLPC lipid bilayers. DSPC data without error bars was only measured once.

Lipid Tail	τ_1 (ps)	τ_2 (ps)	τ_3 (ps)	$\dfrac{A1}{A1+A2}$	$\dfrac{A2}{A1+A2}$
DSPC	1.34	10.40	>>300ps	0.75	0.25
DPPC	1.29 ± 0.13	11.60 ± 0.93	>>300ps	0.75 ± 0.03	0.25 ± 0.04
DMPC	1.01 ± 0.15	7.76 ± 0.83	>>300ps	0.66 ± 0.003	0.34 ± 0.004
DLPC	1.05 ± 0.16	6.07 ± 0.07	>>300ps	0.64 ± 0.01	0.36 ± 0.07

An interesting effect is seen when ergo is incorporated into the shorter chain length liposomes composed of DLPC and DMPC. The data, fits and residuals are shown in Figure 4.12
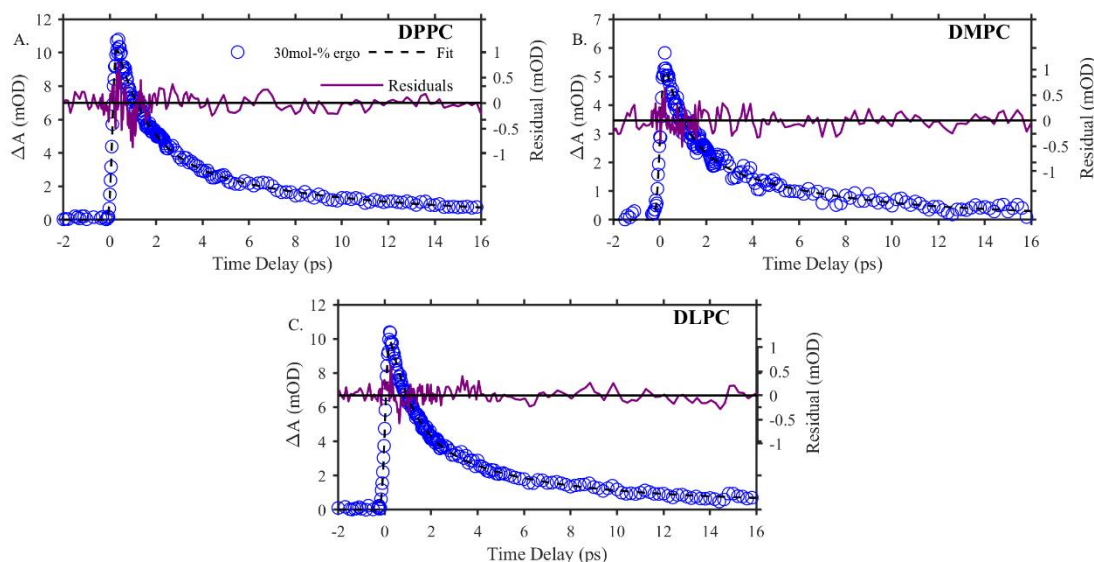
Figure 4.12: Fits (black dash) and residuals (purple) to a 30mol-% loading of ergo (blue circles) in (A) DPPC, (B) DMPC and (C) DLPC at 480 nm.

Table 4.4 summarizes the time constants and amplitudes obtained from the fits. The lifetimes

obtained for ergo in DPPC are slightly longer than those obtained in DMPC and DLPC.

However, the lifetimes of ergo in lipid tail lengths between 14-12 carbons are essentially

identical, although more measurements are needed to establish accurate error bars. This contrasts

with DHC where a steady decrease is observed from DPPC to DMPC to DLPC.

Table 4.4: Table of time constants and amplitudes. Fast (A1) and slow (A2) decay components relative to the total amplitudes obtained for a 30mol-% loading of ergo in DMPC and DLPC lipid bilayers. Measurements without error bars were only done once.

Lipid Tail	τ_1 (ps)	τ_2 (ps)	τ_3 (ps)	$\dfrac{A1}{A1 + A2}$	$\dfrac{A2}{A1 + A2}$
DPPC	1.37 ± 0.29	7.80 ± 1.27	>>300	0.66 ± 0.42	0.34 ± 0.42
DMPC	0.91	5.95	>>300	0.60	0.40
DLPC	0.98	5.25	>>300	0.63	0.37

The similarity between the kinetics in the two shorter lipids may indicate that the tails of DMPC and DLPC are too short to significantly interact with the double bond in ergo (Figure 4.9) yielding nearly identical results in each lipid and comparable to DHC. Another possibility is that ergo orders the DLPC and DMPC membrane in a similar way and differently for DPPC[9]. However, the removal of the interaction between the double bond in ergo in DLPC is further supported by the kinetics of ergo being comparable to the kinetics of DHC where only the cyclohexadiene chromophore and surrounding rings interact with the lipid. Unlike the case of DLPC, DMPC may have a tail length that is long enough to interact with the double bond in ergo, however more measurements in these two lipids are needed to accurately distinguish the lifetimes.

DHC-acetate does not incorporate into the DLPC lipid bilayer since it is less lipophilic than DHC and ergo, and thus was not measured in these liposomes. Due to the COVID-19 pandemic, we were not able to measure the ESA of DHC-acetate in DMPC lipid bilayers.

Liposome Curvature

Although the longest lifetimes of the different provitamins appear to be slightly different in DPPC lipids, we note that Table 2.2 (Chapter 2) illustrates that the size distribution of liposomes is influenced by the specific provitamin incorporated. This raises the question of the influence of liposome curvature on the dynamics. The lifetimes measured here may show a trend of decreasing lifetime with increasing particle size. To test this, the kinetics of DHC in DPPC were measured as a function of liposome size and thus, curvature. It is hypothesized the smaller curvature observed for DHC may constrain the molecule more such that the ring-opening process is slower, while a liposome with less curvature may offer some 'extra room' for the molecule to ring open, as observed in the size distribution and lifetime for ergo in DPPC. To show that DHC

is different from its analogs, and that the differences are not simply due to liposome size, DHC

loaded liposomes were tested at ~75 nm and 190 nm on the same day. The range tested covers

the upper and lower size bounds that are observed for DHC, ergo and DHC-acetate in DPPC as

well as DHC in DLPC and DMPC lipids. The results for DHC in DPPC lipids are summarized in

Table 4.5.

Table 4.5: Summary of time constants and amplitudes for a 30mol-% loading of DHC in DPPC lipid bilayers as a function of liposome size between ~75-190 nm. Measurements without error bars were only measured once. Fast (A1) and slow (A2) decay components relative to the total amplitudes.

Size (nm)	τ_1 (ps)	τ_2 (ps)	τ_3 (ps)	$\dfrac{A1}{A1+A2}$	$\dfrac{A2}{A1+A2}$
78.77 ± 3.86	0.91	9.23	>>300	0.70	0.30
149.29 ± 6.04	1.30 ± 0.13	11.60 ± 0.93	>>300	0.75 ± 0.04	0.25 ± 0.04
193.8 ± 1.08	1.14	10.70	>>300	0.72	0.28

It does not appear that the curvature influences the kinetics within the range of the variations

between the provitamins and lipids (150 to 190 nm), however making the lipids smaller may

have a slight influence on the kinetics of DHC. In addition, the amplitudes of the fast and slow

components are the same within error, further indicating that the kinetics are essentially the same

between 75-190 nm for DHC in DPPC liposomes. This indicates that liposome size is not a

dominant factor and that ergo and DHC-acetate have different effects on the lipid environment.

Summary of Time Constants and Amplitudes

This section will present a summary of the time constants and amplitudes obtained for the heterogeneity, provitamin interactions, lipid tail length and membrane curvature studies. The purpose here is to identify key factors that contribute to the long component observed for DHC, ergo and DHC-acetate in the lipid bilayer environment and to understand why the slow component is different from solution measurements (Chapter 3). Figure 4.13 summarizes the slowest life measured for DHC in the lipid membrane. The fast component is nearly the same for all experiments and therefore not plotted.
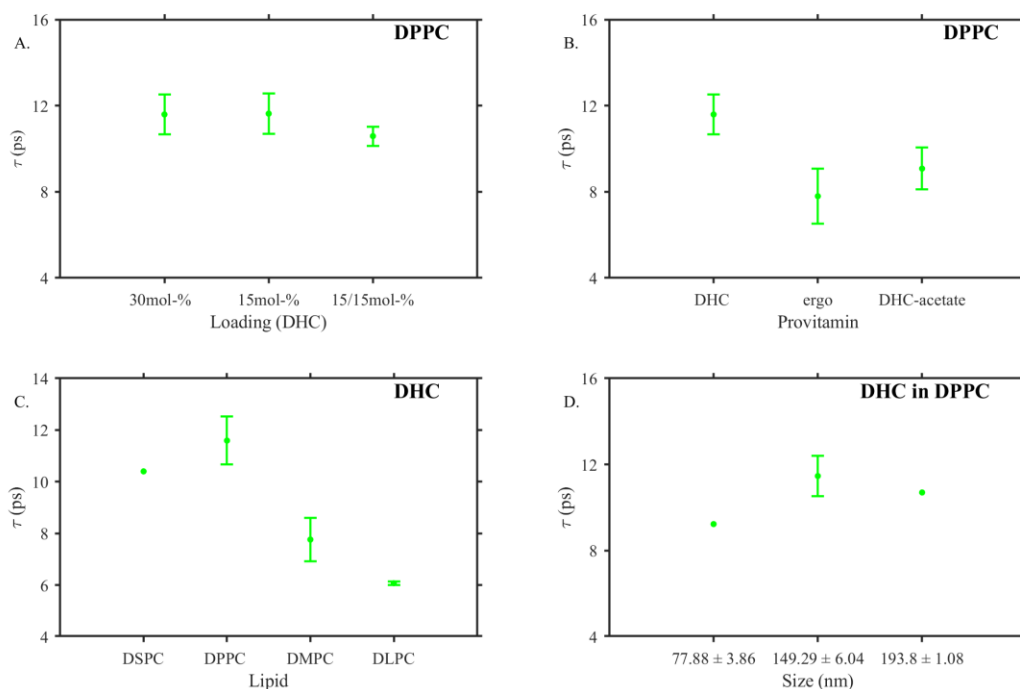
Figure 4.13: Long component (τ_2) of DHC (green) in lipid bilayers as a function of (A) sterol loading, (B) van der Waals and hydrogen bonding, (C) lipid tail length and (D) liposome size.

The longest time constant (τ_2) for DHC in DPPC does not vary significantly with loading or with liposome size. The type of sterol appears to influence the lipid environment since the long components of each of the three provitamins are not the same, as they were in solution.

However, the largest effect observed on τ_2 is when the lipid tail length is changed, thus changing membrane fluidity. Figure 4.14 shows that the bifurcation of the fast and slow component appears to be most dependent on the type of sterol and membrane fluidity. Possible mechanisms to account for these observations are discussed in the next section.
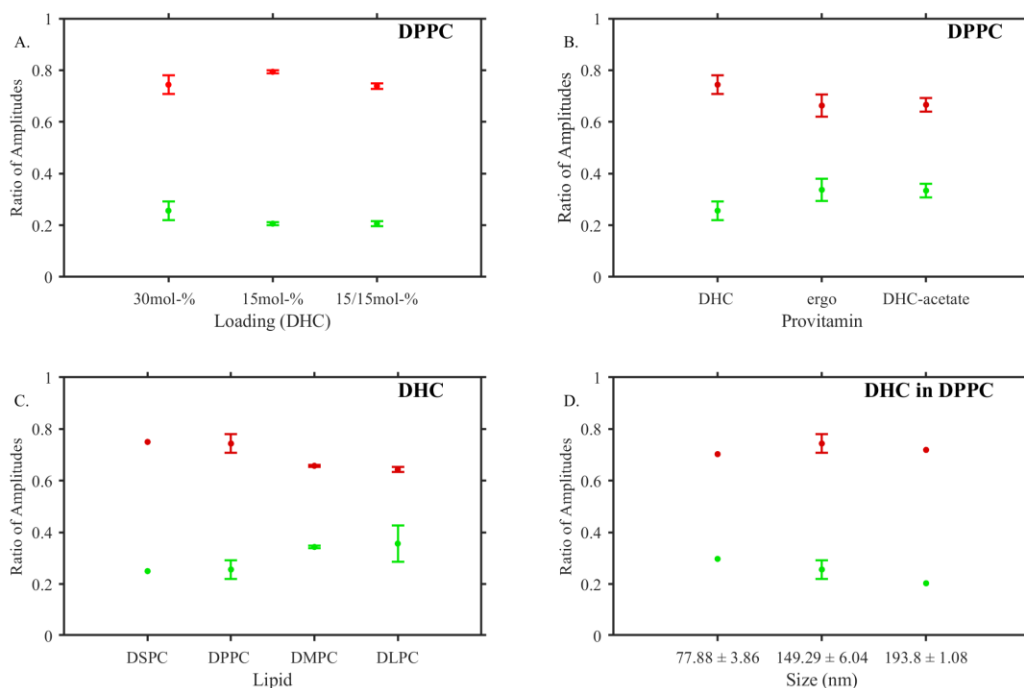
Figure 4.14: Relative amplitudes of the fast (red) and slow time component (green) obtained for DHC in lipid bilayers as a function of (A) sterol loading, (B) van der Waals and hydrogen bonding, (C) lipid tail length and (D) liposome size. Amplitudes obtained from the DADS at 480 nm for each plot, where the relative contributions of the fast component is A/(A+B) and the relative contributions of the slow component is B/(A+B).

Physical assignment of time constants of DHC and analogs in DPPC lipid bilayers:

There are several possible mechanisms through which the lipid bilayer could influence the excited state lifetime. These include the heterogeneity of the lipid matrix, van der Waals interactions, hydrogen bonding and membrane fluidity. The ultimate goal here is to identify the key factors involved in slowing down the ring-opening process in a lipid environment when compared to bulk solution.

The lipid bilayer containing sterol is known to contain solid-ordered phases and liquid-ordered phases, therefore it is not unreasonable to believe that the fast component found in the provitamins can be assigned to population in the liquid-ordered phase and the slow component assigned to a population in the solid-ordered phase. Time resolution tests were taken in LUMOS with an IRF ~200 fs to test if the fast component found was an average of two faster ones. It should be noted that the shorter IRF indicates shorter pulses which give rise to strong solvated electron effects that may distort the kinetics. The fits as shown in Figure 4.4 do not suggest that the excited state absorption is composed of 3 decay components, although this cannot be ruled out. As in solution, none of the measurements contains evidence of spectral narrowing characteristics of vibrational cooling. This indicates that the longer time component is not solely a consequence of an energy transfer from the molecule to the environment in the excited state.

Another possibility is that the lipid environment alters the potential energy surface, although there is not significant evidence for this in either the ground state or excited state spectra.

The most likely explanation is friction on the reaction coordinate. This friction can be estimated using viscosity. For example, the lifetime of DHC in DLPC is significantly shorter than DPPC. Nojima and Iwata[10] used the fluorescence lifetime of trans-stilbene in liposomes to estimate the viscosity in all four of the lipids used in our study. The viscosity of the lipid bilayers were estimated from the photoisomerization rate constant of S_1 trans-stilbene obtained from the fluorescence lifetime. The data was best modeled with a biexponential decay function and attributed to the two solvation environments in the lipid bilayer. The most viscous environment in DPPC and DLPC are estimated to be about 1500 cP and 54 cP, repspectively[10]. While the exact values should be taken with a healthy level of skepticism, it is significant that the friction

in DPPC is significantly higher than in DLPC. In comparison to the observations in solution, the measurements in the lipid bilayer may indicate the friction has to be extremely high to alter the kinetics of DHC. The lipid bilayer may be above the threshold for the kinetics of DHC to be significantly altered. Additional evidence is that the most viscous environment in the DSPC bilayer was reported to be1500 cP[10], which may explain why the observed kinetics and amplitudes are similar as DPPC. Interestingly, the kinetics for DHC and ergo in DMPC (97 cP) fall between DPPC (1500 cP) and DLPC (54 cP)[10]. This is also consistent with membrane compressibility measurements done by Bui *et al.*[9] For a 30mol-% loading of ergo, the DPPC and DLPC lipid bilayer are reported to have a compressibility moduli of 73.2 ± 2.2 mN/m and 152.7 ± 0.6 respectively[9]. It is not surprising that the lifetime for DHC is longer than ergo and DHC-acetate since the different structures of the molecules could alter the lifetimes in the lipid bilayer. Overall, the measured lifetimes of DHC and ergo are similar in DLPC, but 2-3x faster than in the DPPC environment. The similarity between DHC and ergo in the DLPC bilayer may indicate that only the sterol rings interact with the membrane, which are identical for ergo and DHC. Thus, the membrane ordering properties of these two provitamins may be similar if the double bond in ergo cannot change the environment. This is consistent with measurements of the excited state decay of DHC and ergo in solution, where the lifetimes are not distinguishable.

The relative amplitudes of the fast and slow components of the ESA decay may provide additional insight, reflecting the effect of packing within the lipid bilayer modified by tail length or provitamin structure. The differences here are represented by the branching ratios seen for DHC, ergo and DHC-acetate in DPPC (Figure 4.14B). The differences between the three provitamins suggests that van der Waals interactions and hydrogen bonding plays a role in the ring-opening process. The data presented here suggests that van der Waals forces has the most

85

significant impact in constraining the molecule. This is indicated by the lifetimes summarized in Table 4.2 and Table 4.3. In DPPC, the long component in the ring-opening processes for DHC is slower than for both ergo and DHC-acetate. Additional evidence is seen when DHC and ergo are incorporated into the DLPC lipid bilayer. In DLPC, the ring-opening process for DHC and ergo are both significantly faster than the lifetimes measured in DPPC. Environments that allow more structured packing around the provitamin including the tail, impede the ring-opening process for at least part of the population.

The amplitudes of the fast and slow components for DHC and ergo are nearly identical to each other in DLPC, while they are different in DPPC (Figure 4.14C). Thus it appears that the extra double bond in ergo does not interact with the membrane for short lipids. For DHC and ergo in DLPC, the van der Waals forces from the interaction of the provitamin tail with the lipid tail are significantly reduced. However, the hydrogen bonding between the molecule and lipid can still slow down the ring-opening process by restraining motion of the neighboring sterol ring near the cyclohexadiene chromophore (Chapter 3). Although DHC-acetate was not able to be incorporated into the DLPC lipid bilayer, based on the behavior in DPPC and observations in solution, it is expected that lifetime of DHC-acetate would be slightly slower than the 6 ps lifetime observed for DHC, since the larger size of the acetate group may impede the ring-opening motion.

Conclusion

The decay of the excited state in the lipid bilayer is similar to free solution in which a sub-population moves rapidly to the ground state and another is trapped for approximately an order of magnitude longer. To explain the biexponential nature observed in all the lipid data, it is proposed that the mechanism of population transfer is similar to solution, however the lipid slows down the motion of the molecule in the S_1 excited state. The fast ballistic component observed in solution appears to be absent. The ca. 1 to 2 ps component represents the internal conversion of molecules in a fluid-like environment, similar to the process observed in solution. The long decay is unique to liposomes and a result of van der Waals forces imposed on the molecule by the lipid as they pack around the provitamin in regions of lower fluidity. The evidence for this hypothesis is supported by (1) the difference in the longest lifetime (τ_2) measured between DHC and ergo in DPPC, (2) the difference in the longest lifetime between DHC in DPPC and DLPC and (3) the similarity between the time constants for ergo and DHC in DLPC lipid bilayers, where the double-bond in ergo may not interact significantly with the DLPC tails. Additional evidence supporting van der Waals interactions as a key component is shown for the case of DHC-acetate, where the molecule cannot be incorporated into the DLPC lipid bilayer.

References

(1)   Tian, X. Q.; Holick, M. F. A Liposomal Model That Mimics the Cutaneous Production of Vitamin D3: Studies of the Mechanism of the Membrane-Enhanced Thermal Isomerization of Previtamin D3 to Vitamin D3. *J. Biol. Chem.* **1999**, *274* (7), 4174–4179.

(2)   Briuglia, M. L.; Rotella, C.; McFarlane, A.; Lamprou, D. A. Influence of Cholesterol on Liposome Stability and on in Vitro Drug Release. *Drug Deliv. Transl. Res.* **2015**, *5* (3), 231–242.

(3)   Keller, R. K.; Arnold, T. P.; Fliesler, S. J. Formation of 7-Dehydrocholesterol-Containing Membrane Rafts in Vitro and in Vivo, with Relevance to the Smith-Lemli-Opitz Syndrome. *J. Lipid Res.* **2004**, *45* (2), 347–355.

(4)   Berring, E. E.; Borrenpohl, K.; Fliesler, S. J.; Serfis, A. B. A Comparison of the Behavior of Cholesterol and Selected Derivatives in Mixed Sterol-Phospholipid Langmuir Monolayers: A Fluorescence Microscopy Study. *Chem. Phys. Lipids* **2005**, *136* (1), 1–12.

(5)   Cournia, Z. PhD. Thesis. **2006**.

(6)   Bernsdorff, C.; Winter, R. Differential Properties of the Sterols Cholesterol, Ergosterol, Beta-Sitosterol, Trans-7-Dehydrocholesterol, Stigmasterol and Lanosterol on DPPC Bilayer Order. *J. Phys. Chem. B* **2003**, *107* (38), 10658–10664.

(7)   Chen, C.; Tripp, C. P. A Comparison of the Behavior of Cholesterol, 7-Dehydrocholesterol and Ergosterol in Phospholipid Membranes. *Biochim. Biophys. Acta - Biomembr.* **2012**, *1818* (7), 1673–1681.

(8)   Guo, Y.; Pogodin, S.; Baulin, V. A. General Model of Phospholipid Bilayers in Fluid Phase within the Single Chain Mean Field Theory. *J. Chem. Phys.* **2014**, *140* (17).

(9)   Bui, T. T.; Suga, K.; Kuhl, T. L.; Umakoshi, H. Melting-Temperature-Dependent Interactions of Ergosterol with Unsaturated and Saturated Lipids in Model Membranes. *Langmuir* **2019**, *35*, 10640–10647.

(10)   Nojima, Y.; Iwata, K. Viscosity Heterogeneity inside Lipid Bilayers of Single-Component Phosphatidylcholine Liposomes Observed with Picosecond Time-Resolved Fluorescence Spectroscopy. *J. Phys. Chem. B* **2014**, *118* (29), 8631–8641.

Chapter 5

Photoproduct Formation from Provitamins in Solution

Introduction

Upon return to the ground state, provitamin D_3, D_2 and DHC-acetate undergo ring-opening and conformational changes to previtamin D_3, previtamin D_2 or a previtamin D_3-acetate species. Figure 5.1 shows the conformer relaxation process of previtamin D_3.
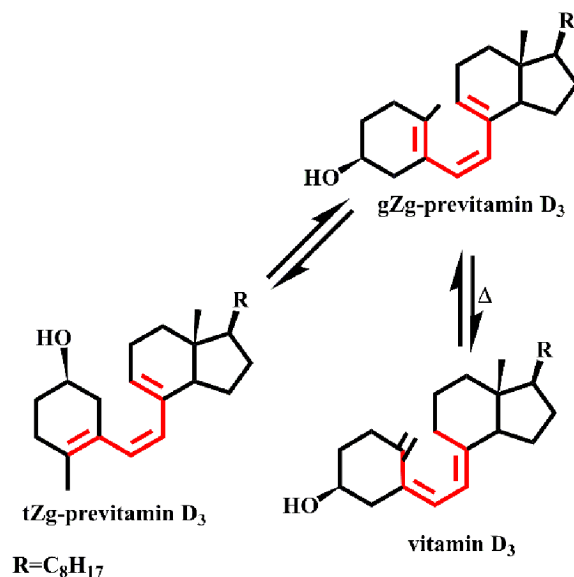
Figure 5.1: Ground state relaxation process of gZg to tZg previtamin D_3. The tZg species is more energetically favorable than the gZg conformation. From the gZg species, the molecule can undergo a hydride shift and thermal relaxation to form vitamin D_3. The photoexcitation of the tZg and gZg species results in other side products, such as tachysterol and lumisterol (Figure 1.1) that are not biologically useful.

As discussed in Chapter 1, Tian and Holick[1] have proposed that the accelerated formation of vitamin D_3 in human skin and DPPC lipid bilayers arises from stabilizing the gZg previtamin D_3 species (Figure 5.1) through hydrogen bonding and van der Waals interactions between the molecule and the lipid. Arruda *et al.*[2] used TD-DFT calculations paired with steady state and time resolved spectroscopic measurements to assign the gZg to tZg relaxation process to be ~7 ps in free solution, where most of the population relaxes down to the tZg conformation. The photoproduct absorption and conformer relaxation of DHC is best monitored between 330 nm and ~250-290 nm in solution, therefore it is necessary to use a UV continuum from 250-400 nm to extend these studies to ergo and DHC-acetate. In order to provide a baseline to test Tian and Holick's proposed liposome model, this chapter will investigate conformer relaxation for DHC, ergo and DHC-acetate in 2-butanol and hexadecane. In Chapter 6, we will use these measurements to interpret the ground state photochemistry in a more constrained liposome environment.

Time Resolved Conformer Relaxation in Solution

The conformer relaxation of DHC and small molecule analogs were studied extensively in solution. Arruda et.al.[2] used time resolved measurements combined with steady state photolysis measurements to understand conformer relaxation on the ground state. Much of the conformer relaxation of the initially formed gZg conformer to tZg previtamin D_3 takes place on a timescale of ~6 to 7 ps and is largely independent of solvent. We have extended these measurements to explore the ground state relaxation of previtamin D_2 and previtamin D_3-acetate in 2-butanol and hexadecane. Following the excitation of the provitamins in 2-butanol and hexadecane, selected time lineouts are illustrated in Figure 5.2. These time lineouts from time resolved measurements in the UV region show that the conformer relaxation process of DHC

analogs, ergo and DHC-acetate are similar to DHC. Following excitation, the difference spectra

of all three provitamins have a ground state bleach at ~270-290 nm and photoproduct absorption

peaking around ~305 nm.
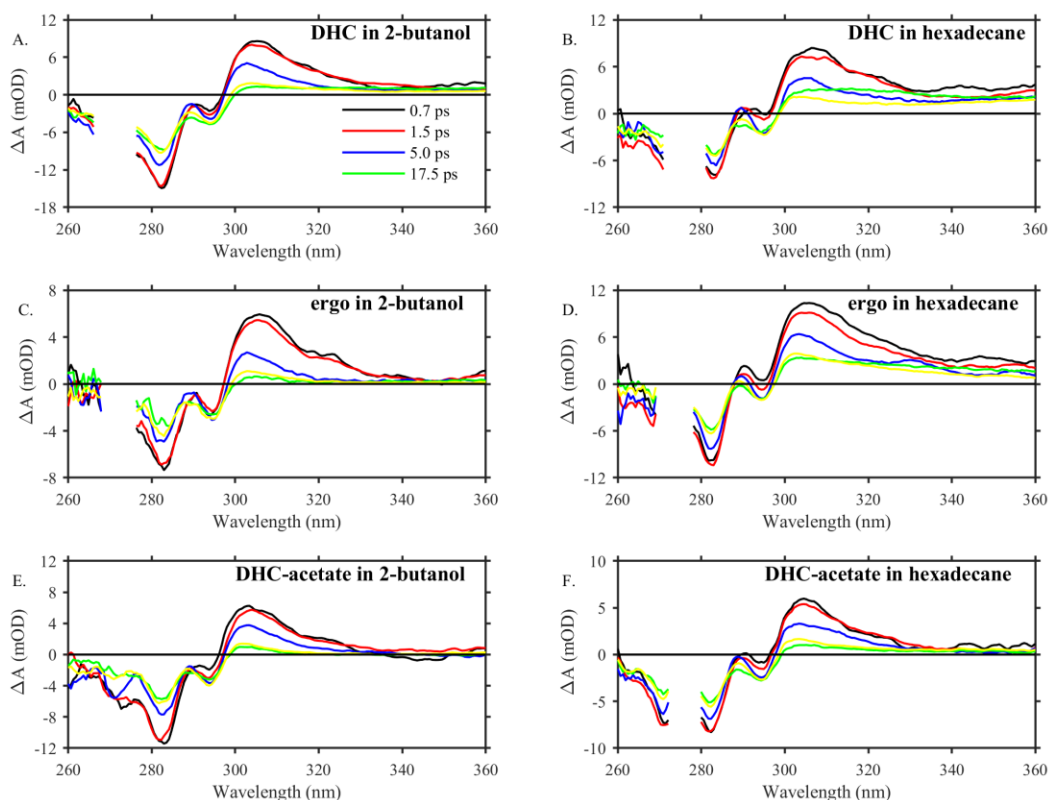
Figure 5.2: Selected UV time delays following excitation of the three provitamins in (A, C, E) 2-butanol and (B, D, F) hexadecane. Pump scatter (removed wavelengths) was removed between 268-275 nm. The legend shown in plot A is the same for all the plots shown.

The time constants of the conformer relaxation process obtained from the global fitting analysis

(described in Chapter 2 and Chapter 3) are similar in 2-butanol, however the relaxation process

of previtamin D_3-acetate appears to be slightly longer in hexadecane. The following section will

summarize the data obtained for the three previtamins in 2-butanol and hexadecane.

Conformer relaxation in 2-butanol: The conformer relaxation data obtained in transient

absorption measurements in 2-butanol required two components to minimize the residuals.

92

Figure 5.3 illustrates the kinetics, fit and residuals at selected wavelengths. The residuals at early times are nearly at baseline. The time constants obtained from the global fits are summarized in Table 5.1. The time constants do not show a distinctive difference between the three compounds in 2-butanol. This suggests that the kinetics do not show substantial contributions from vibrational cooling during the previtamin D relaxation. Such relaxation would result in wavelength dependent constants from 305 to 350 nm[2,3].
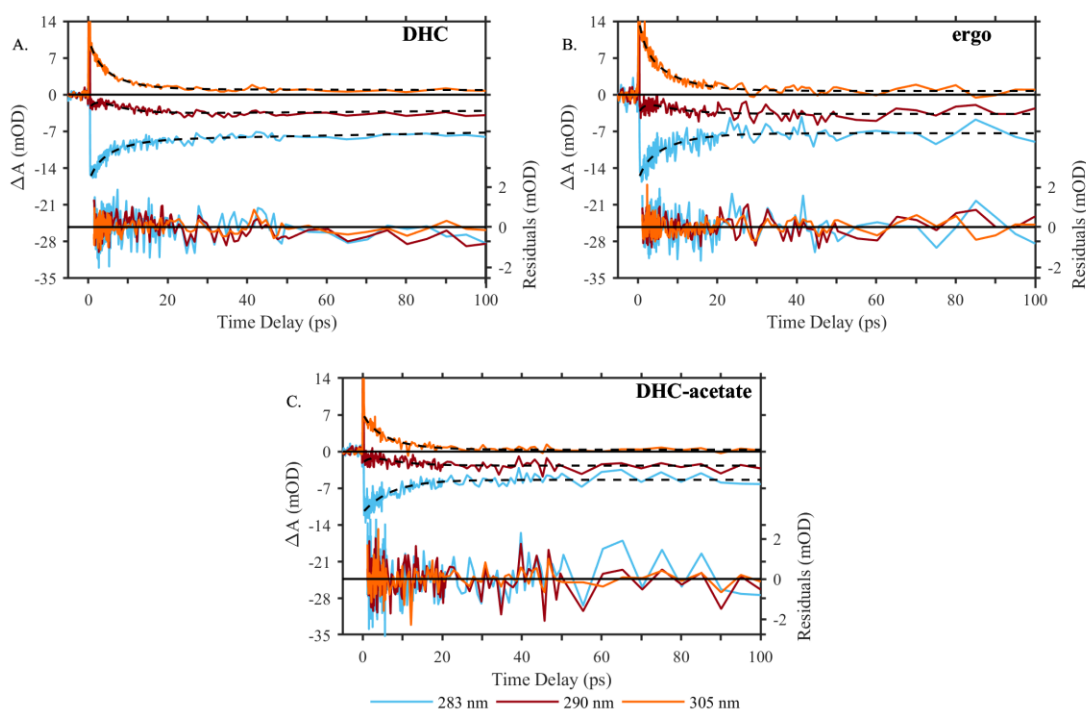
Figure 5.3: Selected UV kinetics plotted at 283 nm, 290 nm and 305 nm (blue, red, orange), fits (black dash) and residuals (shifted for clarity) following excitation of (A) DHC, (B) ergo (scaled) and (C) DHC- acetate in 2-butanol. The legend located at the bottom of plot C is the same for all three plots.

Table 5.1: Summary of conformer relaxation time constants obtained following excitation of the three provitamin D species in 2-butanol. Time constants obtained from a global fit analysis to the data from ~280-400 nm.

Provitamin	τ_1 (ps)	τ_2 (ps)	τ_3 (ps)
DHC	1.29 ± 0.30	6.63 ± 0.48	Permanent >>100ps
ergo	1.41 ± 0.11	6.65 ± 1.81	Permanent >>100ps
DHC -acetate	1.77 ± 0.06	6.65 ± 0.56	Permanent >>100ps

In Chapter 3 we used the DADS obtained for each time component to understand the biexponential nature of the fast and slow components. Here we extend this technique to quantify the time components obtained in the global fit in the UV region. Figure 5.4 shows that the DADS of the time components obtained following excitation of the three provitamins in 2-butanol do not show a distinctive difference. The fast 1.30- 1.70 ps component corresponds to a mixture of excited states of the previtamins, the slow ca. 7 ps component corresponds to conformer relaxation and the long time permanent signal corresponds to the photoproduct formed as reported by Arruda *et al.*[2] Unlike excited state measurement where all time constants were used to interpret the dynamics, the only time components that are relevant to analyze for product formation in the UV data are the slow, 6-7 ps component and the permanent component.
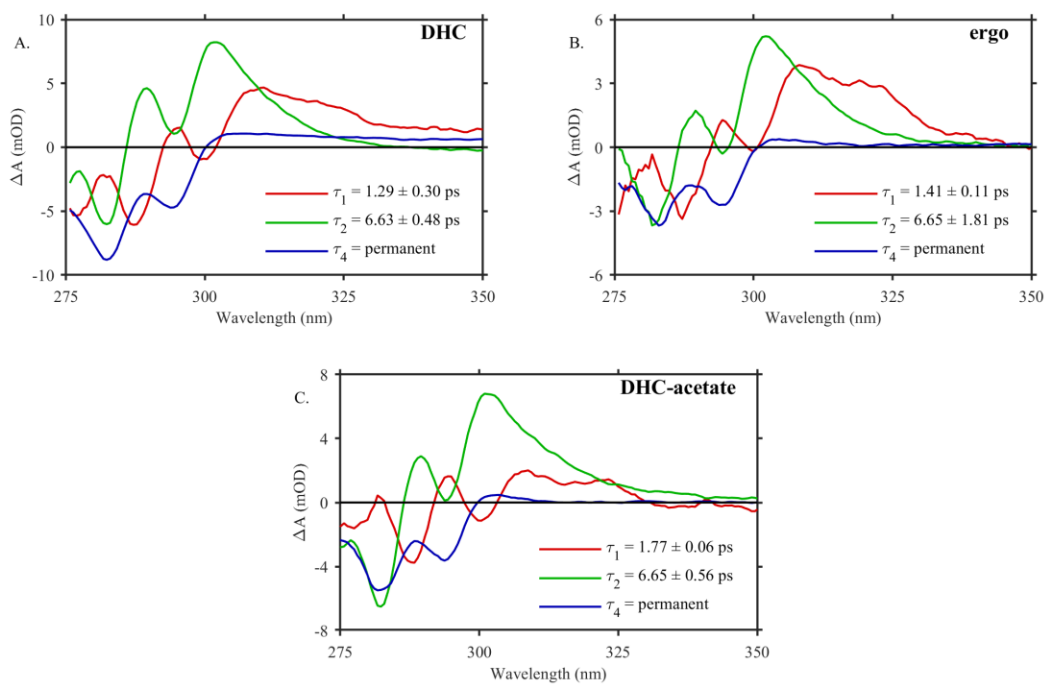
Figure 5.4: UV DADS obtained from the global fit analysis following excitation of (A) DHC, (B) ergo and (C) DHC-acetate in 2-butanol.

Conformer relaxation in hexadecane: The 6-7 ps component obtained from globally fitting the previtamin data in 2-butanol is similar in hexadecane. In this nonpolar environment, the conformer relaxation of previtamin D_2 and previtamin D_3 do not show significant differences. However, the long component of previtamin D_3-acetate becomes slightly more pronounced. Since the noise level of the probe is significantly higher in the UV region compared to the visible region (Chapter 3), the differences between the previtamins are not distinguishable without fitting the data. Figure 5.5 shows selected wavelengths of fits and residuals obtained from globally fitting the data from ~280-400 nm for the three previtamins in hexadecane. The over-under of the residuals at early times, may suggest that vibrational cooling is more pronounced for the relaxation of previtamin D_3-acetate than for previtamin D_3 or previtamin D_2, however more measurements are needed to quantify this feature. The time constants obtained from the global fit are summarized in Table 5.2. As observed in 2-butanol, the time constants do not show a

distinctive difference between previtamin D_3 and previtamin D_2. However, the relaxation of the previtamin D_3-acetate species appears to be slightly longer than the other two compounds.
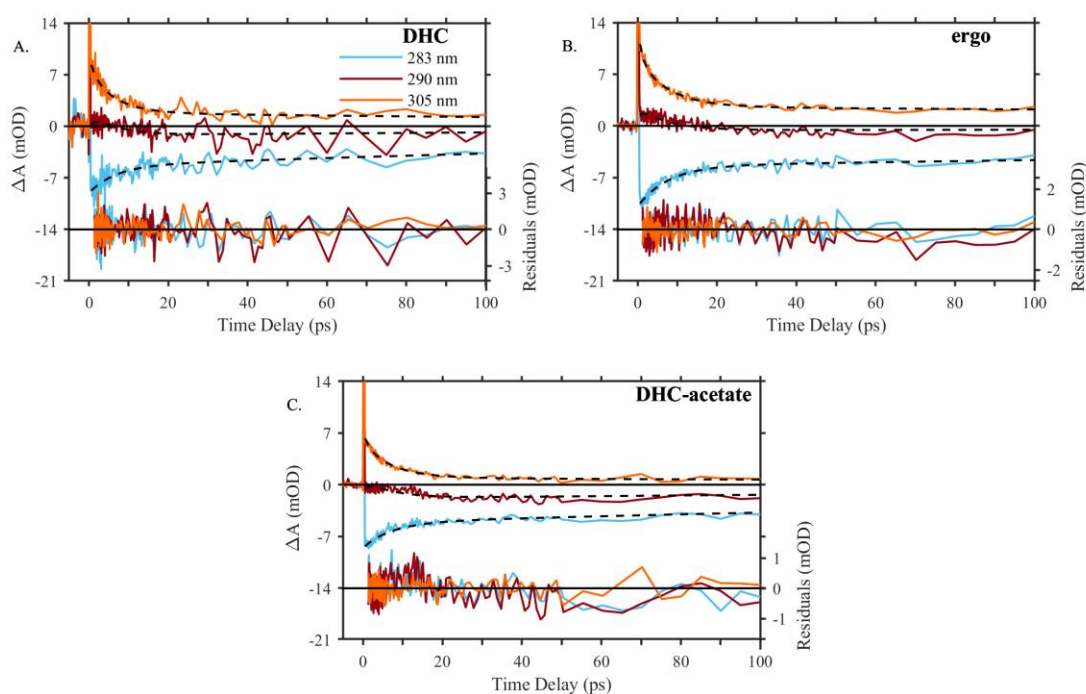
Figure 5.5: Selected UV kinetics plotted at 283 nm, 290 nm and 305 nm (blue, red and orange), fits (black dash) and residuals (shifted for clarity) following the excitation of (A) DHC, (B) ergo and (C) DHC-acetate in hexadecane. The legend in plot A is the same for plots B and C.

Table 5.2: Summary of conformer relaxation time constants obtained following excitation of the three provitamin D species in hexadecane. Time constants obtained from a global fit analysis to the data from ~280-400 nm.

Provitamin	τ_1 (ps)	τ_2 (ps)	τ_3 (ps)
DHC	1.41 ± 0.21	6.35 ± 0.20	Permanent >>100ps
ergo	1.24 ± 0.27	6.72 ± 1.40	Permanent >>100ps
DHC-acetate	1.78 ± 0.47	7.36 ± 0.31	Permanent >>100ps

The fits summarized above suggest that the hexadecane solvent may affect the conformational relaxation by packing around the acetate group and constraining the motion. The DADS for all three compounds in hexadecane are summarized in Figure 5.6. As in 2-butanol, the DADS are

similar for all three compounds. There appears to be a long-lived solvent contribution that varied from run to run. This contribution can be estimated from the plateau between 340 and 360 nm where the previtamin signal should decay to zero. This is consistent with earlier measurements on DHC in alkane solvents[2,4].
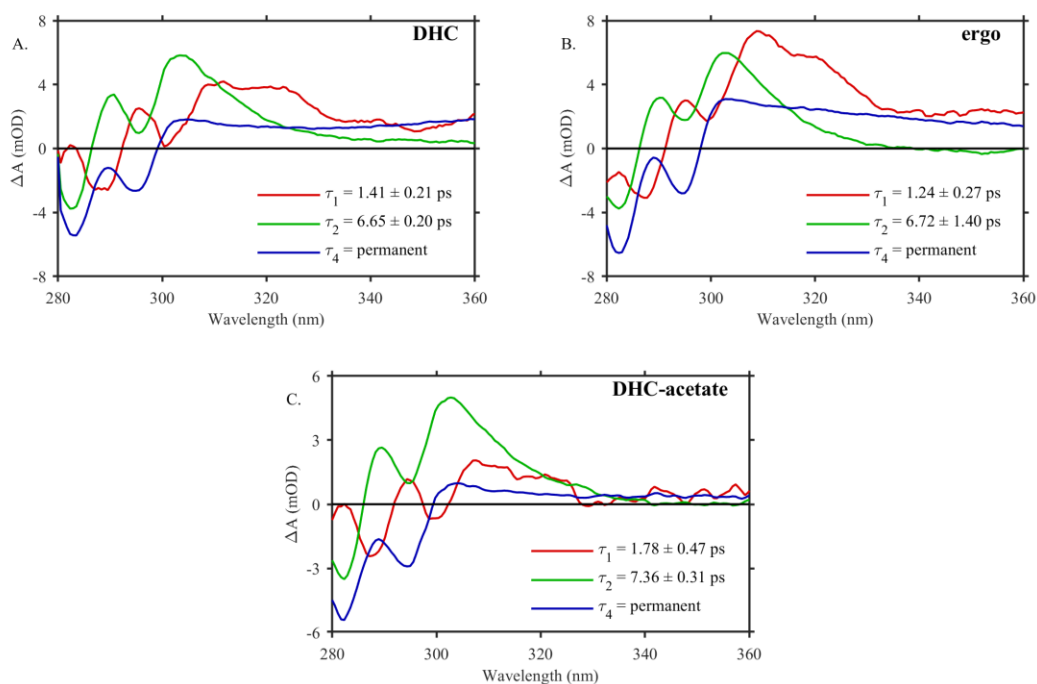
Figure 5.6: UV DADS obtained from the global fit analysis following excitation of (A) DHC, (B) ergo and (C) DHC-acetate in hexadecane.

Steady State Photolysis

The time resolved measurements that were obtained only provided information on processes that occur within the first 100 ps. To understand the distribution of previtamin conformers on a longer timescale, we also investigated the long time photoproduct distribution by steady state techniques. Steady state photolysis studies were done at ~17 °C to determine the long time product spectrum. As demonstrated by Arruda *et al.*[2] a blue shifted spectrum

corresponds to the tZg conformation, whereas a red shifted spectrum identifies contributions of the gZg conformer. Arruda *et al.*[2] has also demonstrated that the steady state difference spectra are similar to the transient data at long times. The most significant difference is in the definition of vibronic structure in the region between 260-300 nm.

Steady state photolysis in 2-butanol and hexadecane: In steady state measurements, the difference spectrum, ΔA, is given by,

$$\Delta A = \text{previtamin}_{t=t'} - \text{provitamin}_{t=0} \tag{5.1a}$$

$$\text{previtamin}_{\text{reconstructed}} = \Delta A + \alpha * \text{provitamin}_{t=0} \tag{5.1b}$$

where t = t' is some time, t' (seconds) after irradiation, t = 0 is the ground state before irradiation and α is a scale factor <<1. An accumulation of side products, such as tachysterol or lumisterol is indicated by structural changes in the depletion region, between 270-300 nm and absorption ~305 nm. A substantial accumulation of side products becomes more apparent in later time scans, especially when the difference signal starts to become positive. The scans that are structurally different than the earliest time point (2s) were not used in any of the reconstructed previtamin D spectra (Equation 5.1b). Figure 5.7 shows the steady state difference spectra in 2-butanol. Although the 4s difference spectra may be good in DHC and ergo, only the 2s lineout was used to construct previtamin D_3, previtamin D_2, and previtamin D_3-acetate.
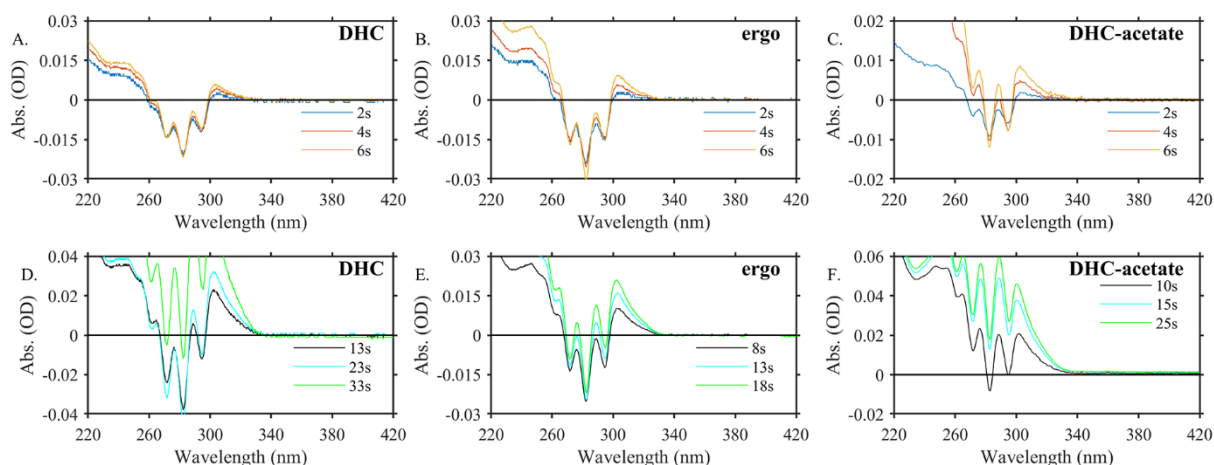
Figure 5.7: Secondary photoproducts, tachysterol and lumisterol that form at late times. The bottom plots show steady state lineouts of the depletion of DHC, ergo and DHC-acetate at (A-C) early and (D-F) late times in 2-butanol. Scaled to relative intensity.

Steady state photolysis measurements were also performed in hexadecane. The criteria for reconstructing the photoproduct spectrum in hexadecane is the same as mentioned above for 2-butanol and in Equation 5.1b. Figure 5.8 shows lineouts of steady state photolysis on DHC, ergo and DHC-acetate in hexadecane. The time lineouts that were used to reconstruct the previtamin D_3, previtamin D_2 and previtamin D_3-acetate spectra were the first 4s, 4s and 2s respectively.
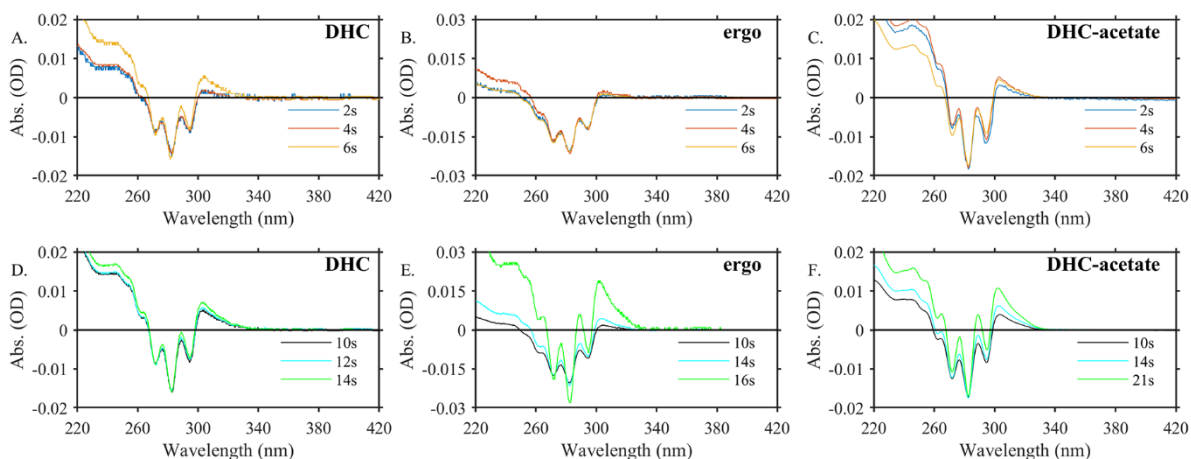
Figure 5.8: Steady state lineouts showing the depletion of DHC, ergo and DHC-acetate at (A-C) early and (D-F) late times in hexadecane. Scaled to relative intensity.

99

Figure 5.9 shows the reconstructed previtamin D_3, previtamin D_2, and previtamin D_3-acetate

species from the steady state photolysis. The three previtamins do not show significant

differences between each other and the peak of the reconstructed photoproduct appears to be

independent of solvent. To estimate the peak and FWHM of the distribution, each previtamin

was fit to a Gaussian function. The Gaussian fit for each previtamin species are illustrated in

Figure 5.10. Table 5.3 summarizes the peak and FWHM of each Gaussian used to fit the data.

The peak of each Gaussian is ca. 260 nm with a FWHM of 6000-6700 cm^{-1}. The Gaussian peak

and FWHM are in agreement with the parameters used for previtamin D_3 in heptane ~6500 cm^{-1} [2]

and ethanol ~6000 cm^{-1} [5].
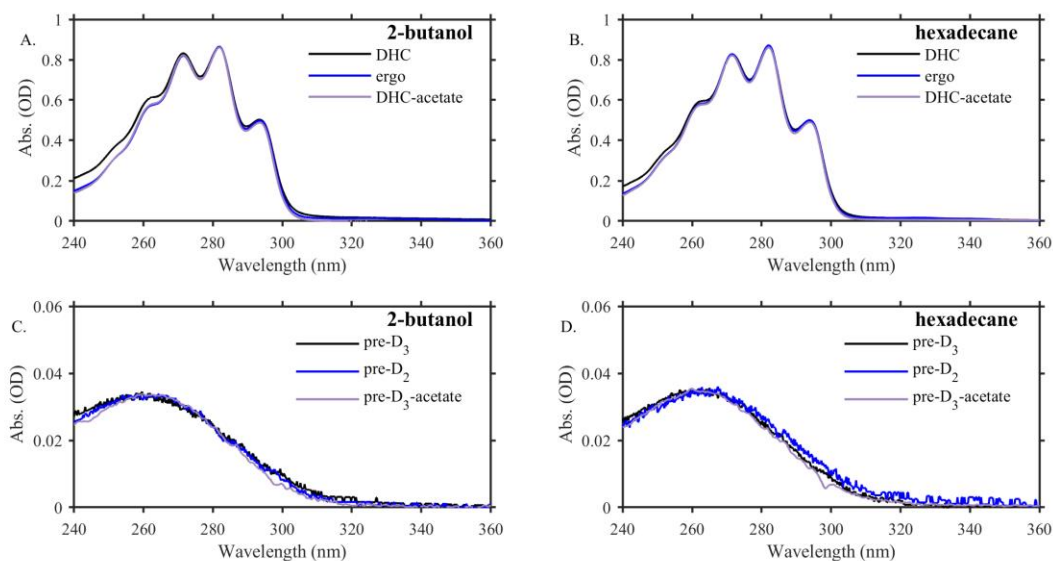
Figure 5.9: Ground state spectra of DHC and analogs in (A) 2-butanol and (B) hexadecane. Estimated previtamin D spectra (obtained from Equation 5.1b) consisting of gZg and tZg conformers in (C) 2-butanol and (D) hexadecane. Plots A-D scaled to relative intensity.
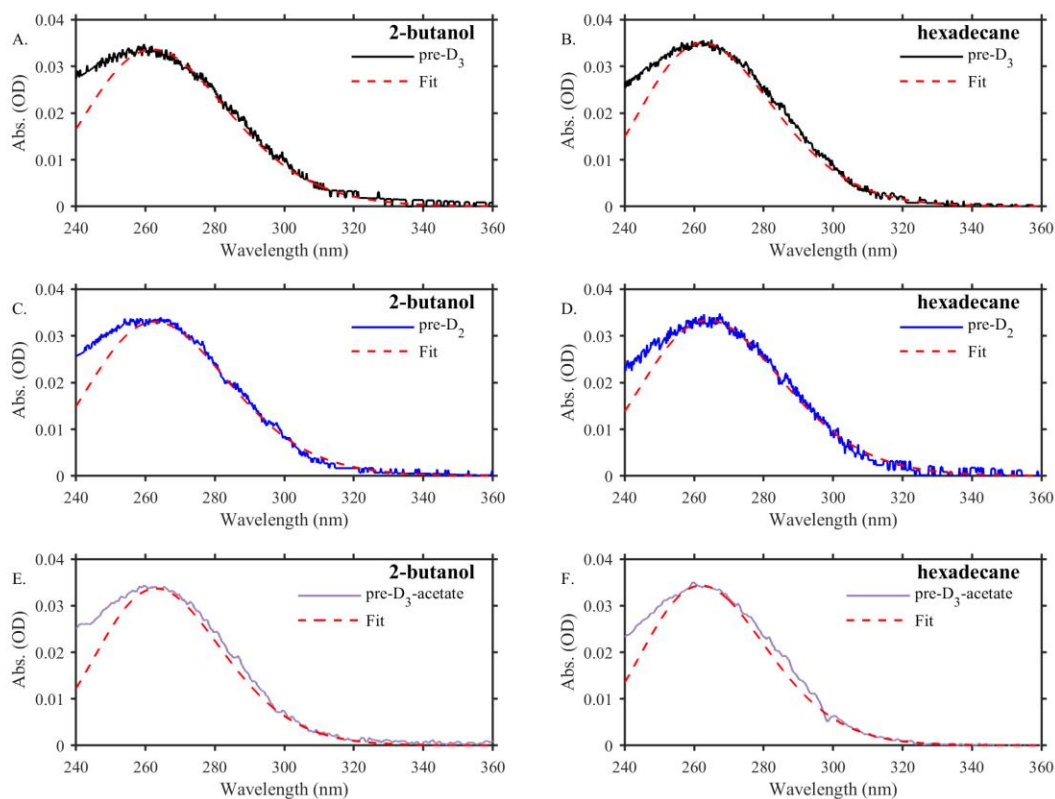
Figure 5.10: Gaussian fit (red dashed) to the three previtamin D species in (A, C, E) 2-butanol and (B, D, F) hexadecane.

Table 5.3: Gaussian parameters used to fit the reconstructed previtamin D species in 2-butanol and hexadecane.

Previtamin species	Peak of Gaussian (nm) in 2-butanol	FWHM of Gaussian (cm^{-1}) in 2-butanol	Peak of Gaussian (nm) in hexadecane	FWHM of Gaussian (cm^{-1}) in hexadecane
pre-D$_3$	261.5 ± 0.8	6672.8 ± 232.6	258.8 ± 3.8	6688.7 ± 237.2
pre-D$_2$	261.5 ± 1.2	6383.0 ± 345.0	261 ± 3.0	7043.4 ± 315.4
pre-D$_3$-acetate	260 ± 3.0	5962.5 ± 75.5	263.5 ± 1.5	5962.5 ± 75.5

Steady state measurements compared to TA: In order to understand the conformer relaxation process observed in transient measurements, we compare the transient products with steady state measurements. In prior measurements studying the conformer relaxation of DHC in solution, the difference spectra obtained from steady state measurements approximately agrees with TA data at long times, although there are some significant differences[2]. Figure 5.11 shows a comparison of the steady state difference spectra compared to early and late time difference spectra following excitation of the three provitamins in both solvents. Time resolved data for previtamin D_3, previtamin D_2 and previtamin D_3-acetate are more structured at early times than at a few hundred of picoseconds after excitation. The sharp structure in the transient data reflects an early time conformer distribution whereas the less structured spectra in later times is suggestive of a change in the previtamin distribution. Of particular significance is the definition of vibronic structure in the steady state difference spectrum compared with less definition in the transient product at ca. 100 ps.
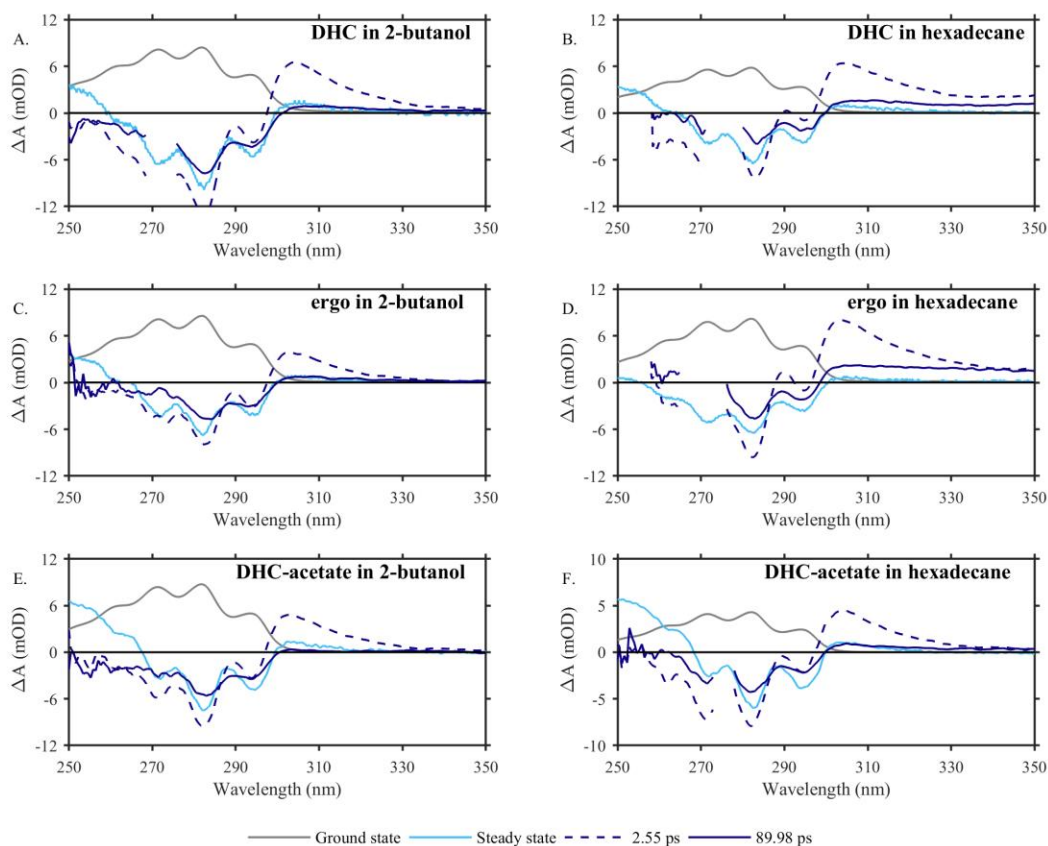
Figure 5.11: Comparison of steady state photolysis (light blue) and transient data for time delays at 2.55 ps (dash blue) and ~100 ps (dark blue) following excitation of the three provitamins in (A, C, E) 2-butanol and (B, D, F) hexadecane. Steady state and ground state scaled for comparison to transient data. The legend located at the bottom is the same for all six plots.

Comparison of time resolved data in 2-butanol and hexadecane: In order to gain a deeper physical insight for the time constants obtained in transient data for the UV region, we use have excited state information obtained in Chapter 3. We have combined the UV and visible data and performed a global fit to the entire spectrum. Figure 5.12 shows the DADS obtained over the region of 260-650 nm following excitation of the three provitamins in 2-butanol and hexadecane. In the UV and visible regions, the difference spectra report on different parts of the photochemical reaction. Since the influence of conformer relaxation, vibrational cooling and excited state behavior on the spectrum is a function of wavelength, fitting the data across the spectrum can alter the lifetimes compared to fitting in respective regions. In Figure 5.12, the first

and second components (red and green) corresponds to the excited state spectra, the third component (blue) corresponds to gZg to tZg conformer relaxation and the fourth component (cyan) corresponds to photoproduct formation in the UV region and a solvent component in the visible region.
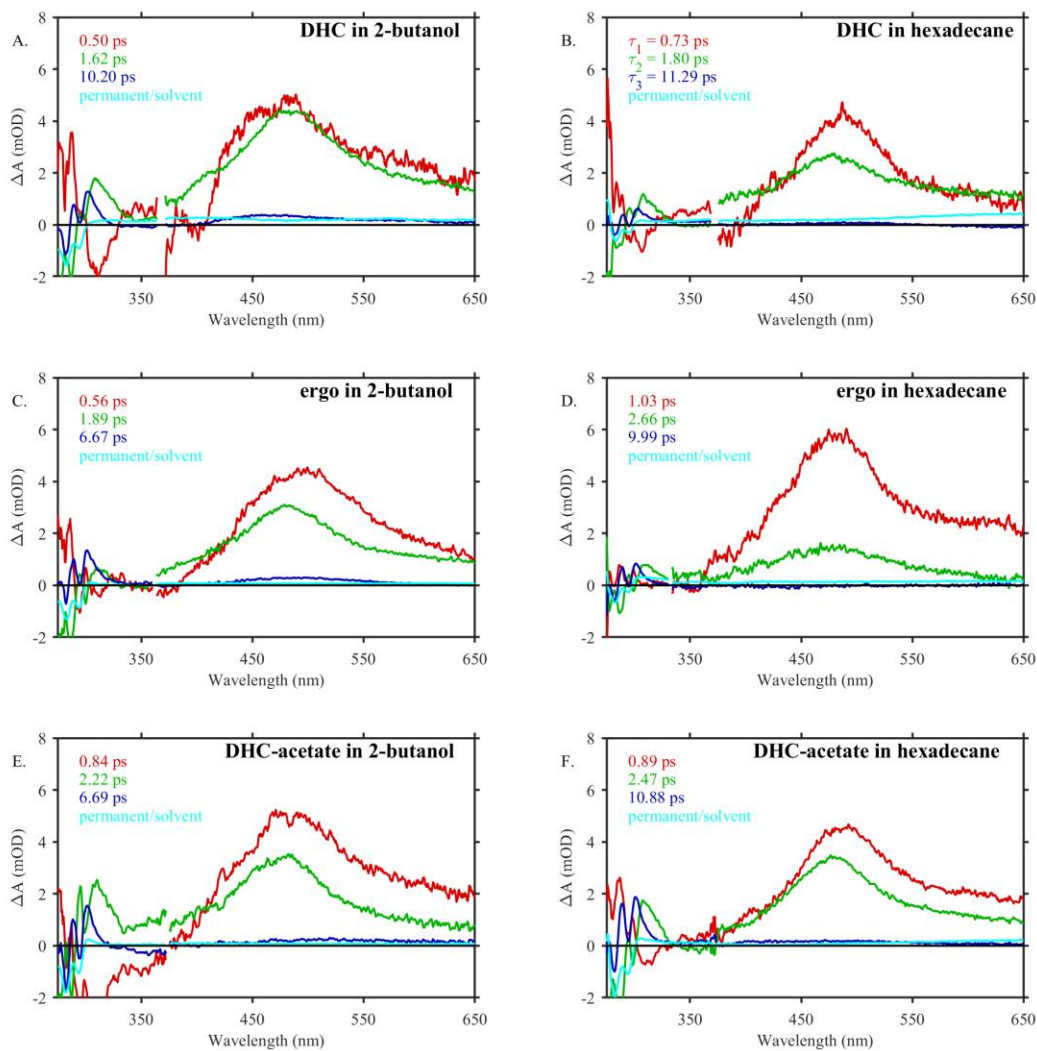
Figure 5.12: DADS for the three previtamins in (A, C, E) 2-butanol and (B, D, F) hexadecane obtained from a global fit from ~260-650 nm. The removed wavelengths are where separate UV (250-400 nm) and visible (350-700 nm) data was concatenated. Figures scaled to relative intensities.

Photoproduct distribution in 2-butanol and hexadecane: To further explore the relaxation process observed for the three previtamins in 2-butanol and hexadecane we use the steady state results to interpret the kinetics observed at ~ 283 nm. Figure 5.13 (A-B) shows a comparison of the bleach signal for the three compounds in 2-butanol and in hexadecane. The recovery observed in the bleach signal is suggestive of conformer relaxation[2]. Figure 5.13 (C-D) shows that the center of the reconstructed previtamin D_2 and previtamin D_3-acetate species are nearly identical to previtamin D_3 in the two solvents. The blue shifted spectra suggests that most of the distributions of the three previtamins are in the tZg conformation in the steady state measurements[2].The decay of the bleach in the transient measurements reflects the increase in the tZg population on a picosecond timescale.
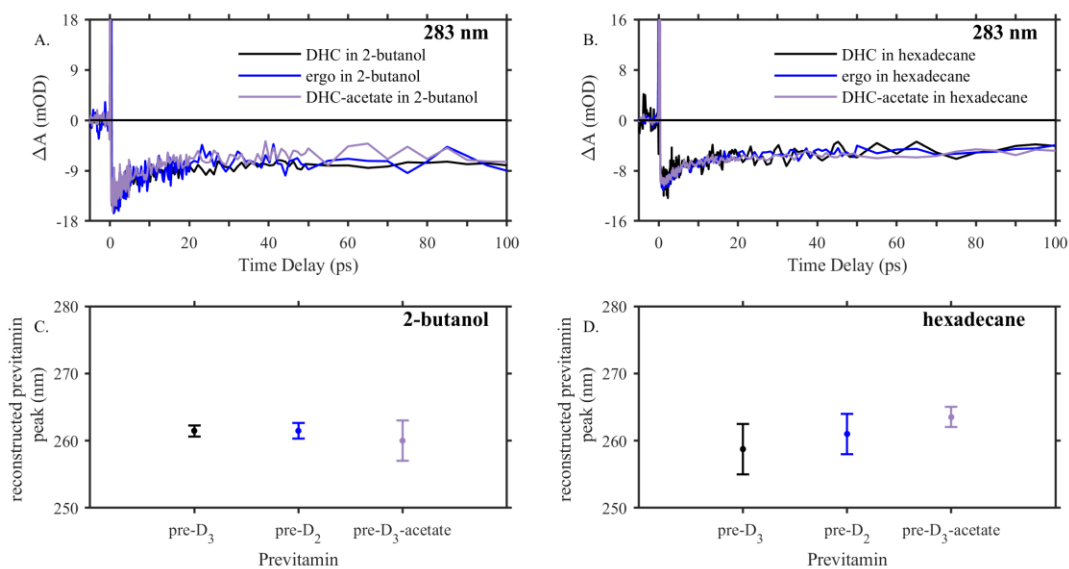
Figure 5.13: Bleach signal comparison at 283 nm of the three previtamins in (A) 2-butanol and (B) hexadecane. Kinetics scaled to relatives intensities. Peak of reconstructed photoproducts in (C) 2-butanol and (D) hexadecane.

It is not surprising that the distribution of the previtamin conformers are similar in 2-butanol and hexadecane. However, the timescale for the isomerization process is different in these two solvents. In hexadecane, the conformer relaxation of previtamin D-acetate ($\tau_2 = 7.36 \pm 0.31$ ps) is

slightly longer than the conformer relaxation of previtamin D_2 ($\tau_2 = 6.72 \pm 1.40$ ps) and previtamin D_3 ($\tau_2 = 6.35 \pm 0.20$ ps). In 2-butanol, the timescale for conformer isomerization is similar for the three previtamins ($\tau_{2, D3} = 6.63 \pm 0.48$ ps, $\tau_{2, D2} = 6.65 \pm 1.81$ ps, $\tau_{2, D3\text{-}acetate} = 6.65 \pm 0.56$ ps). The only significant difference observed is for previtamin D-acetate in hexadecane. All of the other time constants are the same within error. The solvent viscosity for 2-butanol is slightly higher than hexadecane (3.10 cP and 3.03 cP, respectively)[6], although the difference is not significant. It is possible that the size of the acetate group could slow down the gZg to tZg isomerization, however the size of the acetate group does not suggest to play a significant role since the relaxation time is similar to previtamin D_3 and previtamin D_2 in 2-butanol. This solvent viscosity cannot account for any difference in the isomerization process of previtamin D_3-acetate in 2-butanol and hexadecane.

In 2-butanol, all three previtamins have the ability to hydrogen bond to the solvent. This would make the relaxation process longer than in hexadecane rather than shorter. Because there is not a solvent dependence for previtamin D_3 and previtamin D_2, hydrogen bonding is unlikely to explain the observation for previtamin D_3-acetate. Since the size of the acetate group and hydrogen bonding do not appear to be the important factors, the acetate group may experience a specific packing effect in hexadecane that influences both excited state decay (see Chapter 3) and conformer relaxation.

Conclusion

The purpose of this study was to test the conformer relaxation of the previtamin D_3 analogs, previtamin D_2 and previtamin D_3-acetate, in a simple environment where previtamin D_3 was already well studied. The conformer relaxation process is similar for all three previtamins. Our results show that all three molecules have a bleach signal from ~250-300 nm and prompt photoproduct absorption ~305 nm. In 2-butanol, the lifetimes obtained for the gZg to tZg conformational relaxation are independent of the specific previtamin ($\tau_{2, D3} = 6.63 \pm 0.48$ ps, $\tau_{2, D2} = 6.65 \pm 1.81$ ps, $\tau_{2, D3\text{-}acetate} = 6.65 \pm 0.56$ ps). In hexadecane, the conformational relaxation from the gZg to tZg previtamin D_3–acetate species is slightly longer ($\tau_2 = 7.36 \pm 0.31$ ps) compared to dynamics in 2-butanol ($\tau_2 = 6.65 \pm 0.56$ ps) and to the other previtamins ($\tau_{2, D3\text{-}hex} = 6.35 \pm 0.20$ ps, $\tau_{2, D2\text{-}hex} = 6.72 \pm 1.40$ ps). Steady state measurements in 2-butanol and hexadecane show that the distribution of the reconstructed photoproducts for previtamin D_2 and previtamin D_3-acetate are nearly identical to previtamin D_3. The blue shift relative to the provitamin spectra suggests that most of the distribution is in the tZg conformation. The solvent does not appear to significantly alter the shape or peak of the reconstructed previtamin spectra.

The studies in this chapter show that conformer relaxation from the gZg to tZg takes place for all three previtamins on ~6-7 ps timescale in free solution where the process is nearly independent of previtamin and polarity of the solvent. The product formed within 100 ps is similar to the steady state product, although there is evidence for more conformational heterogeneity.

The next chapter will discuss the conformational relaxation of the three previtamins in lipid membranes. The two significant results from this chapter that are relevant to the membrane environment are hydrogen bonding (2-butanol) and packing effects from long alkane tails

(hexadecane). The fits from the global analysis of our transient spectra suggest that these parameters do not significantly alter the conformer relaxation process between the three previtamins in the free solution environment. Therefore, any significant changes in the liposomes can be attributed to the lipid environment and are not inherent properties of the specific molecules.

References

(1)   Tian, X. Q.; Holick, M. F. A Liposomal Model That Mimics the Cutaneous Production of Vitamin D3: Studies of the Mechanism of the Membrane-Enhanced Thermal Isomerization of Previtamin D3 to Vitamin D3. *J. Biol. Chem.* **1999**, *274* (7), 4174–4179.

(2)   Arruda, B. C., Peng, J., Smith, B. Spears, K. G., Sension, R. J. Photochemical Ring-Opening and Ground State Relaxation in α-Terpinene with Comparison to Provitamin D 3 Photochemical Ring-Opening and Ground State Relaxation in α-Terpinene with Comparison to Provitamin D 3 Brenden C . Arruda , Jian Peng , Broc Smith , K. *J. Phys. Chem.* **2012**.

(3)   Arruda, B. C.; Smith, B.; Spears, K. G.; Sension, R. J. Ultrafast Ring-Opening Reactions: A Comparison of α-Terpinene, α-Phellandrene, and 7-Dehydrocholesterol with 1,3-Cyclohexadiene. *Faraday Discuss.* **2013**, *163*, 159–171.

(4)   Tang, K. C.; Rury, A.; Orozco, M. B.; Egendorf, J.; Spears, K. G.; Sension, R. J. Ultrafast Electrocyclic Ring Opening of 7-Dehydrocholesterol in Solution: The Influence of Solvent on Excited State Dynamics. *J. Chem. Phys.* **2011**, *134* (10).

(5)   Fuss, W.; Ho, T.; Hering, P.; Kompa, K. L.; Lochbrunner, S. Ring Opening in the Dehydrocholesterol - Previtamin D System Studied by Ultrafast Spectroscopy. **1996**, 921–927.

(6)   Lide, D. R.; Baysinger, G. CRC Handbook of Chemistry and Physics: A Ready-Reference

Book of Chemical and Physical Data. *Choice Rev. Online* **2004**, *41* (08), 41-4368-41–

4368.

Chapter 6

Photoproduct Formation from Provitamins in Lipid Bilayers

Introduction

Upon returning to the ground state, previtamin D_3, previtamin D_2 and previtamin D_3-acetate undergo conformational relaxation to form a stable previtamin species (Figure 5.1). Tian and Holick[1] proposed that DPPC lipid bilayers closely mimic the human skin environment by stabilizing the gZg previtamin D_3 species. To test the contributions of the lipid environment to gZg stabilization, we use spectroscopic methods to probe the conformations and relaxation of previtamin D_3 in lipid bilayers. This chapter will explore conformational relaxation in terms of hydrogen bonding, van der Waals interactions and lipid tail length. The relaxation of previtamin D_3 will be compared to the relaxation of previtamin D_2 and previtamin D_3-acetate in DPPC liposomes to identify van der Waals and hydrogen bonding effects. To investigate the influence of the lipid tail length on the conformational relaxation, previtamin D_3 will be explored in DLPC lipid bilayers. The results in free solution, discussed in Chapter 5 will be used to interpret the results.

Time Resolved Conformer Relaxation in DPPC Lipid Bilayers

Having performed the necessary background measurements (Chapter 2 and Chapter 5) we are now ready to study the conformer relaxation in DPPC lipid bilayers using UV probe wavelengths ranging from ~275-360 nm. These measurements were performed using 265 nm excitation and a 30mol-% provitamin loading. Selected time delay lineouts from time resolved data are shown in Figure 6.1. The transient spectra in Figure 6.1 are characterized by overlapping ground state bleach, excited state absorption, and photoproduct absorption between 270 nm and 290 nm. The bleach diminishes above ~290 nm and is followed by an immediate peak of product absorption at ~305 nm. This product absorption dominates the longer wavelengths, similar to our observation in solution measurements. The offset that is presented in the data at long times is most likely a contribution from thermal lensing (Chapter 2).
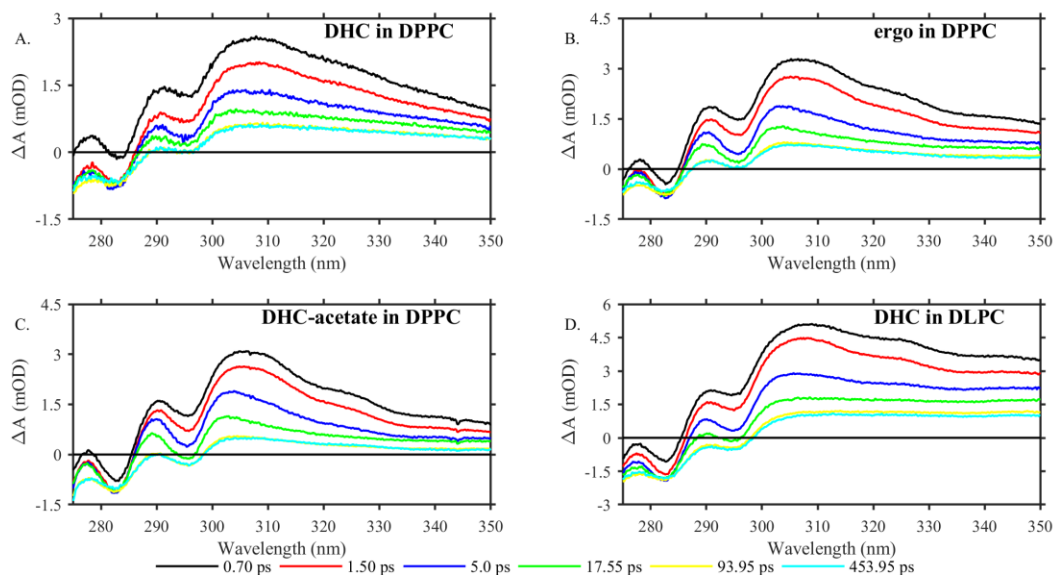
Figure 6.1: Selected time delays following excitation of 30mol-% loadings of (A) DHC, (B) ergo, (C) DHC-acetate in DPPC and (D) DHC in DLPC.

The data was fit using a global fitting program as described in Chapter 3. Selected wavelengths of the kinetics, fits, and residuals are illustrated in Figure 6.2. The analysis shows

that the relaxation of the three previtamins in lipid bilayers is significantly lengthened compared to solution measurements. The lifetimes obtained from the global fit are summarized in Table 6.1. Since the lifetimes of the three previtamins are nearly identical for time delays from -5 to 500/800 ps, van der Waals and hydrogen bonding do not play a significant role during the initial steps of the conformer relaxation. Measurements of previtamin D_3 in DLPC are comparable to measurements taken in DPPC for similar time delays. Therefore, the initial relaxation process does not appear to be dependent on the lipid tail length.
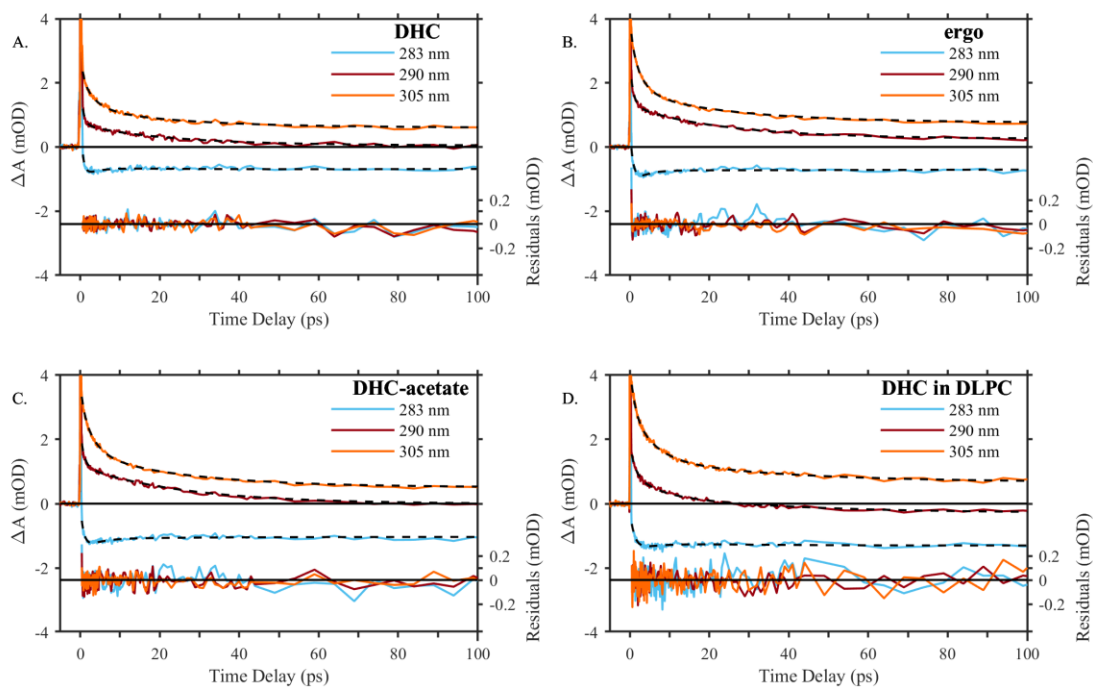
Figure 6.2: Selected UV kinetics (blue, red and orange), fits (black dash) and residuals (shifted for clarity) following excitation of 30mol-% loadings of (A) DHC, (B) ergo, (C) DHC- acetate in DPPC and (D) DHC in DLPC.

Table 6.1: Summary of time constants obtained following excitation of (30mol-% loadings of) DHC, ergo or DHC-acetate in lipid bilayers. Time constants obtained by globally fitting the data from ~275-350 nm.

Provitamin (30mol-%)	τ_1 (ps)	τ_2 (ps)	τ_3 (ps)	τ_4(ps)
DHC (DPPC)	0.79 ± 0.27	3.07 ± 0.77	26.02 ± 2.65	Permanent >>500ps
ergo (DPPC)	0.86 ± 0.08	3.23 ± 0.48	24.85 ± 1.12	Permanent >>500ps
DHC-acetate (DPPC)	0.67 ± 0.27	3.00 ± 0.62	24.80 ± 2.17	Permanent >>500ps
DHC (DLPC)	1.12 ± 0.01	5.0 ± 0.566	31.53 ± 4.47	Permanent >>500ps

The DADS (decay associated difference spectra) obtained from the global fit are plotted in Figure 6.3. As we saw in UV solution measurements (Chapter 5), the fast component in the kinetic decay is quantified as a mixture of photoproduct excited states and does not contain information about conformer relaxation. The second component observed in the lipid bilayer kinetics (ca. 3-5 ps) is suggestive of vibrational cooling or an excited state contribution, whereas the third component is suggestive of the conformer relaxation. The third, ca. 25 ps, and permanent components are of interest since they contain information on the photoproduct formation and the ground state relaxation.
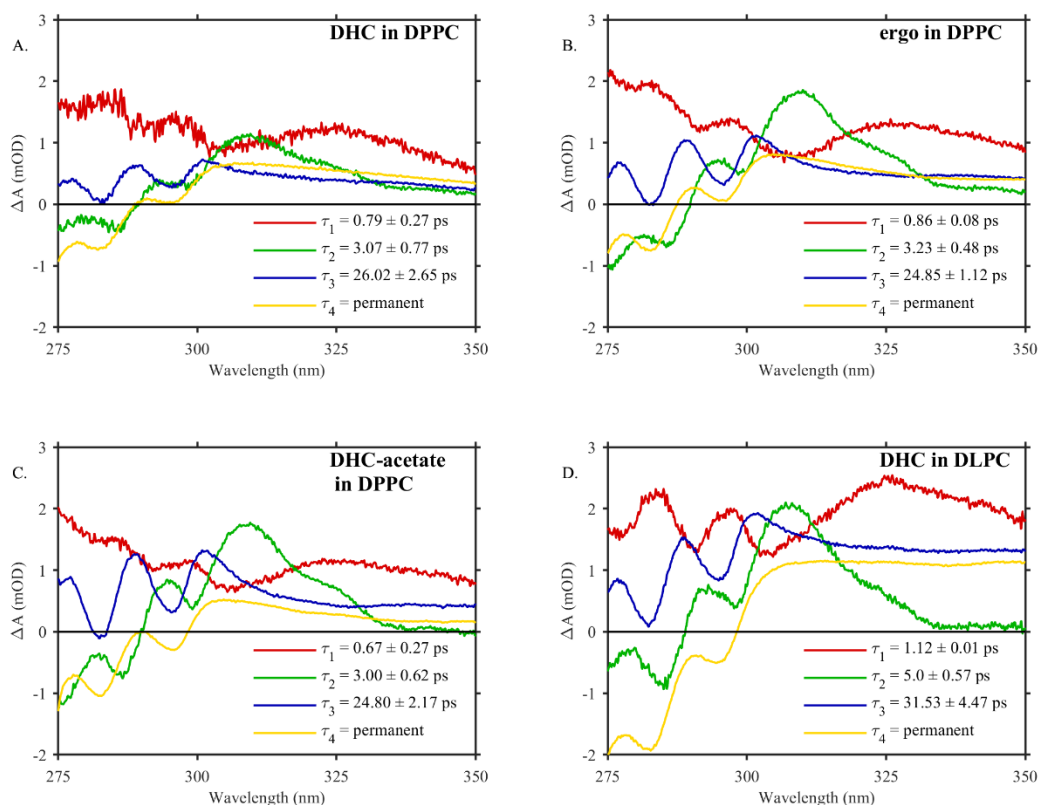
Figure 6.3: DADS obtained from the global fit routine following the excitation of 30mol-% loadings of (A) DHC, (B) ergo, (C) DHC-acetate in DPPC liposomes and (D) DHC in DLPC.

Steady State Photolysis of Provitamins in Liposomes

Steady state photolysis measurements for the three provitamins were performed to determine the photoproduct spectrum and conformer distribution in liposomes. Figure 6.4 shows selected time delay lineouts following excitation of 30mol-% DHC, ergo and DHC-acetate in DPPC. To reconstruct the spectra for the three previtamin D species in liposomes, the methods used in solution (Equation 5.1a and 5.1b), discussed in Chapter 5 were used. In Figure 6.4, the secondary photoproduct accumulation at ~305 nm appears to be slower in the lipid environment than in solution. It should be noted that, although structural changes appear to be slower in the liposome environment compared to solution, the difference spectra for DHC and ergo do not

appear to change within the first 20 seconds. To quantify the rate of secondary photolysis further, measurements need to be performed with similar starting concentrations in the lipid bilayer and solution environment. When constructing previtamin D_3, previtamin D_2, and previtamin D_3-acetate species, only the earliest time lineouts up to 8 seconds, 6 seconds and 4 seconds were used respectively to ensure that secondary products do not contaminate the results.
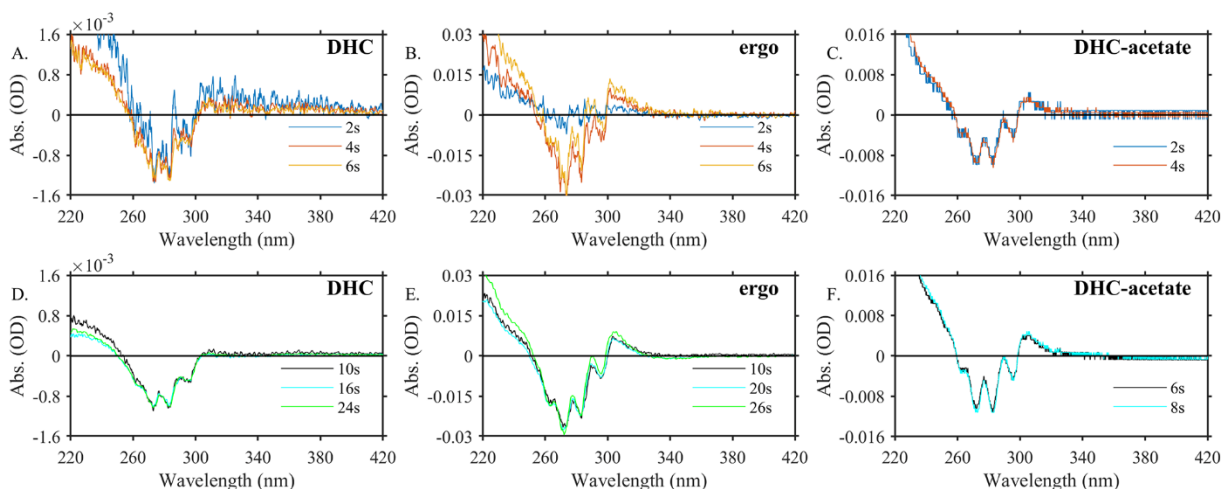
Figure 6.4: Steady state lineouts following excitation of 30mol-% loadings of DHC, ergo and DHC-acetate at (A-C) early and (D-F) late times in DPPC lipid bilayers. Scaled to relative intensity.

Figure 6.5A show the ground state spectra of the three provitamins in anisotropic DPPC lipid bilayers. Figure 6.5B shows the ground state spectra of DHC and ergo in DPPC compared to isotropic solution. The spectra are red shifted ~1 nm in the DPPC liposome environment compared to solution. The reconstructed previtamin D spectra in DPPC are shown in Figure 6.5C and compared to solution in Figure 6.5D .To quantify the reconstructed previtamin D spectra, a sum of two Gaussian functions was used to fit the data (see Figure 6.6 and Table 6.2). Although two Gaussians were not required in solution, the requirement for the two Gaussians in the lipid environment may reflect the heterogeneity of fluid and non-fluid environments in the liposome.
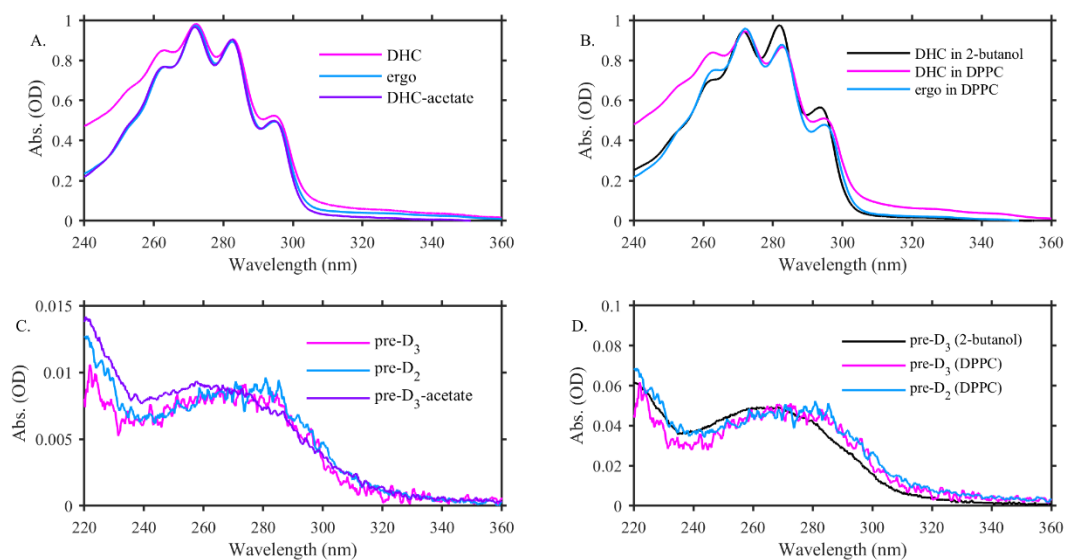
Figure 6.5: (A) Ground state comparison between (30mol-% loadings of) DHC (magenta), ergo (light blue) and DHC-acetate (purple) in DPPC lipid bilayers. (B) Ground state comparison between DHC and ergo in DPPC and DHC in 2-butanol (black), (C) Reconstructed previtamin D species in DPPC and (D) comparison to previtamin species in 2-butanol. Figures scaled to relative intensity. Ground state spectra scaled to ~1 OD at ~272 nm. Reconstructed previtamin D spectra scaled to relative intensities.
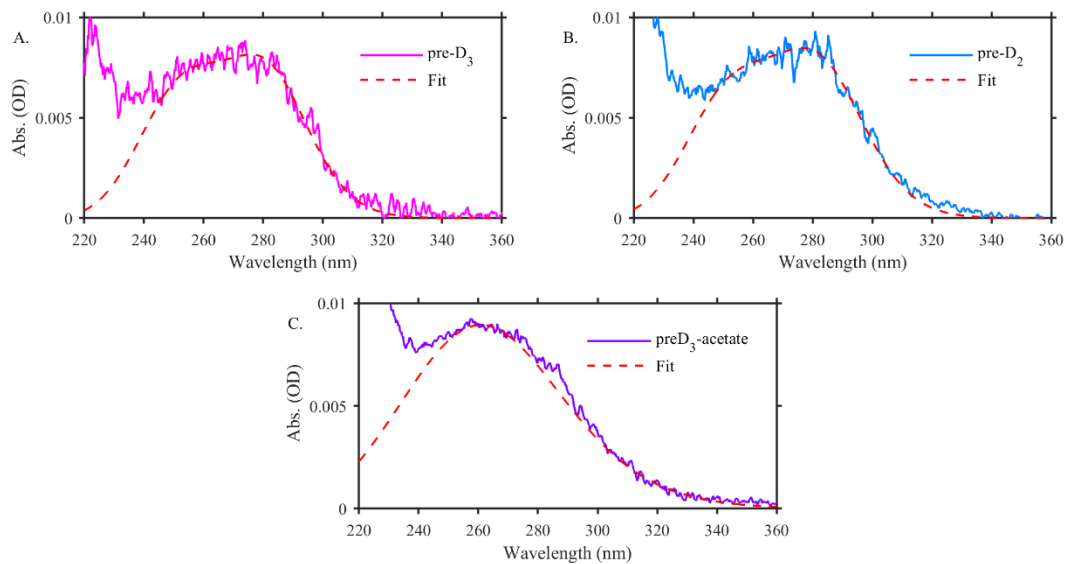
Figure 6.6: Sum of two Gaussians used to fit (red dashed) the reconstructed previtamin D species in DPPC lipid bilayers. Figures scaled to relative intensities.

117

Table 6.2: Summary of peak values for the reconstructed previtamins in DPPC lipid bilayers.

Previtamin	Peak of Gaussian #1 (nm)	FWHM of Gaussian #1 (cm^{-1})	Peak of Gaussian #2 (nm)	FWHM of Gaussian #2 (cm^{-1})
pre-D_3	284.3 ± 0.4	3661.5 ± 114.8	258.8 ± 3.0	6928.5 ± 618.0
pre-D_2	284.3 ± 0.9	3392.5 ± 492.0	259 ± 3.7	6764.2 ± 163.0
pre-D_3-acetate	275.0 ± 5.0	6073.0 ± 2991.5	250.50 ± 0.5	5382.5 ± 3961.4

The spectra of the previtamins are red shifted from the ground state spectra of the provitamins, in agreement to the spectra of gZg previtamin D_3 at 91K[2]. The peak of the absorption of the previtamin D_3-acetate in DPPC is slightly blue-shifted with respect to previtamin D_3 and previtamin D_2. In comparison to solution (Chapter 5), the previtamin D_3 and previtamin D_2 spectra are red shifted ~15 nm (Figure 6.5D). The observed red shift and the analysis done by Arruda *et al.*[3] on DHC and solution suggests that there is a higher distribution of gZg conformers in the lipid bilayer compared to solution. The blue shift in the previtamin D_3-acetate spectrum (Table 6.2) suggests that the tZg conformation makes a larger contribution to the population, in agreement with the hypothesis that the absence of hydrogen bonding to the head group destabilizes the gZg conformation.

Steady state measurements were extended to DHC in DLPC to probe the conformer distribution in a significantly shorter lipid tail length. Figure 6.7 shows photolysis lineouts at early and late times. The spectra do not appear to change significantly for the time scales from 2 to 18 seconds, however, only the first 2 seconds were used to construct the steady state photoproduct.
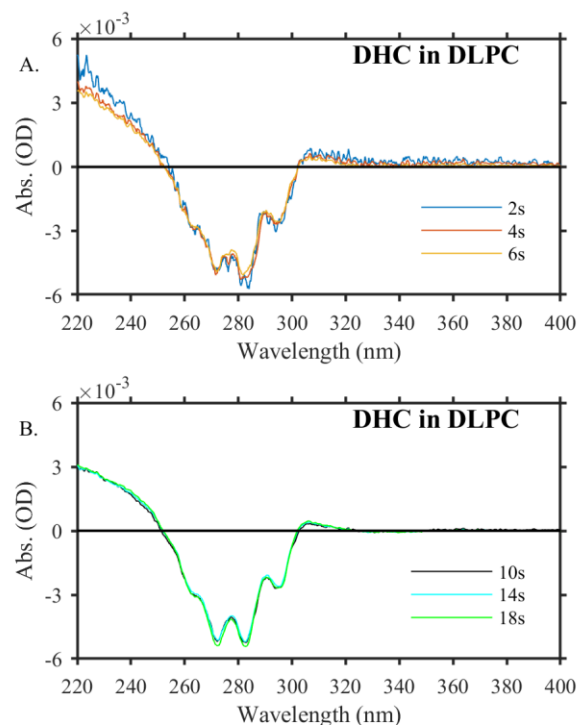
Figure 6.7: (A) Steady state photolysis of a 30mol-% loading of DHC in DLPC at (A) early times and (B) late times. Both figures scaled to relative intensity.

DLPC with its shorter alkane tail results in liposomes that are more fluid than DPPC liposomes at room temperature[4,5]. A comparison of the ground state and reconstructed product spectra for DHC in DPPC and DLPC is shown in Figure 6.8. The ground state spectra are essentially identical (Figure 6.8A). Thus, we can directly compare the less rigid DLPC environment to a more rigid DPPC environment without complications that are introduced by the spectral shift bias that is present in the comparison between measurements in solution and lipids (Figure 6.5B and Figure 6.8B). In order to remove any bias that comes from adding back the ground state, Figure 6.8C shows the minimum amount of ground state needed to reconstruct the previtamin D_3 species in DPPC compared to the maximum amount of ground state of DHC in DLPC. The maximum and minimum amount of ground state was determined based on the amount of structure appearing on the reconstructed photoproduct spectrum. Adding more ground state results in a positive structure in the photoproduct spectrum while adding less results in negative

features at the same wavelengths. In DLPC liposomes the previtamin D_3 spectrum is clearly blue

shifted relative to that observed in DPPC liposomes. The spectrum in DLPC looks similar to the

reconstructed photoproduct in solution (Figure 6.6C). A sum of two Gaussian functions was used

to fit the data. The peak of the two Guassians are 256.2 ± 2 nm and 254.7 ± 3.5 nm with a

FWHM of 7658.5 ± 62.3 cm^{-1} and 11238.9 ± 535.2 cm^{-1}, respectively. The similarity of the

peaks suggest that only one Gaussian is required, as observed in solution. The spectrum of

previtamin D_3 in DLPC is blue shifted with respect to the previtamin D_3 spectrum in DPPC. This

is consistent with the hypothesis that the gZg conformer is stabilized in the DPPC liposomes, but

not in the more fluid DLPC liposomes or in solution.
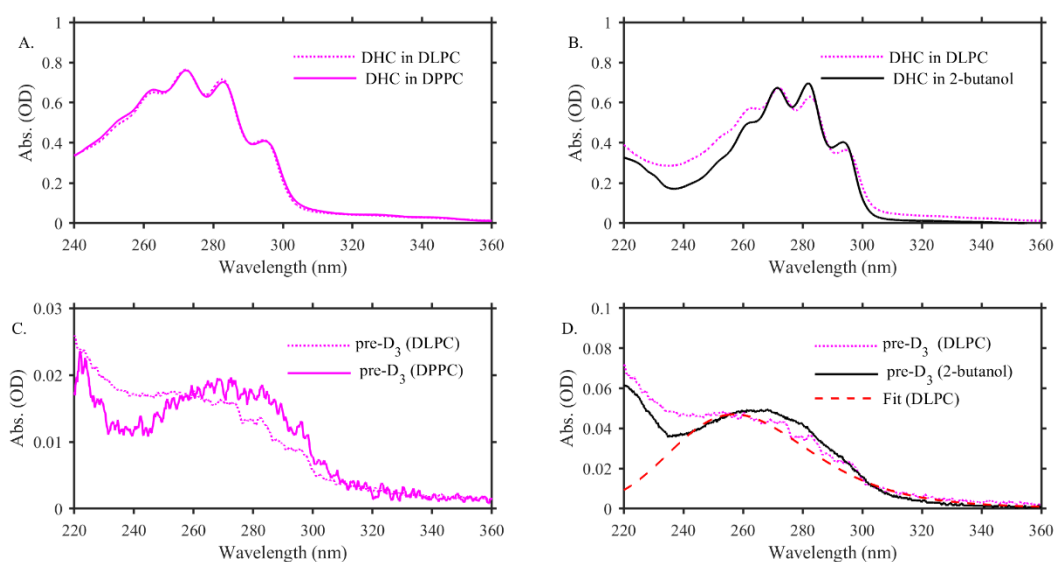
Figure 6.8: (A) Ground state comparison between (30mol-% loadings of) DHC in DLPC (magenta dotted) and DPPC lipid bilayers (magenta). (B) Ground state comparison between DHC in DLPC and solution (black). (C) Comparison between the reconstructed photoproduct of previtamin D_3 in DLPC to DPPC and (D) to solution. Also shown in (D) is the fit (red dashed) to the reconstructed previtamin D_3 spectrum in DLPC. Figures scaled to relative intensities.

Figure 6.9 shows a comparison of the steady state photoproduct spectra with the

picosecond transient absorption measurements. The comparison between the transient

measurements and the steady state results show a change in photoproduct distribution during

early times (10 ps) and late times (>> 400 ps). The late time delay lineouts are in close

agreement to steady state results except there is an offset in the data that most likely reflects

contributions from thermal lensing (Chapter 2). Of particular significance is the definition of

vibronic structure in the steady state difference spectrum compared with the definition in the

transient product at ca. 450 ps. In comparison to solution (Chapter 5), the difference in the

definition is not as large, suggesting that the lipid bilayers may narrow the conformational space

that the molecules are able to explore.
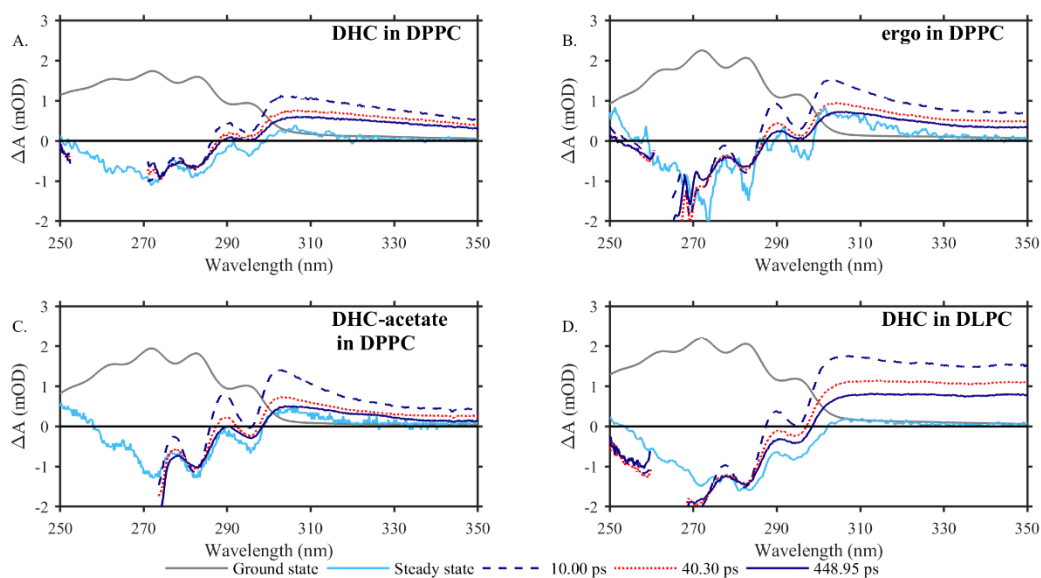
Figure 6.9: Ground state of the provitamins (gray) in (A-C) DPPC and (D) DLPC in comparison to the steady state spectra (light blue) and transient absorption data at time delays of 10 ps (dash blue), 40.30 ps (red dots) and >400 ps (solid blue). Steady state and ground state scaled for comparison to transient data. Transient data in DLPC scaled to same intensity as the other 3 panels. The legend at the bottom is the same for all four plots. All provitamin loadings were measured at 30mol-%.

Time Resolved Data in The Excited State and Ground State

For an accurate interpretation of the UV dynamics, the data is best fit including visible contributions from 350-700 nm. The UV relaxation following excitation of the three provitamins in the lipid bilayer environment, was concatenated with visible data (Chapter 4) and the global fit routine was used to fit the entire spectrum ~275 to 650 nm. Figure 6.10 shows the DADS following excitation of the three provitamins in the lipid bilayer environment. As in our solution analysis (Chapter 5), the difference spectra in the UV and visible regions report on different parts of the photochemical reaction. Since the influence of conformer relaxation, vibrational cooling and excited state behavior is a function of wavelength, fitting the data across the spectrum can alter the lifetimes compared to fitting the data in the respective regions. In Figure 6.10, the first and second components correspond to the excited state spectra, the third component (blue) corresponds to conformer relaxation from the gZg to tZg species, and the fourth component (cyan) corresponds to photoproduct formation in the UV region and a background component in the visible region. This background may contain contributions from solvated electrons in water as well as thermal lensing in the visible region. The precise time constants determined for the excited state decay are significantly different when UV contributions are included, compared to fitting only the visible absorption region (Chapter 4). However, the excited state lifetime is still longer compared to solution measurements (Chapter 3 and 5). The differences likely result from the number of relaxation components present in the UV region. The noise level of the measurement is insufficient to allow accurate fitting to the number of components actually present in the data.
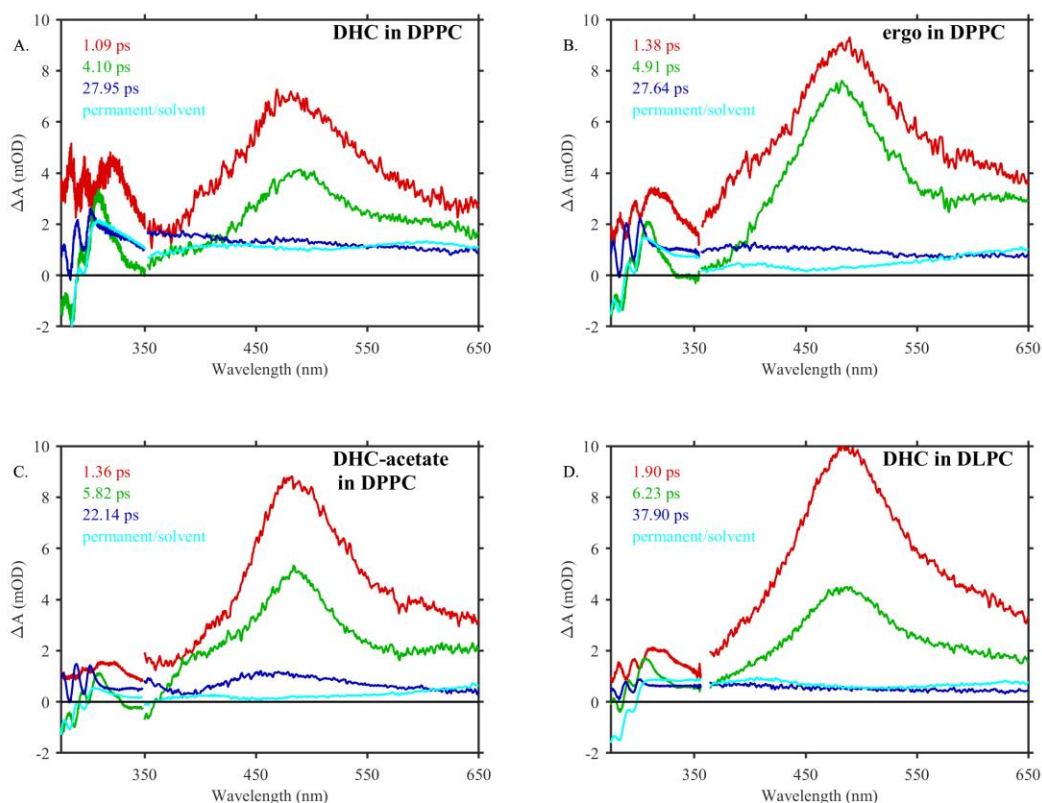
Figure 6.10: DADS obtained after a global fit to the concatenated data from ~275-650 nm following excitation of (30mol-% loadings of) (A) DHC, (B) ergo, (C) DHC-acetate in DPPC and (D) DHC in DLPC lipid bilayers. The removed wavelength regions are where separate UV and visible data was concatenated together. Spectra scaled to relative intensities.

Time resolved kinetics and photolysis in lipid bilayers compared to solution: As previously shown in Table 6.1, the relaxation time of the three previtamins within the first 500 ps are similar in the DPPC lipid bilayer with a relaxation time of ca. 25ps. The initial conformer relaxation of gZg to tZg previtamin D_3 does not appear to be significantly dependent on the lipid tail length since there is not a significant difference between the relaxation time in DPPC and DLPC lipid bilayers. Although we do not see a significant difference in the DPPC and DLPC lipid environment, the kinetics in the lipid bilayer are significantly different compared to solution. Figure 6.11A and Figure 6.11B shows the comparison between the bleach signal of the three previtamins in 2-butanol and in the lipid bilayers at 283 nm. It is important to point out that

in the lipid bilayer (Figure 6.11B), the bleach remains essentially constant, while ground state

conformational relaxation or a ground state recovery component is present in the solution data

(Figure 6.11A). Figure 6.11C and Figure 6.11D shows the peak of the Gaussian fit to the

reconstructed previtamin species in solution and in the lipid environment. The distribution of

gZg and tZg conformers appears to be most dependent on the fluidity of the environment.
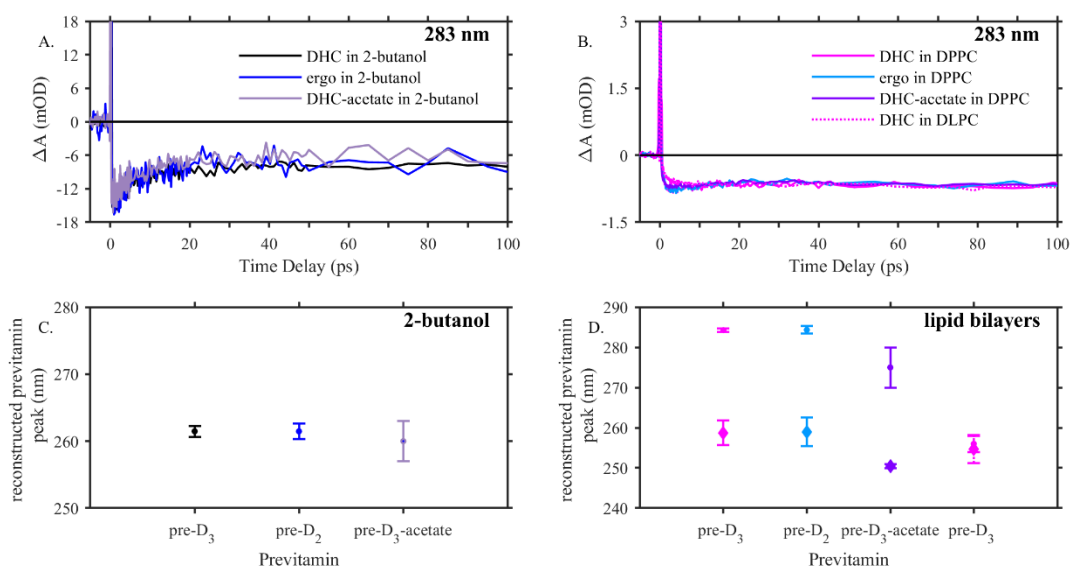
Figure 6.11: (A) Kinetics at 283nm showing that the bleach signal in solution is different from (B) the kinetics in the lipid bilayer (with a 30mol-% provitamin loading). Solution and lipid measurements scaled to relative intensities. Peak of the reconstructed previtamin D species in (C) 2-butanol and in (D) lipid bilayers. The circles and diamonds represent the peaks of the first and second Gaussian used to fit each of the previtamin D spectra, respectively.

Discussion

In this section we will discuss possible explanations for the difference in isomerization of gZg to tZg in solution and in the lipid bilayer environment. In steady state measurements, we observe a red shift of the three previtamin D spectra in the DPPC lipid bilayer medium compared to what was previously reported in solution[3] or in Chapter 5. The lipid bilayer medium is a complex anisotropic medium with hydrogen bonding, van der Waals interactions and lipid domains, all playing a potential role. The lipid environment is overall more viscous and rigid than the environment in solution[3,6]. Two Gaussians are needed to fit the reconstructed previtamin D spectra. The fit to the reconstructed previtamin D spectra in steady state measurements suggests that the lipid environment influences the product distribution. The distribution of fluid and non-fluid regions of the lipid bilayer may be responsible for the photoproduct distribution. The rigid regions of the DPPC bilayer could stabilize a higher distribution of the gZg previtamin species, resulting in a red shift to the overall spectra of the three previtamins when compared with DLPC and isotropic solution. The reconstructed spectrum of previtamin D_3 (peaking at ca. 275 nm) appears to be similar to the reconstructed spectrum of previtamin D_2 However, the reconstructed spectrum of previtamin D_3-acetate (peaking ca. 260 nm) is slightly blue shifted relative to previtamin D_3 and D_2 in the DPPC lipid environment suggesting that hydrogen bonding to the lipid head group constrains the isomerization.

In solution (Chapter 5), the environment is homogenous and the conformer distribution mostly relaxes down to the tZg species. Thus, only one Gaussian is required to fit the reconstructed previtamin D spectra. The observed previtamin spectra are blue shifted and similar (peaking at ca. 260 nm). The reconstructed spectra of the previtamin D_3, previtamin D_2 and previtamin D_3-acetate in 2-butanol do not show a significant difference compared to the

125

respective photoproducts in hexadecane (that peaks ca. 260 nm). The second Gaussian used to fit each of the three reconstructed previtamin D spectra in the lipid bilayer environment has a peak near this region and does not depend on the specific lipid or previtamin. This suggests that this component may reflect contributions from the tZg conformation.

In the DLPC lipid bilayer, the similarity between the peak of the first and second Gaussian used to fit the spectrum suggests that the DLPC lipid bilayer cannot form regions as rigid as the DPPC environment. Thus, allowing a higher distribution of gZg conformers to relax to the tZg species, despite hydrogen bonding to the lipid head groups. The reconstructed previtamin D_3 spectrum in DLPC (peaking ca. 260 nm) is blue shifted compared to the spectrum in DPPC (peaking ca. 275 nm). In DPPC there is a noticeable difference between the FWHM of each Gaussian. This suggests that there is a lower distribution of gZg previtamin D_3-acetate conformers compared to gZg previtamin D_3 and D_2 conformers. The second Gaussian used to fit the reconstructed previtamin D_3 and previtamin D_2 spectra in DPPC peaks ca. 260 nm and has a FWHM that is nearly twice as broad as the first Gaussian that peaks ca. 280 nm. For the blue shifted previtamin D_3-acetate in DPPC and previtamin D_3 in DLPC, the ratio of the two FWHM of each Gaussian used to fit the data are between 1 and 1.5 times the first FWHM that peaks on the redder edge of each spectrum. The hypothesis that the second Gaussian may reflect contributions from the tZg distribution is in agreement with the blue shifted spectrum of these two compounds. The FWHM ratio between the second and first Gaussian may suggest that most of the distribution is in the tZg conformation, with a higher distribution in the absence of hydrogen bonding and in the more fluid DLPC membrane.

The results observed here are consistent with the membrane model proposed by Tian and Holick[1] (Chapter 1). The blue shift that is observed for previtamin D_3 in DLPC and previtamin

D$_3$-acetate in DPPC may suggest that longer time delays in transient measurements, on the order of nanoseconds or microseconds, would show additional conformer relaxation from gZg to tZg species. This would be most obvious in the decrease of the bleach at ~270/280 nm, where the transition from gZg to tZg makes a significant contribution in solution.

In solution, solvent molecules have the freedom to diffuse around the solute, whereas the lipids in the liposome environment are oriented and structured. Besides the rigid environment of the solvent, it is also important to consider how the cyclohexadiene chromophore is oriented within the bilayer. Another factor that can influence how the previtamins 'twist' to form a stable previtamin D species is the orientation of the molecules with respect to the solvent. The sterol ring of the previtamins are not in the same plane as the lipid tails. Although cholesterol and DHC only structurally differ by a single bond, DHC is reported to disorder the lipid bilayer while cholesterol orders the membrane[7,8,9,10]. The effect of DHC-acetate on the lipid bilayer has not been specifically explored however, it is hypothesized that the size of the acetate group disrupts the ordering of the bilayer, which may push away neighboring lipids. The blue shift of previtamin D$_3$-acetate in steady state measurements may indicate that the non-planarity, the absence of hydrogen bonding, and the disruption of lipid packing may impose less constraint on the previtamin D$_3$-acetate species, allowing a higher distribution of gZg conformers to isomerize to the tZg species.

One of the major differences between solution and the liposome environment is that the liposome environment is not isotropic. In the lipid bilayer, the molecule is proposed to be solvated within the alkyl tails of the bilayer, where the tails hinder any motion the molecule may undergo[1]. Although the incorporation of DHC has the effect of disordering the membrane[7,11,9], the solvated DHC molecules have fewer degrees of freedom since they cannot be incorporated

into the hydrophilic regions near the head group, or anywhere in the presence of an aqueous solution. In comparison to solution, the ground state spectra of the three provitamins in the lipid bilayer (Figure 6.5) are ~1 nm red shifted, similar to the red shift observed in a liquid crystal medium[12].

Dmiternko *et al.*[12] demonstrated that the rotation barrier from gZg to tZg is a function of the molecule alignment to the solvent molecules. For nematic liquid crystals in the isotropic phase at 77 °C, the formation of tachysterol (Figure 1.1) was lower compared to ethanol solutions. However for nematic crystals in the mesophase at 24 °C, tachysterol accumulation was higher than in ethanol solutions. It is expected that the more viscous medium (isotropic phase) would suppress tachysterol formation than ethanol, however Dmiternko *et al.* reported that the mesophase nematic crystals (even more viscous than isotropic phase) was a more favorable medium for tachysterol accumulation than ethanol. The FWHM of the second Gaussian that peaks ca. 260 nm suggests that the photochemistry of previtamin D_3 observed in the DPPC lipid membrane environment maybe consistent with the liquid crystal results.

In another study, Terenetskaya *et al.*[13] reported UV absorption measurements on the photoconversion of DHC in silica gel/solvent matrices. In the presence of an adsorbed water layer on the silica dioxide surface, the repulsion between the hydrophobic parts of DHC (and photoisomers) to the surface increased the rotation barrier of gZg to tZg isomerization. In the lipid membrane model[1], hydrogen bonding occurs between the carbonyl groups of the phospholipids and hydroxyl group of the molecule and the alkane tail of the molecule is located between the alkane tails of the lipids. Since the molecule tails are solvated within the tails of the lipid it is not energetically favorable for the nonpolar part of the molecule to interact with the polar part of the lipid, it is possible that this restricts motion and increases the rotation barrier

from gZg to tZg, thus red shifting the overall spectrum of the three previtamins in DPPC at early times.

Another possible mechanism is that the initial gZg conformer is thermally hot and may transfer energy to the nearby lipid tails, slightly disordering them by inducing a localized heating, facilitating isomerization from gZg to tZg in the more fluid regions. This proposed mechanism may help explain the different spectra observed for previtamin D_3 in a fluid (DLPC) and ridged (DPPC) environment.

To bridge the gap between isotropic and anisotropic environments, the ratio between ethanol-water mixtures can be tuned to construct micelles in water-rich environments[13,12], which constrains the solvated molecule within the hydrophobic region and ethanol-rich environments that allow for conformational flexibility. For these two environments, Dmiterrnko found that the formation of tachysterol was inhibited in the constrained water-rich environment. Our data shows that conformational change in hexadecane is not constrained, despite being the same carbon length as DPPC (Table 5.2 and 5.3). This agrees with Dmiternko's findings.

Overall the biologically relevant reaction is the conversion from gZg previtamin D_3 to vitamin D_3. The solvation environment may either increase the rotational barrier from gZg to tZg or the relative stability of the gZg conformer. Since a higher barrier will only slow down the formation of equilibrium, it is likely that an increase in the relative stability of the gZg conformer is more significant in promoting vitamin D formation. This stabilization is a function of the specific environment. While solution measurements may provide insight into the conformer relaxation, the solvation environment is not biologically relevant for vitamin D formation. Our time resolved measurements suggest that the molecule experiences significant friction from the lipid bilayer and unfavorable geometries for rotation due to the structure imposed by

hydrophobic and hydrophilic regions of the lipid and constraint of the tails (See Figure 4.1 and 4.9). These factors may stabilize the gZg conformer. The extra kinetic energy from the resonant pump wavelength may allow the molecule to overcome these barriers to form the tZg species for a portion of the population. Reports in literature have shown vitamin D production to be most efficient within wavelengths of 290 nm[14,15,16] . This may lower the energy input to the system such that the gZg conformers cannot make it over the barrier as easily. Thus, locking a higher distribution in the gZg conformation.

In time resolved measurements, the constraints and properties of the bilayer discussed above certainly plays a role in the observed time constants. The fast 700-800 fs component is assigned to be the excited state as observed in solution, the 3 ps component suggests that there is an early excited contribution in the that cannot be resolved in visible data (Chapter 4) and the 25 ps component may arise from the constraint imposed by the lipid bilayer that increases the time it takes for the gZg / tZg distribution to reach equilibrium. In comparison to solution, that data suggests that we observe a larger long lived distribution of the gZg conformer in transient absorption data and in steady state photolysis measurements.

Conclusion

In the lipid bilayer, the transient kinetics observed within the first 500 ps are nearly independent of previtamin and membrane rigidity, but are elongated by ~3.5x compared to solution measurements. Unlike solution measurements (Chapter 5 and Figure 6.11), the bleach signal in the lipid environment does not show significant conformer relaxation dynamics. The three reconstructed previtamin D species in solution indicate that most of the distribution favors the tZg conformer. The reconstructed previtamin D_3 and previtamin D_2 spectra in the DPPC environment appear to be red shifted, suggesting a higher distribution of gZg conformers. A blue shift is present for the previtamin D_3-acetate in DPPC and previtamin D_3 in DLPC, consistent with Tian and Holick's proposed mechanism and a lower population of gZg conformers in these liposomes. One Gaussian is needed to fit the reconstructed previtamin spectra in solution. The fits are nearly identical for all three previtamins (with a peak ca. 260 nm and a FWHM of 6700 cm^{-1}), whereas a sum of two Gaussians are needed in the lipid environment. This is consistent with the heterogeneity of each environment. The solution environment is homogeneous and the lipid bilayer can have fluid and non-fluid regions. The mechanism behind gZg stabilization appears to be a trade-off between solvent organization, viscosity of the lipid, and specific interactions within the lipid bilayer. The anisotropic lipid structure, hydrogen bonding, and the viscosity of the bilayer may increase the barrier of the gZg to tZg isomerization and/or the relative stability of the gZg conformer. The DPPC lipid environment likely increases the rotation/viscosity barrier for gZg to tZg isomerization, whereas the DLPC environment may have a slightly lower barrier, comparable to solution.

References

(1)   Tian, X. Q.; Holick, M. F. A Liposomal Model That Mimics the Cutaneous Production of Vitamin D3: Studies of the Mechanism of the Membrane-Enhanced Thermal Isomerization of Previtamin D3 to Vitamin D3. *J. Biol. Chem.* **1999**, *274* (7), 4174–4179.

(2)   Fuß, W.; Lochbrunner, S. The Wavelength Dependence of the Photochemistry of Previtamin D. *J. Photochem. Photobiol. A Chem.* **1997**, *105* (2–3), 159–164.

(3)   Arruda, B. C., Peng, J., Smith, B. Spears, K. G., Sension, R. J. Photochemical Ring-Opening and Ground State Relaxation in α-Terpinene with Comparison to Provitamin D 3 Photochemical Ring-Opening and Ground State Relaxation in α-Terpinene with Comparison to Provitamin D 3 Brenden C . Arruda , Jian Peng , Broc Smith , K. *J. Phys. Chem.* **2012**.

(4)   Bui, T. T.; Suga, K.; Kuhl, T. L.; Umakoshi, H. Melting-Temperature-Dependent Interactions of Ergosterol with Unsaturated and Saturated Lipids in Model Membranes. *Langmuir* **2019**, *35*, 10640–10647.

(5)   Guo, Y.; Pogodin, S.; Baulin, V. A. General Model of Phospholipid Bilayers in Fluid Phase within the Single Chain Mean Field Theory. *J. Chem. Phys.* **2014**, *140* (17).

(6)   Nojima, Y.; Iwata, K. Viscosity Heterogeneity inside Lipid Bilayers of Single-Component Phosphatidylcholine Liposomes Observed with Picosecond Time-Resolved Fluorescence Spectroscopy. *J. Phys. Chem. B* **2014**, *118* (29), 8631–8641.

(7)   Benesch, M. G. K.; Lewis, R. N. A. H.; McElhaney, R. N. A Calorimetric and Spectroscopic Comparison of the Effects of Cholesterol and Its Immediate Biosynthetic Precursors 7-Dehydrocholesterol and Desmosterol on the Thermotropic Phase Behavior and Organization of Dipalmitoylphosphatidylcholine Bilayer Membrane. *Chem. Phys. Lipids* **2015**, *191*, 123–135.

(8)   Chen, C.; Tripp, C. P. A Comparison of the Behavior of Cholesterol, 7-Dehydrocholesterol and Ergosterol in Phospholipid Membranes. *Biochim. Biophys. Acta - Biomembr.* **2012**, *1818* (7), 1673–1681.

(9)   Staneva, G.; Chachaty, C.; Wolf, C.; Quinn, P. J. Comparison of the Liquid-Ordered Bilayer Phases Containing Cholesterol or 7-Dehydrocholesterol in Modeling Smith-Lemli-Opitz Syndrome. *J. Lipid Res.* **2010**, *51* (7), 1810–1822.

(10)   Róg, T.; Vattulainen, I.; Jansen, M.; Ikonen, E.; Karttunen, M. Comparison of Cholesterol and Its Direct Precursors along the Biosynthetic Pathway: Effects of Cholesterol, Desmosterol and 7-Dehydrocholesterol on Saturated and Unsaturated Lipid Bilayers. *J. Chem. Phys.* **2008**, *129* (15).

(11)   Bernsdorff, C.; Winter, R. Differential Properties of the Sterols Cholesterol, Ergosterol, Beta-Sitosterol, Trans-7-Dehydrocholesterol, Stigmasterol and Lanosterol on DPPC Bilayer Order. *J. Phys. Chem. B* **2003**, *107* (38), 10658–10664.

(12)   Dmitrenko, O.; Orlova, T.; Terenetskaya, I. Medium Controlled Photochemistry of Provitamin D: From Solutions to Liquid Crystals. *J. Mol. Liq.* **2018**, *267*, 428–435.

(13)   Terenetskaya, I.; Dmitrenko, O.; Eremenko, A. CONFORMATIONAL PHOTOCHEMISTRY REACTION MEDIA CONTROL. **1995**, *21*, 653–664.

(14)   Kalajian, T. A.; Aldoukhi, A.; Veronikis, A. J.; Persons, K.; Holick, M. F. Ultraviolet B Light Emitting Diodes (LEDs) Are More Efficient and Effective in Producing Vitamin D3 in Human Skin Compared to Natural Sunlight. *Sci. Rep.* **2017**, *7* (1), 6–13.

(15)   Holick, M. F. Biological Effects of Sunlight, Ultraviolet Radiation, Visible Light, Infrared Radiation and Vitamin D for Health. *Anticancer Res.* **2016**, *36* (3), 1345–1356.

(16)   Kostas, A. Generation of Previtamin D3 from Tachysterol3 : A Novel Approach for Producing Vitamin D3 in the Winter. *Bost. Univ. thesis* **2015**.

Chapter 7

Conclusions and Extended Ideas

Summary of Work

The excited state dynamics and photoproduct relaxation of three Provitamin D compounds, 7-dehydrocholesterol (DHC), ergosterol (ergo) and DHC-acetate were probed using broad band transient absorption and steady state spectroscopy. Measurements were performed in isotropic solution and in anisotropic lipid bilayers. The visible transient absorption spectra (~350-650 nm), presented in Chapter 3 and 4 provide insight into the trapping mechanism that contributes to the biexponential nature of the excited state decay in solution and in the liposome environment. In solution (Chapter 3), the biexponential decay of the excited state corresponds to a ballistic, 500 fs component, and ~2 ps slow component. On the potential energy surface, these time constants are attributed to a fast population of molecules that decay rapidly from the excited to ground state and a longer lived trapped population. Ergo appears to have the same dynamics as DHC in both 2-butanol and hexadecane, whereas DHC-acetate appears to have slightly longer time constants in these environments. The difference may come from the size of the acetate group impeding the ring-opening process. In the liposome environment (Chapter 4), the kinetics of the three compounds do not behave the same way as they do in solution and they show differences based on membrane fluidity, hydrogen bonding and van der Waals interactions.

We hypothesized that the ballistic component is absent and the biexponential decay arises from specific influences on the provitamins in (liquid-ordered) fluid (~1-1.5 ps) and (solid-ordered) non-fluid regions (6-11ps) of the lipid bilayer.

UV transient absorption studies (~250-350 nm), in solution and liposomes (Chapter 5 and 6), provide insight on the first 5-500 ps process of gZg to tZg relaxation. The relaxation takes place ~6-7 ps in solution, nearly independent of the compound. Steady state measurements in Chapter 5 show that the reconstructed previtamin D_2 and previtamin D_3-acetate are similar to previtamin D_3 and are nearly independent of solvent. In solution, one Gaussian band representing the tZg species peaks at ca. 260 nm with a FWHM ca. 6700 cm^{-1}, in agreement with measurements done by Arruda[1]and Fuss[2]. However, in the DPPC lipid environment (Chapter 6), the three reconstructed previtamin D spectra are best modeled using two Gaussians, while in the DLPC environment only one Gaussian is needed. The FWHM and peak of each Gaussian may provide insight into the gZg and tZg distribution in non-fluid and fluid environments. The peak of both previtamin D_3 and previtamin D_2 species are red shifted (ca. 275 nm) with respect to previtamin D_3-acetate in DPPC (ca. 260 nm), previtamin D_3 in DLPC (ca. 260 nm), and the previtamin D species in solution (ca. 260 nm). The red shift suggests the gZg stabilization is a function of hydrogen bonding and ridgidity of the environment. This is consistent with the small amplitude component of 25 ps that is observed in time resolved measurements, suggesting that the gZg species is stabilized longer in the lipid bilayer environment than in solution. The distributions of the reconstructed previtamins in the lipid bilayers and solution are in agreement with the membrane model proposed by Tian and Holick[3]. Other studies have attributed the heterogeneity of the lipid bilayer to account for multiple fitting parameters required to fit data in

liposomes[4,5]. This is consistent with our fits to the excited state decay and to the steady state previtamin distributions obtained in lipid bilayers.

Extended Ideas

Since the measurements explored in this dissertation suggest that the initial steps involved in vitamin D_3 formation depends on specific interactions between the molecule and the lipid environment, the lifetimes can be further explored by preforming additional experiments and computational simulations. The following sections outline experimental and computational work that could be done to gain a deeper understanding of the results presented in this dissertation. These experiments will not only provide additional information to understand vitamin D_3 formation in mammalian skin, but may provide structural insight about the membrane environment to further understand the Smith-Lemi-Opitz syndrome (SLOS).

Experimental:

1. <u>Nanosecond-microsecond time delays</u>: Transient data taken out to time delays of 800 ps shows a steady bleach signal, nearly independent for all three compounds and all lipid environments. However, the previtamin D_3 in DLPC and previtamin D_3-acetate in DPPC spectra in steady state measurements (seconds) are blue shifted relative to previtamin D_3 and previtamin D_2 spectra in DPPC, suggesting that the absence of hydrogen bonding and increased membrane fluidity allows gZg to tZg relaxation. Transient absorption measurements out to time delays of nanoseconds or microseconds should show additional conformer relaxation from gZg to tZg and allow characterization of this process (Figure 6.11).

2. <u>Wavelength dependent studies on the nanosecond to microsecond time scale</u>: Reports in literature have shown vitamin D production to be most efficient with excitation wavelengths of ca. 290 nm[6,7,8]. To explore the gZg to tZg conformer relaxation in the lipid bilayer and the reason for this efficiency, a wavelength dependent study with excitation wavelengths over the range of 265-300 nm and probe time delays from picoseconds to nanoseconds or microseconds should be performed. The long time scale would allow us to explore gZg to tZg conformer relaxation using the ground state bleach and photoproduct absorption from (below) 260 to 300 nm as a probe.

3. <u>Temperature dependent studies</u>: Preliminary studies of the gZg to tZg relaxation were performed for 30mol-% DHC in DPPC ranging from ~16-56 °C. To complete this work, curvature studies in the UV are also needed since the liposomes compress and expand below and above room temperature. Figure 7.1 shows sample UV kinetics traces and the melting curve (taken with Nano DSC) for 30mol-% DHC in DPPC as a function of temperature. A summary of the liposome size, polydispersity index (PDI) and time constants obtained from the fit to the data are presented in Table 7.1. The melting temperature of 30mol-% DHC in DPPC in Figure 7.1 is less than 41 °C, in agreement with measurements reported by Benesch[9]. Surprisingly, τ_3 increases with temperature, but is similar above and below the melting temperature. More work is needed to sort this out. In addition, it is hypothesized that the DMPC lipid membrane may be more sensitive to temperature measurements since the melting point (of pure DMPC) is at room temperature (24 °C). Since (pure) DLPC has a melting point of -2 °C, it is hypothesized that temperature measurements will not show any affect, thus these measurements are less

important. Temperature dependent measurements should be performed using DMPC as

well as DPPC.
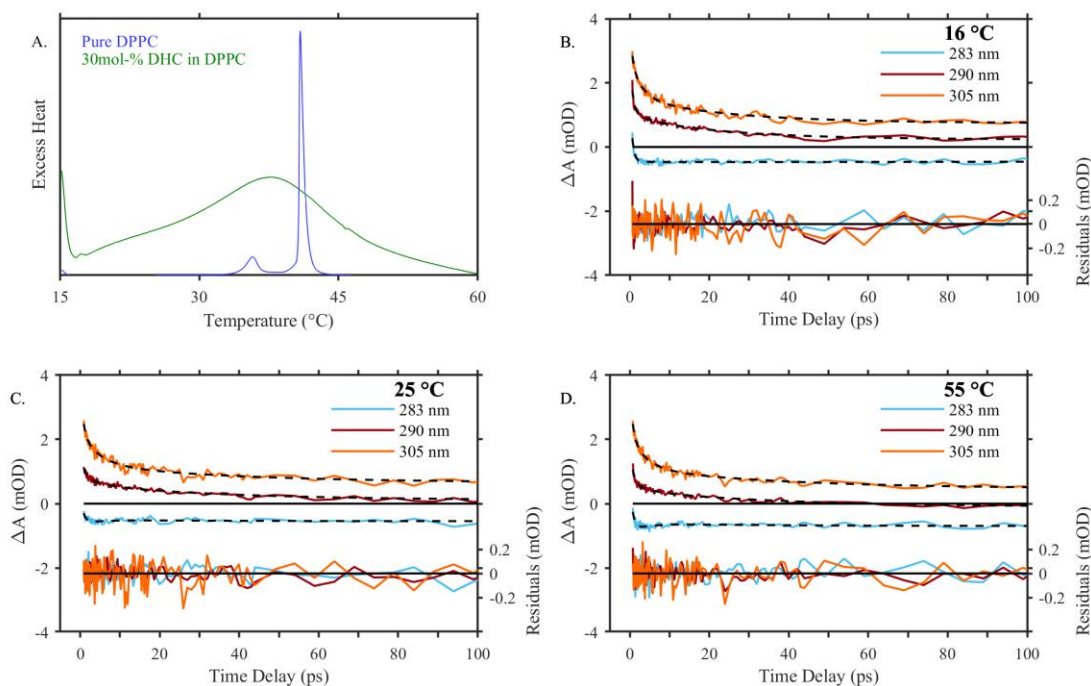
Figure 7.1: (A) Differential scanning calorimetry measurements of pure DPPC (blue) and a 30mol-% loading of DHC in DPPC (green). The pretransition and main transition of DPPC are shown at ~35 °C and 41 °C, respectively. Figures scaled to relative intensities. Conformer relaxation kinetics for a 30mol-% loading of DHC in DPPC at temperatures of (B) 16 °C, (C) 25 °C and (D) 55 °C.

Table 7.1: Time constants and liposome distribution obtained for a 30mol-% loading of DHC in DPPC as a function of temperature.

Temperature (°C)	Size (nm) and PDI	τ_1 (ps)	τ_2 (ps)	τ_3 (ps)	τ_4 (ps)
17	142.10 ± 0.44 0.10 ± 0.02	0.52	2.80	23.40	Permanent
27.7	144.8 ± 4.22 0.07 ± 0.02	0.74	4.65	37.30	Permanent
56.6	156.40 ± 158.60 0.06 ± 0.01	0.75	4.03	37.17	Permanent

4. <u>Loading Studies</u>: Preliminary heterogeneity tests were conducted for various loadings and cholesterol (CHL) mixtures of DHC in DPPC (Chapter 3) at ~22-24 °C in the visible region. The excited state decay does not appear be dependent on loadings of 15/0, 15/15 and 30/0mol-% DHC/CHL in DPPC. When probing in the UV region, preliminary loading studies at 25 °C for loadings of 30-50mol-% do not appear to contribute to conformer relaxation. The kinetics are illustrated in Figure 7.2. Table 7.2 summarizes the time constants and liposome distributions. The noise in the data presented for 15mol-% may alter the fit since the kinetics appear to be similar for 30 and 50mol-% loadings. The DPPC bilayer may be too rigid to alter the dynamics, therefore it would be useful to conduct these studies again with DMPC or DLPC in the visible and UV regions including picosecond to microsecond time delays.
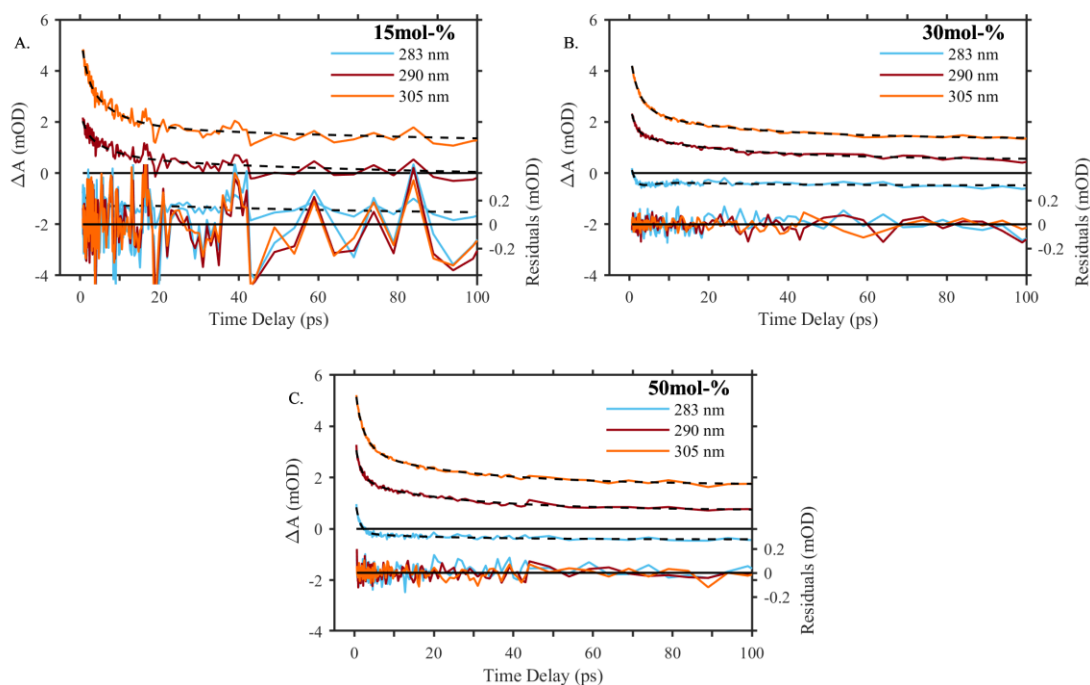
Figure 7.2: Conformer relaxation kinetics of DHC in DPPC for loadings of (A) 15mol-%, (B) 30mol-% and (C) 50mol-% at 25 °C.

Table 7.2: Time constants and liposome distribution obtained (at room temperature) for DHC in DPPC as a function of loading.

Loading (mol-%)	Size (nm) and PDI	τ_1 (ps)	τ_2 (ps)	τ_3 (ps)	τ_4 (ps)
15	120.33 ± 2.50 0.11 ± 0.02	1.23	7.14	90.90	Permanent
30	149.29 ± 6.04 0.08 ± 0.02	0.79 ± 0.27	3.07 ± 0.77	26.02 ± 2.65	Permanent
50	145.33 ± 0.56 0.27 ± 0.32	1.04	3.18	22.78	Permanent

5. <u>Egg PC tests</u>: The double bond in Egg PC (Figure 1.10) is located near sterol structure of DHC and analogs, ergo and DHC-acetate. Although the chain length is comparable to DPPC and DSPC, the double bond may allow the lipids to be flexible enough to loosen the constraint around the chromophore, thus speeding up the excited state dynamics and conformer relaxation dynamics on the ground state. If the double bond in Egg PC allows the tails to be flexible enough, steady state results may show a similar photoproduct distribution as in DLPC.

Computational work:

To further quantify experimental results, simulations are needed to understand the excited state behavior in solution and in the lipid bilayer.

1. <u>MD simulations in solution</u>: As discussed in Chapter 3 and 5, the size of the acetate group on DHC-acetate may impede motion in both the excited and ground state. To further quantify the dynamics, MD simulations will be useful to explore how the acetate group affects the ring-opening and conformational relaxation of the molecule.

2. <u>MD simulations in lipid bilayers</u>: To understand the heterogeneity of the lipid bilayer for each provitamin, the fluid and non-fluid regions need to be quantified for each specific provitamin as a function of temperature and lipid tail length. As discussed in Chapter 4 and 5, each of these regions may play a role in the ring-opening process and in the gZg stabilization.

Conclusion

The photochemistry of DHC in the excited state and in the ground state appears to be more dependent on the lipid tail length than on other lipid parameters. In the DPPC lipid environment, the ring-opening process is completed within ca. 11 ps, while in DLPC, the process is completed within 6 ps. In the ground state, the DPPC environment appears to stabilize a higher distribution of gZg conformers when the molecule is able to hydrogen bond to the lipid head group, while the DLPC environment appears to allow more gZg conformers to relax to the tZg conformation. Since the measurements done in this dissertation suggest that the DPPC lipid environment produces a significantly higher yield of vitamin D_3 than a shorter tail length lipid or a solution environment, Tian and Holick's proposed membrane model[3] is considered as a good simple model to understand vitamin D_3 formation in the human skin environment.

References

(1)   Arruda, B. C., Peng, J., Smith, B. Spears, K. G., Sension, R. J. Photochemical Ring-Opening and Ground State Relaxation in α-Terpinene with Comparison to Provitamin D 3 Photochemical Ring-Opening and Ground State Relaxation in α-Terpinene with Comparison to Provitamin D 3 Brenden C . Arruda , Jian Peng , Broc Smith , K. *J. Phys. Chem.* **2012**.

(2)   Fuss, W.; Höfer, T.; Hering, P.; Kompa, K. L.; Lochbrunner, S.; Schikarski, T.; Schmid, W. E. Ring Opening in the Dehydrocholesterol-Previtamin D System Studied by Ultrafast Spectroscopy. *J. Phys. Chem.* **1996**, *100* (2), 921–927.

(3)   Tian, X. Q.; Holick, M. F. A Liposomal Model That Mimics the Cutaneous Production of Vitamin D3: Studies of the Mechanism of the Membrane-Enhanced Thermal Isomerization of Previtamin D3 to Vitamin D3. *J. Biol. Chem.* **1999**, *274* (7), 4174–4179.

(4)   Chen, C.; Tripp, C. P. A Comparison of the Behavior of Cholesterol, 7-Dehydrocholesterol and Ergosterol in Phospholipid Membranes. *Biochim. Biophys. Acta - Biomembr.* **2012**, *1818* (7), 1673–1681.

(5)   Nojima, Y.; Iwata, K. Viscosity Heterogeneity inside Lipid Bilayers of Single-Component Phosphatidylcholine Liposomes Observed with Picosecond Time-Resolved Fluorescence Spectroscopy. *J. Phys. Chem. B* **2014**, *118* (29), 8631–8641.

(6)   Kalajian, T. A.; Aldoukhi, A.; Veronikis, A. J.; Persons, K.; Holick, M. F. Ultraviolet B Light Emitting Diodes (LEDs) Are More Efficient and Effective in Producing Vitamin D3 in Human Skin Compared to Natural Sunlight. *Sci. Rep.* **2017**, *7* (1), 6–13.

(7)   Holick, M. F. Biological Effects of Sunlight, Ultraviolet Radiation, Visible Light, Infrared Radiation and Vitamin D for Health. *Anticancer Res.* **2016**, *36* (3), 1345–1356.

(8)   Kostas, A. Generation of Previtamin D3 from Tachysterol3 : A Novel Approach for Producing Vitamin D3 in the Winter. *Bost. Univ. thesis* **2015**.

(9)   Benesch, M. G. K.; Lewis, R. N. A. H.; McElhaney, R. N. A Calorimetric and Spectroscopic Comparison of the Effects of Cholesterol and Its Immediate Biosynthetic Precursors 7-Dehydrocholesterol and Desmosterol on the Thermotropic Phase Behavior and Organization of Dipalmitoylphosphatidylcholine Bilayer Membrane. *Chem. Phys. Lipids* **2015**, *191*, 123–135.